CENTRAL RESEARCH LIBRARY
DOCUMENT COLLECTION

Oak Ridge National Laboratory

Molten-Salt Reactor Program

Semiannual Information Meeting

APRIL 20, 1971

OAK RIDGE, TENNESSEE

Summaries of the Presentations

OAK RIDGE NATIONAL LABORATORY
CENTRAL RESEARCH LIBRARY
DOCUMENT COLLECTION
LIBRARY LOAN COPY
DO NOT TRANSFER TO ANOTHER PERSON
If you wish someone else to see this document, send in name with document and the library will arrange a loan.
UCN-7969
(3 3-67)

OAK RIDGE NATIONAL LABORATORY
OPERATED BY UNION CARBIDE CORPORATION • FOR THE U.S. ATOMIC ENERGY COMMISSION

MOLTEN-SALT REACTOR PROGRAM

Semiannual Information Meeting
April 20, 1971

Summaries of the ORNL Presentations

M. W. Rosenthal, Director
R. B. Briggs, Associate Director
P. N. Haubenreich, Associate Director

CONTENTS

Paper No.		
1	Conclusions from MSRE Operation and Post-Operation Examination	P. N. Haubenreich
2	Migration of Noble-Metal Fission Products in the MSRE	E. L. Compere
3	Performance of Hastelloy N in the MSRE and Its Improvement for Future Reactors	H. E. McCoy
4	Chemical Studies Involving Control of Tritium in Molten-Salt Reactors	S. Cantor
5	Chemical Processing Development for MSBR's	L. M. Ferris
6	Development of Processing Plant Materials	J. R. DiStefano
7	Graphite Development	W. P. Eatherly
8	Status and Plans for the Engineering Technology Program	Dunlap Scott
9	Development of MSBR Bubble Generator and Bubble Separator	C. H. Gabbard
10	Influences of Physical Properties and Entrance Region Conditions on Molten-Salt Heat Transfer	J. W. Cooke
11	Exploration of the Design of an MSR Demonstration Plant	E. S. Bettis

PROGRAM

Morning Session, 9:00 - 12:00

9:00	Introduction	M. W. Rosenthal
9:10	Conclusions from MSRE Operation and Post-Operation Examination	P. N. Haubenreich
9:35	Migration of Noble-Metal Fission Products in the MSRE	E. L. Compere
9:55	Performance of Hastelloy N in the MSRE and Its Improvement for Future Reactors	H. E. McCoy
10:20	Chemical Studies Involving Control of Tritium in Molten-Salt Reactors	S. Cantor
10:40	Intermission	
10:55	Chemical Processing Development for MSBR's	L. M. Ferris
11:20	Development of Processing Plant Materials	J. R. DiStefano
11:40	Graphite Development	W. P. Eatherly
12:00	LUNCH	

Afternoon Session, 1:30 - 4:00

1:30	Introduction	R. B. Briggs
1:40	A Utility-Sponsored Independent Technical Evaluation of MSBR Technology	Deslonde R. deBoisblanc (Ebasco Services)
2:20	Status and Plans for the Engineering Technology Program	Dunlap Scott
2:45	Intermission	
3:00	Development of MSBR Bubble Generator and Bubble Separator	C. H. Gabbard
3:20	Influences of Physical Properties and Entrance Region Conditions on Molten-Salt Heat Transfer	J. W. Cooke
3:40	Exploration of the Design of an MSR Demonstration Plant	E. S. Bettis
4:00	Adjourn	

1. Conclusions from MSRE Operation and Post-Operation Examination

Paul N. Haubenreich

The MSRE was intended to demonstrate the practicality of the molten-salt reactor concept, so great emphasis was placed on making the reactor safe, reliable and maintainable. It proved to be so, and within 3 years after nuclear operation began in 1965 the original goals of the MSRE were met and surpassed. Then, in an extension of the experimental program, the uranium was removed from the fuel salt by fluorination and ^{233}U was substituted. The reactor operated another 14 months, yielding much new information, before the final shutdown in December 1969. Between November 1970 and February 1971, limited examinations were carried out to supplement the observations made during operation.

Radiation in the reactor and drain tank cells (on the order of 100 R/hr) required all the work to be done through shielding, with tools and procedures especially developed for the tasks. The control rods, drives and thimbles were removed and part of one thimble was taken for examination. The top of the graphite core was viewed, then one graphite bar was removed. The interior of the fuel pump bowl was also viewed, through an opening left by excision of the sampler cage with an abrasive tool. A plasma torch was used to cut out a portion of the primary heat exchanger shell. Sections of 6 tubes were then cut out. Part of the thermal shield around the reactor was removed and a sample of thermal insulation obtained for analysis in support of tritium studies. Heaters were removed from the suspected location of a small leak that had occurred during the final shutdown. The leaked salt (2 - 3 in.^{3}) was observed and the freeze valve containing the leak was cut out. The flowmeter in the coolant salt system was calibrated and the large salt piping outside the reactor cell was removed for use in development loops. Patches were fastened over the holes in the pump tank and heat exchanger, the severed ends of lines were plugged, and the containment cells were sealed to conclude the on-site work. Meanwhile the rod thimble, core graphite bar, sampler cage, heat exchanger tubes, and the leaking freeze valves were examined in hot cells.

Operation of the MSRE showed that the fuel was, as expected, immune to radiation damage and tolerant of the buildup of fission and corrosion products. Noble gases were stripped, "noble metals" were deposited on surfaces, and other fission products remained stably in the salt. Most of the tritium from the fuel was removed through the offgas system but substantial fractions diffused out through hot metal walls. Simple refuelling of MSRs was demonstrated by the routine additions of UF_4-LiF and PuF_3 during operation and the on-site fluorination of the fuel. Predicted and observed nuclear characteristics, including long-term reactivity behavior, agreed very well.

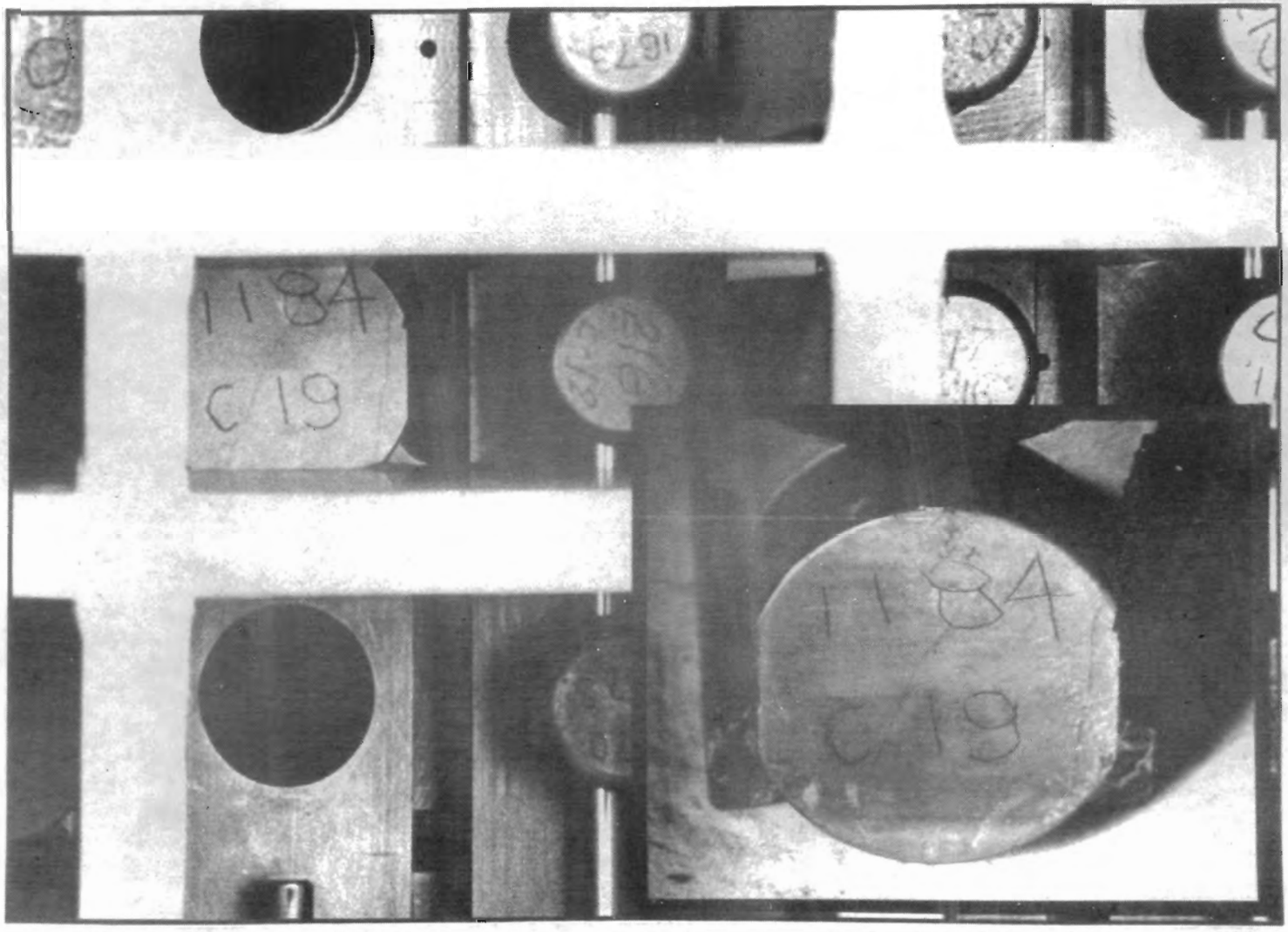

Fig. 1-1. LOWER END OF A GRAPHITE MODERATOR ELEMENT BEFORE AND AFTER EXPOSURE IN THE MSRE

Comparison of hot cell photograph (inset) with the photograph of the core during assembly shows no perceptible change in more than 20,000 hr in 1200°F salt in the MSRE core.

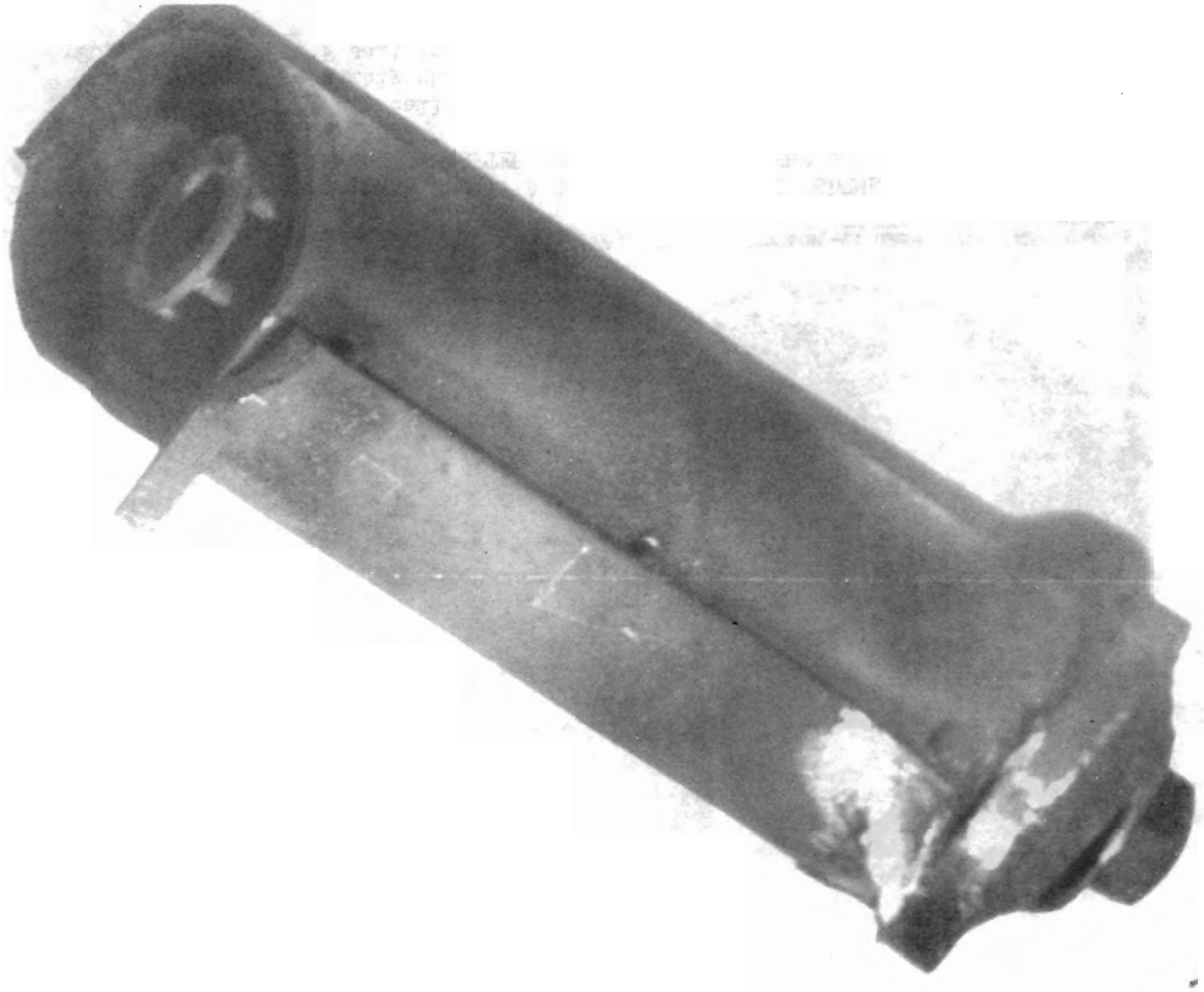

Fig. 1-2. SAMPLER CAGE AND BAFFLE FROM THE FUEL PUMP BOWL

Surfaces above the salt are covered with sootlike deposits. (The bright area is from the cutting operation.) The cage and the inside of the baffle have deposits tentatively ascribed to reduction of corrosion products by exposure of beryllium there.

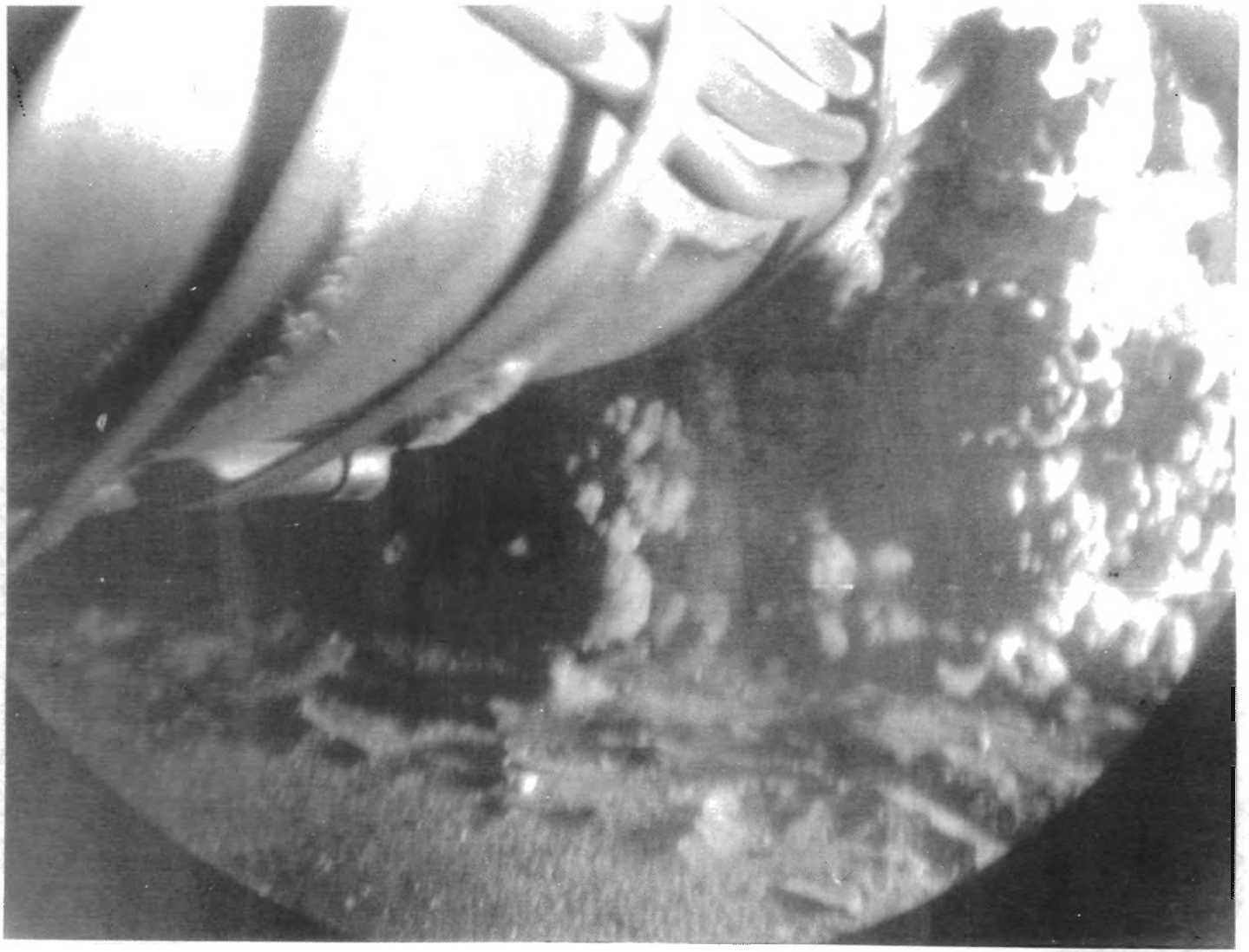

Fig. 1-3. CLOSEUP VIEW OF SALT NEAR FREEZE VALVE FV-105

The drain line and 1/8-in.-dia. thermocouple sheaths loom at upper left. During the final shutdown, 2 to 3 in.^{3} of salt escaped through a small crack near the freeze valve air shroud and froze in this knobby mass. A late modification of the shroud to increase air flow caused unexpectedly high thermal stresses during each cycle, ultimately resulting in the crack.

2. Migration of Noble-Metal Fission Products in the MSRE

E. L. Compere

The behavior of the noble metal fission product isotopes in molten salt reactor fuel is less well understood than that of the gaseous or salt seeking isotopes. The tendency of these elements to deposit on surfaces could give rise to some accumulation of neutron poisons on core graphite, the development of significant afterheat problems in heat exchangers in the unlikely event of simultaneous emptying of fuel and coolant salts, and appreciable complication of maintenance and processing. Their transport in the MSRE is of interest in order to distinguish mechanisms of interest to MSBR designs.

The transport paths and lags of noble metal fission products in the MSRE have been examined using all available data on the activity ratio of two isotopes of the same element, 39.6-day ^{103}Ru and 367-day ^{106}Ru. Data from graphite and metal surveillance specimens exposed for various periods and removed at various times, for material taken from the off-gas system, and for salt and gas samples and other materials exposed to pump bowl salt, were compared with appropriate inventory ratios and with values calculated for indicated lags in a simple compartment model. This model, as implied in earlier reports, assumes that salt rapidly loses ruthenium fission product formed in it, some to surfaces and most to a separate mobile "pool" of noble metal fission product, presumably particulate or colloidal and located to an appreciable extent in pump bowl regions. Some of this "pool" material is deposited on surfaces, and it appears to be the source of the off-gas deposits. All materials sampled from or exposed in the pump bowl appear to receive their ruthenium activity from the pool of retained material. Adequate agreement of observed data with indications of the model has resulted when holdup periods of 45-90 days were assumed.

Examination of the sampler cage and mist shield excised in January 1971 from the MSRE pump bowl revealed that all surfaces were covered with a deposited film, generally gray-black, over unattacked metal. These films contained carbon, fuel salt fluorides, structural metals, fission products dominated by noble metal isotopes and ^{137}Cs, and tritium. Much but probably not all of the structural metals could be debris from cutting operations. Tritium/carbon atom ratios of $\sim 1 \times 10^{-4}$ are consistent with non-trivial exchange with hydrogen in tars resulting from the cracking of lubricating oil which leaked into the pump bowl. A very high proportion, relative to calculated inventory per gram of fuel salt, was observed for all noble metal fission isotopes: ^{95}Nb, ^{99}Tc, ^{103}Ru, ^{106}Ru, ^{125}Sb and ^{127m}Te. The relative proportions of ^{103}Ru and ^{106}Ru isotopes, and the quantities of deposit suggest that these deposits were accumulated over a long period and that several percent of the reactor inventory of noble metal isotopes is deposited in the pump bowl. Thickest deposits were noted on the sample cage rods and inner mist shield walls below the surface, suggesting the steady agglomeration and deposition of suspended material in the less agitated regions.

The MSBR pump-gas separator circuits are indicated to be less susceptible to such behavior, since they should not encounter the combination of conditions developed in the MSRE pump bowl.

ORNL-DWG 70-5192

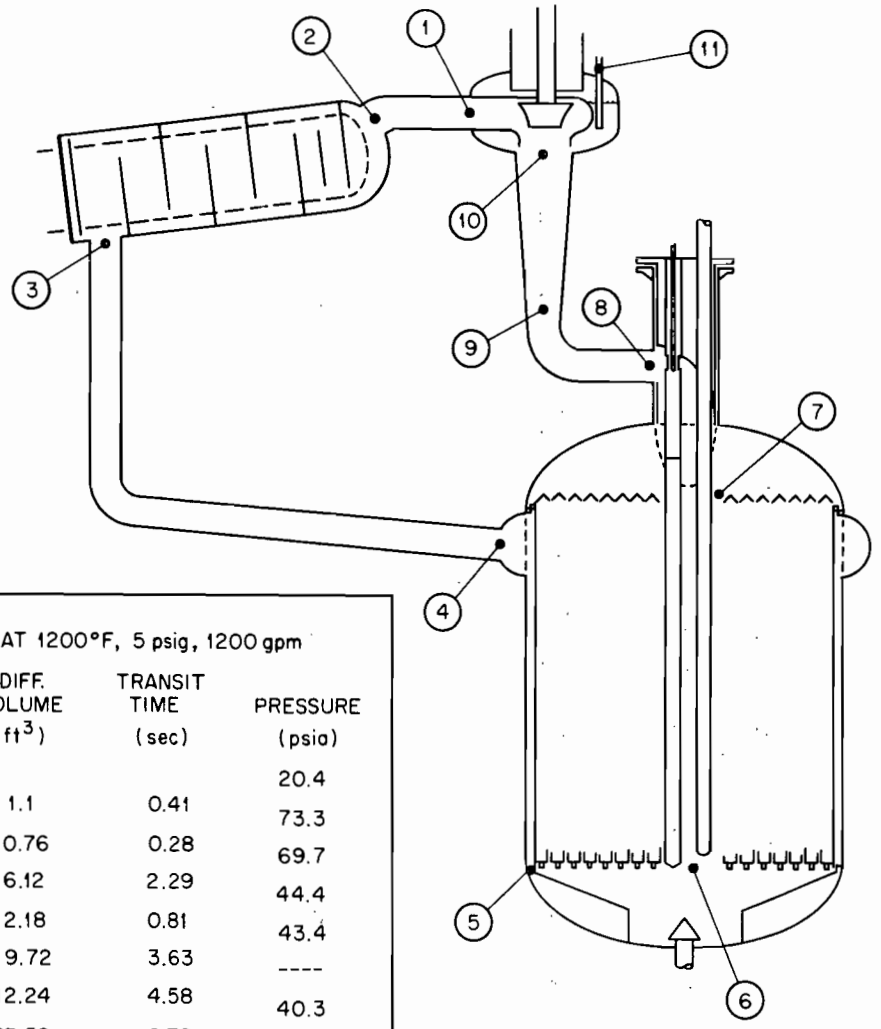

LOOP DATA AT 1200°F, 5 psig, 1200 gpm

POSITION	DIFF. VOLUME (ft^3)	TRANSIT TIME (sec)	PRESSURE (psia)
10			20.4
1	1.1	0.41	73.3
2	0.76	0.28	69.7
3	6.12	2.29	44.4
4	2.18	0.81	43.4
5	9.72	3.63	----
6	12.24	4.58	40.3
7	23.52	8.79	35.5
8	11.39	4.26	25.8
9	1.37	0.51	----
10	0.73	0.27	20.4

Fig. 2-1. MSRE FUEL CIRCULATION LOOP

1960 liters of fuel salt require ∿ 26 seconds for full circuit. Pump bowl holds additional ∿ 82 liters of salt, has inflow 4.1 ℓ/sec. Areas: Loop metal, 7.9 x 10^5 cm^2; graphite; fuel channels, 1.32 x 10^6 cm^2; total graphite 2.28 x 10^6 cm^2.

ORNL-DWG 70-14514

Noble Metal Fission Products

During MSRE Runs 19 and 20

Isotope	Percentage of Total Inventory in Given Location		
	Salt	Graphite	Metal
^{95}Nb	0-20	12	11
^{99}Mo	11-83	12	60
^{103}Ru	.4-21	4	5
^{106}Ru	.2-10	3	5
^{129}Te	.6-11	2	-
^{132}Te	.7-17	-	60
^{131}I	38-70	.2	6

Fig. 2-2. Noble metal isotopes deposit on metal and graphite surfaces. The amounts in salt are erratic but generally too low to account for entire inventory.

ORNL-DWG 70-14513

FISSION PRODUCT ACCUMULATION MODELS

1. OVERALL INVENTORY

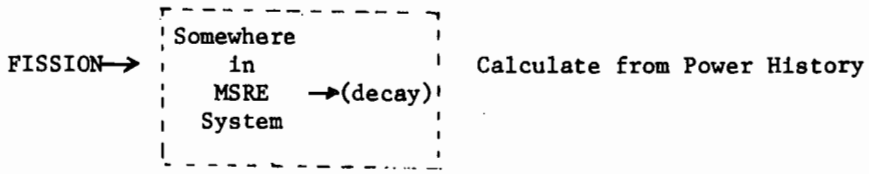

2. IF RETAINED IN SALT

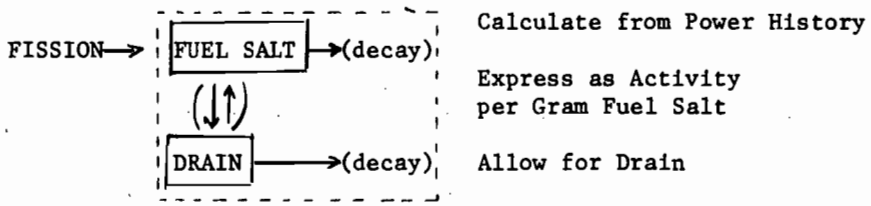

3. IF LOST RAPIDLY FROM SALT

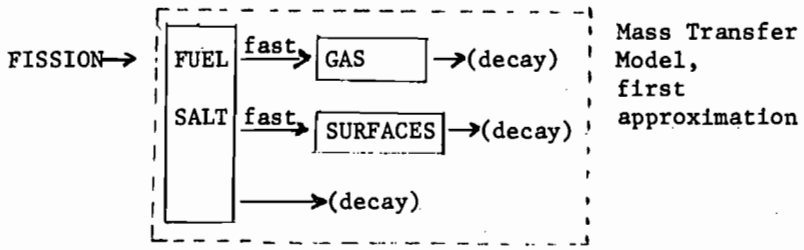

Fig. 2-3. Inventory is calculated from power history. Simple mass transfer model assumes prompt deposition on surfaces or into offgas.

ORNL-DWG 70-14516

Mass Transfer in MSRE

Briggs (1968)

$$\frac{dC}{dt} = \frac{P \cdot B \cdot y}{V_{salt}} - C \left(\frac{K_{gr} \cdot S_{gr} \cdot A_{gr}}{V_{salt}} + \frac{K_{met} S_{met} A_{met}}{V_{salt}} \cdot \frac{K_{Bub} \cdot S_{Bub} \cdot A_{Bub}}{V_{salt}} + \lambda \right)$$

where $B = 3.1 \times 10^{16}$ fiss/sec. Mw(th)

S = sticking fraction

Let $K_{isotope} = R \cdot K_{xenon}$

Assume $S = 1$, neglect λ

In English units (cu ft, hr. etc)

for MSRE at 8 Mw, .001 void fraction, .02 inch bubbles

$$\frac{dC}{dt} = 1.22 \times 10^{19} \cdot y - C \left(\frac{.06 \cdot R \cdot 1500}{73} + \frac{.7 \cdot R \cdot 600}{73} + \frac{2 \cdot R \cdot 260}{73} \right)$$

$$= 1.22 \times 10^{19} \cdot y - C\,(1.2 \cdot R + 5.7 \cdot R + 7.1 \cdot R), \quad \frac{\text{atoms}}{\text{cu ft. hr.}}$$

Thereby: steady state conc. $= 8.6 \times 10^{17} \cdot y/R$, atoms/cu ft.

Meanlife in fuel $= \frac{1}{14.R}$ hr.

Fig. 2-4. Direct mass transfer plays a part in removal of noble metals from salt. A retention time of ∿4 minutes gives very low concentration in salt. Over half to off-gas via bubbles.

ORNL-DWG 70-14539

DIRECT MASS TRANSFER COMMENTS

Concentration in salt of dissolved isotope amounts to 4 minutes production.

About 10^{11} atoms enter a .02 inch diameter bubble in the 8 minute cycle. Equivalent to about 1% of monolayer of given isotope on bubble surface, or a 1 micron particle.

Partition between metal and graphite surfaces and elsewhere (bubbles?) OK.

Rapid atom transport to surfaces precludes small colloids.

Bubble transport OK if sticking fraction is high. (As suggested by Blankenship hypothesis).

Dissolved isotope concentration (.001 to .00001) x inventory. Too low.

Short retention time implies production ratio of isotopes in salt samples and pump bowl gas samples. Inventory ratios should be found on surfaces and in offgas accumulations.

Fig. 2-5. Direct mass transfer model does not agree with pump bowl sample data. Amounts and activity ratios of isotopes, suggest a holdup phase may be involved.

ORNL-DWG 70-14538

HOLDUP PERIOD FROM ISOTOPE ACTIVITY RATIO

with steady state, at a fractional release rate of 1 /θ from holdup pool

$$\frac{A_1}{A_2} = \frac{Y_1}{Y_2} * \frac{(H_2 + .693 * \theta)}{(H_1 + .693 * \theta)}$$

θ = Holdup Period

H = Halflife

as produced (no holdup)

$$\frac{A_1}{A_2} = \frac{Y_1}{Y_2} * \frac{H_2}{H_1}$$

infinite holdup, no release from accumulation region

$$\frac{A_1}{A_2} = \frac{Y_1}{Y_2}$$

Fig. 2-6. Activity ratios for two isotopes of the same element will equal inventory if accumulated by prompt deposition. Holdup phase will fall between inventory and production, offgas or other deposits from holdup will be below inventory.

ORNL-DWG 70-13503

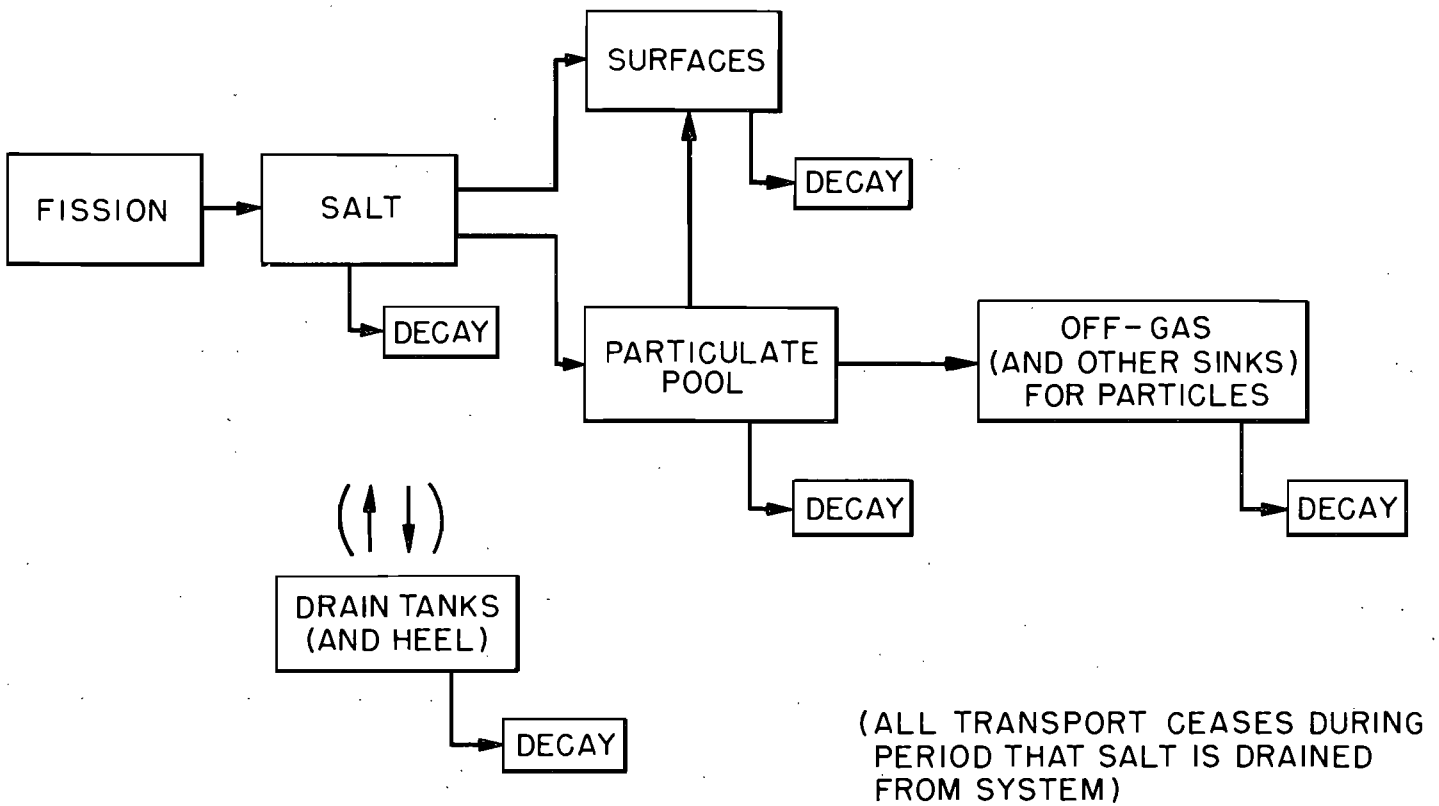

Fig. 2-7. Differential equations describing transport of atoms from one state or compartment to another are fitted into a Runge-Kutta numerical integration scheme, with MSRE power history as input. Isotope activity ratios can be estimated for various assumptions for model and transport rate.

ORNL-DWG 70-14279

Ruthenium Isotope Activity Ratios of Surveillance Specimens

Observed vs Calculated (dpm ^{103}Ru/dpm ^{106}Ru)

Exposure, Runs	Material	Observed Ratios: Median underlined	Calculated Values of Ratio: Net Inventory	Plus Deposition from Holdup (45 day)	(O.G.)
8 - 11	Graphite	20^3,22,$\underline{23}^3$ 25^2,27,52	25.5	19.2	(15.9)
8 - 14	Graphite	$\underline{9}^5$, 12	11.4	8.4	(6.8)
12- 14	Graphite	11,12^6,(>12),$\underline{13}^2$,(>13),14,(>14),16,17	16.7	11.6	(9.3)
	Metal	10^3,$\underline{11}$,12^2,15			
8 - 18	Graphite	6^2, $\underline{7}^3$, 8	9.8	7.2	(5.7)
	Metal Basket	$(3.5)^2$			
15- 18	Graphite	2,10,11^2,$\underline{12}^4$, 13,14,15^2,16,21,27	19.7	14.9	(12.3)
	Metal	6,$\underline{7}^3$,8,9,10			
19- 20	Graphite	10^2,11,$\underline{12}^4$,13^2,14,3200	21.7	13.4	(9.6)
	Metal	6,7^4,8,10^3,$\underline{11}^3$,12^2,$13^3$15			

Fig. 2-8. Ru activity ratios of all surveillance specimens are shown. They fall somewhat below inventory, indicating both direct deposition and deposition after holdup.

ORNL-DWG 70-14278

Ruthenium Isotope Activity Ratios of Off-Gas Line Deposits

Observed vs Calculated (dpm ^{103}Ru/dpm ^{106}Ru)

I. Jumper Section of Line 522, exposed Dec. 1966 - March 25, 1968

Sample	Obs. Ratio	Calc. Values of Ratio	
Flextool	2.4	Production	58
Upstream hose	2.4	Net inventory	12.1
Downstream hose	4.1		
Inlet Dust	7.3	Net Deposit if	
Outlet Dust	4.4	45 day holdup	7.0
		90 day holdup	5.5

II. Specimen Holder, Line 522, exposed Aug. 1968 - June 1969

Bail End	9.7	Production	43
Flake	5.0	Net inventory	19.7
Tube Sections (recount 7/70, corr)	5.4, 5.9 (6, 2)	Net Deposit if	
		45 day holdup	12.3
		90 day holdup	9.3

III. Overflow Tank Off-Gas Line (523), exposed 1965 to June 1969

Valve V523	8.0	Inventory	9.6
Line 523	11.3, 13.7, 13.3		
Valve HCV 523	13.3, 12.5, 10.0	Net Deposit if	
		45 day holdup	5.8
		90 day holdup	4.3

Fig. 2-9. Ru activity ratios of deposits from offgas line are generally below inventory, indicating holdup. Diversion of gas flow from line 522 to line 523 in May 1969 would diminish calculated ratio for line 522 and increase it for line 523.

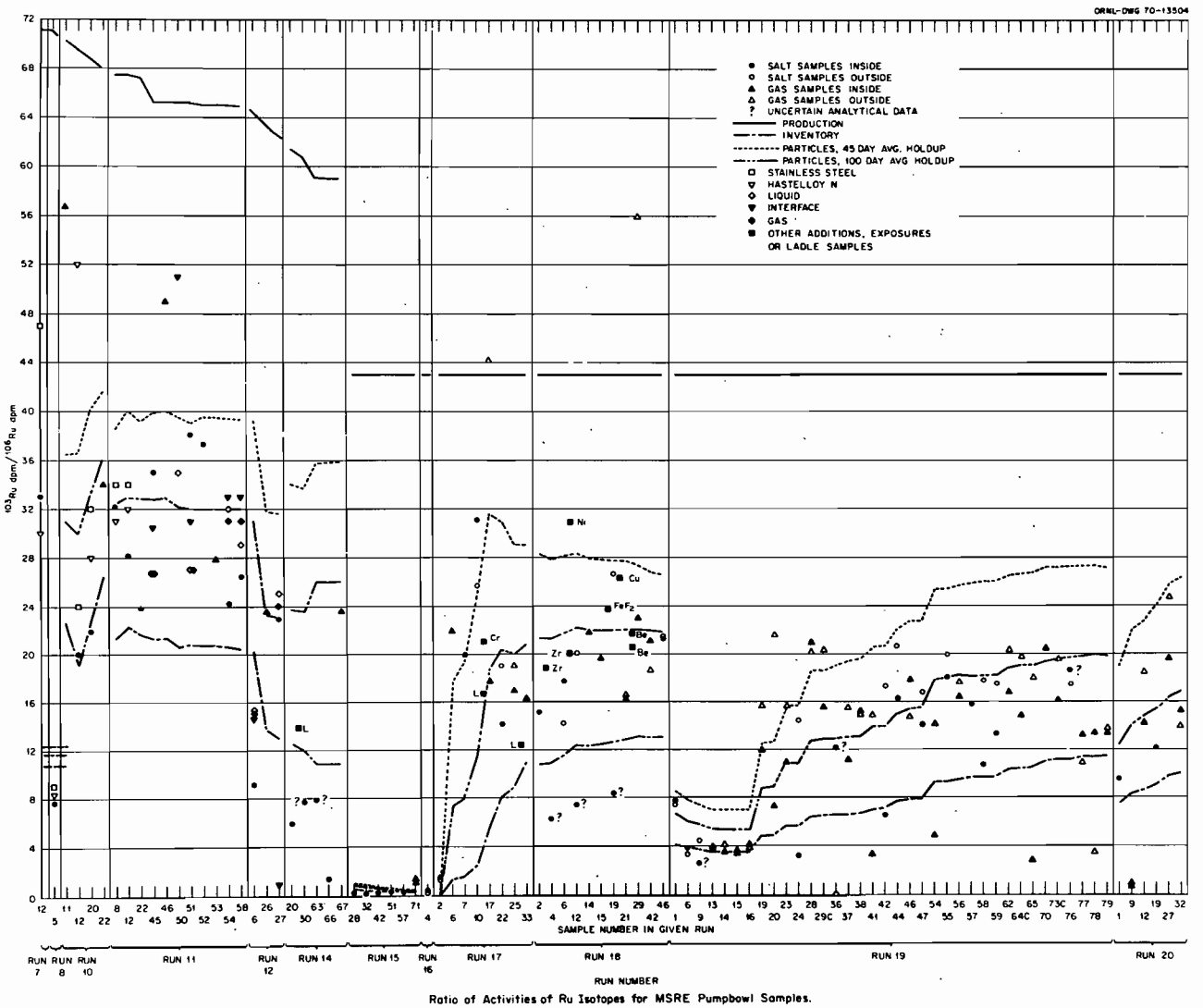

Fig. 2-10. Samples of all kinds fall generally above inventory and below production, indicating significant holdup. Gas and salt samples have similar ratios.

ORNL-DWG 70-14540

PARTICULATE HOLDUP COMMENTS

Deposition can be operative without or in parallel with any direct transport to bubbles.

Pump bowl liquid surface indicated to be a major holdup region.

Retention in system for an extended period is indicated.

Concentration in pump bowl samples would vary with entrainment fluctuation.

Age data from isotope ratios is consistent with observation on surveillance specimens, offgas accumulations, and pump bowl samples.

Gas borne material possibly mostly on salt mist. Even to offgas.

Losses can occur to offgas, and also to overflow tank, pump bowl shed roof, system crevices and to some extent to system surfaces.

Differences in MSBR may be important.

Fig. 2-11. A holdup phase, presumably particulate, for noble metal isotopes is consistent with data for Ru isotopes.

ORNL-DWG 69-10172A

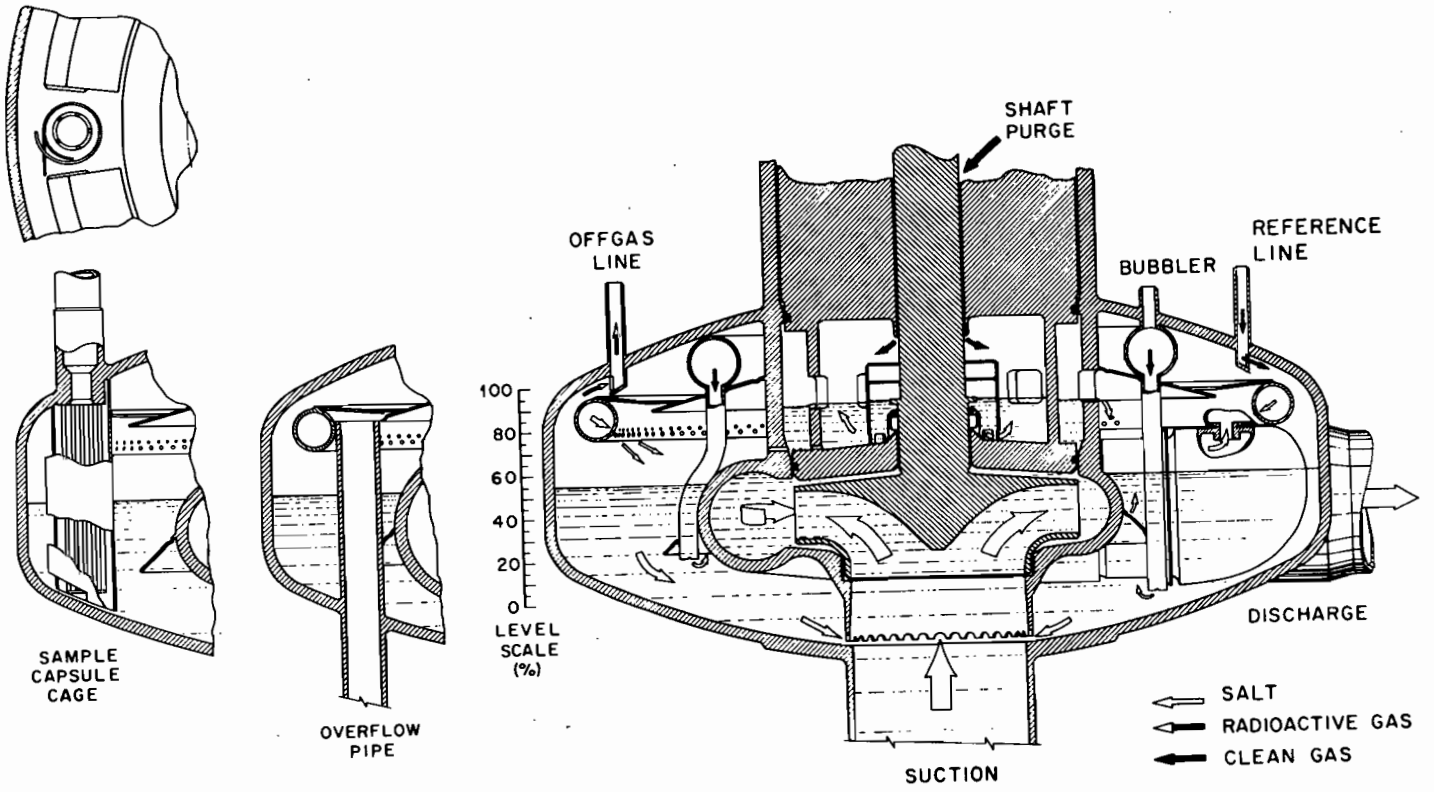

Fig. 2-12. MSRE PUMP BOWL

The pump bowl spray permits removal of gases into the helium offgas: The contents of the fuel loop pass through the pump bowl each ∿500 sec. Helium flow is ∿8 liters/min through ∿54 liter gas space. A few cc/day of oil lubricant also leak in. The capsules with fusible plugs, for liquid or gas samples, are lowered into the space contained within a spiral mist shield.

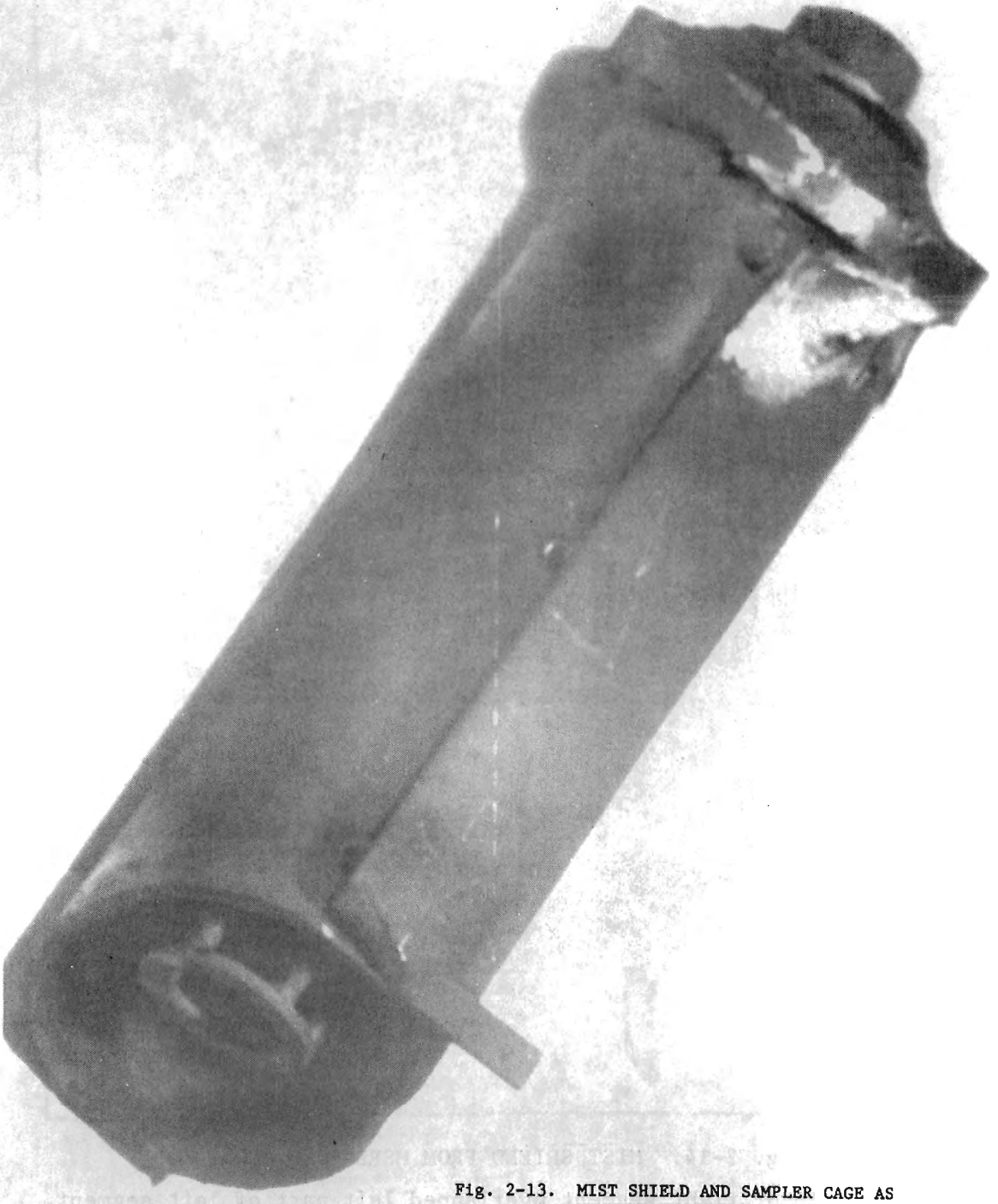

Fig. 2-13. MIST SHIELD AND SAMPLER CAGE AS REMOVED FROM MSRE PUMP BOWL.

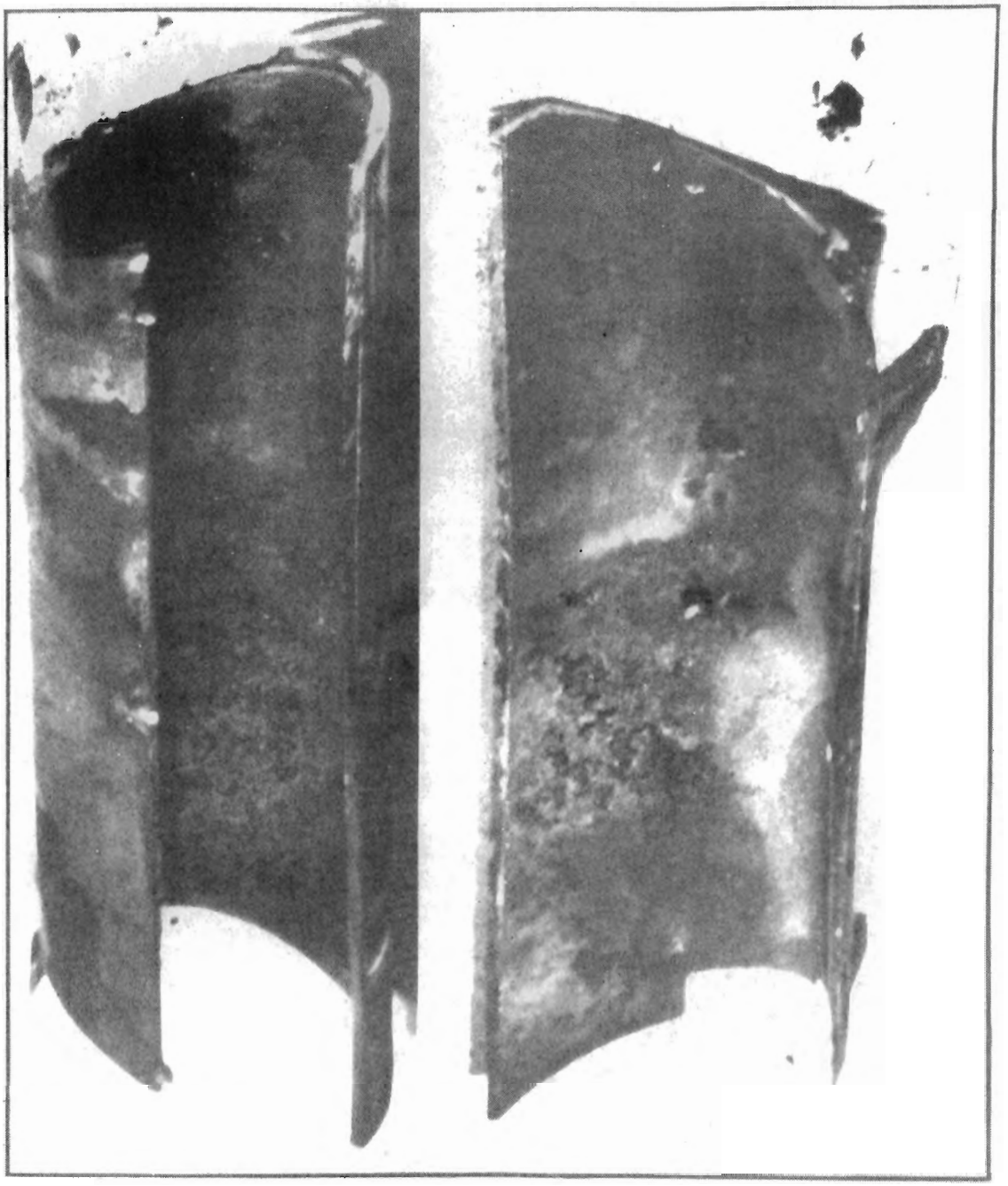

Fig. 2-14. MIST SHIELD FROM MSRE PUMP BOWL.

Right half of right segment overlapped left part of left segment, liquid level about halfway up.

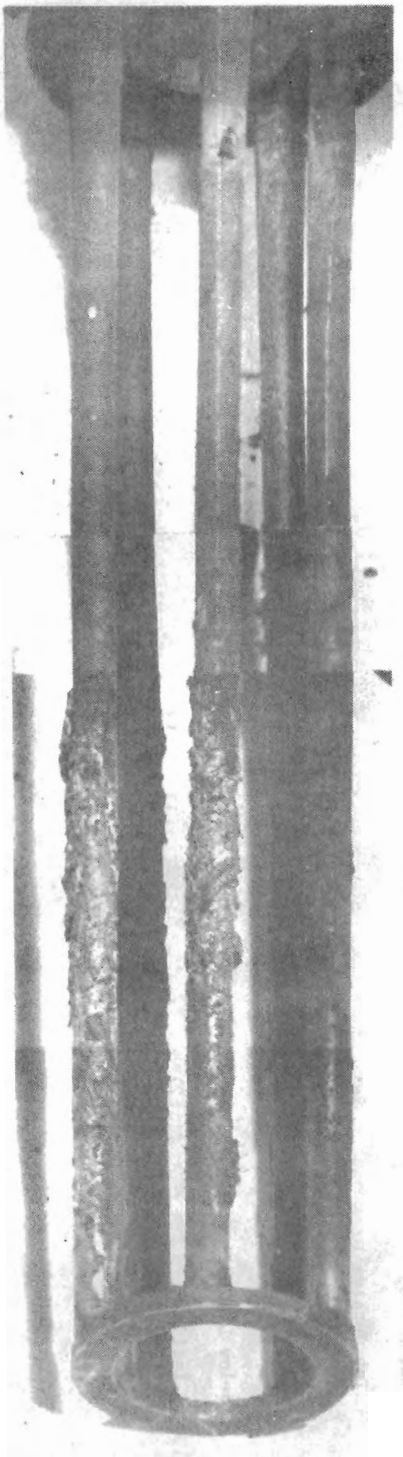

Fig. 2-15. SAMPLER CAGE FROM INSIDE MIST SHIELD. Bottom ring scraped earlier.

ORNL-DWG 71-3594

Chemical and Spectrographic Analysis of Deposits from Mist Shield, MSRE Pump Bowl

		Composition, %									
Sample	mCiT/g	C	UF_4	LiF	BeF_2	ZrF_4	Ni	Mo	Cr	Fe	Mn
Loose Particles Pump Bowl Bottom	14	7		22	18	∿1	∿25	∿3	∿1.5	∿.8	∿.8
Mist Shield:											
Latch Stop	89	28		10	10	∿1	∿8	∿3	∿.8	∿.8	<.5
Top Outside				6	5.	-	-	14	-	-	-
Inside				6	3	-	-	-	-	-	
Middle Outside				3	2	-	-	5	-	-	
Below Liquid Surface:											
Inside #1	21			11	13	∿1	∿8	∿3	∿4	∿3	<.5
Inside #2				10	8	1	11	3	2	7	
Cage Rod			.35	20	15	2	3	2	2	12	
Bottom Outside				5	3	-	9	13	-	-	
Inside				9	6	3	9	6	1	8	
Nominal Compositions											
MSRE Fuel			(1)	(42)	(36)	(20)					
Hastelloy-N							(.69)	(16)	(7)	(5)	(∿1)

- Sought; not found spectrographically.

Fig. 2-16. Deposits from mist shield contain carbon, fuel salt, metal constituents, some of which is doubtless from cutting debris.

ORNL-DWG 71-3595

Radiochemical Analysis of Deposits from Mist Shield, MSRE Pump Bowl

Isotope	^{99}Tc	^{95}Nb	^{103}Ru	^{106}Ru	^{125}Sb	^{127m}Te	^{137}Cs	^{95}Zr	^{144}Ce
Halflife	2.1×10^5y	35d (after ^{95}Zr)	39.6d	367d	2.7y	105d	30y	65d	284d
Sample activity per gram expressed as fraction of MSRE inventory activity/grams fuel salt.									
Latch Stop	-	260	360.	1000	6	70	3.1	<.5	<.2
Top Outside	-	120	170.	330	100	100	9.5	<.5	<.2
Inside	-	∿40	∿240	270	1000	70	4.3	<.5	<.2
Middle Outside	-	280	530	650	560	50	8.0	<.5	<.2
Below Liquid Surface:									
Inside #1	-	350	160	220	270	140	.6	<.5	.13
Inside #2	460	150	290	310	70	100	1.1	<.5	<.2
Cage Rod	-	300	220	690	200	190	.2	<.5	<.2
Bottom Outside	-	<60	<60	1200	170	230	3.2	<.5	<.2
Inside	-	∿16	∿15	190	50	30	0.32	<.5	.11

Fig. 2-17. Noble metal isotopes are all highly concentrated in pump bowl deposits; ∿ 5% of the mass of the deposits is indicated to be noble metal fission products.

3. Performance of Hastelloy N in the MSRE and Its Improvement for Future Reactors

H. E. McCoy

Several components of the MSRE have been removed for examination after 26,000 hr of operation at 650°C. The results of our work on the coolant circuit were reported at the last MSRP Information Meeting and we could find no evidence of corrosion. During the past few months we have removed several parts from the primary circuit including a graphite moderator element, a Hastelloy N control rod thimble, the sample assembly from the pump bowl, a lost copper sample tube, the shell and several tubes from the primary heat exchanger, and a freeze valve that failed as operation was terminated. The graphite moderator element was in excellent condition with no detectable dimensional changes (Fig. 3–1). There was a shallow layer about 2 mils deep on many of the Hastelloy N surfaces that we attribute to cold working, but no metallographic evidence of corrosion. All metal surfaces exposed to the fuel salt exhibited intergranular cracking to a depth of 5 to 10 mils during a room temperature tensile test (Fig. 3–2). The copper capsule was extremely brittle (Fig. 3–3). The failure in the freeze valve was located and attributed to thermal fatigue (Fig. 3–4).

Efforts to develop a modified Hastelloy N with improved resistance to thermal neutron irradiation have concentrated on commercial scale-up of several alloys that looked promising based on laboratory melts. These alloys contained small additions of Ti, Hf, and Nb. The commercial alloys containing Ti and Nb had postirradiation properties about equivalent to those of our laboratory melts, but the properties of the commercial alloys containing Hf were inferior to those of the laboratory melts (Figs. 3–5, 3–6, 3–7). This observation is associated with the different precipitate distributions obtained in the laboratory and the commercial melts.

The corrosion of Hastelloy N in sodium fluoroborate is being studied in four thermal convection loops and in two pump loops. The corrosion rate is very sensitive to the impurity content of the salt and acceptable corrosion rates can be obtained if the impurity content is kept low. One pump loop is currently being repaired and the second, a more versatile system, is undergoing preoperational checks (Fig. 3–8).

The corrosion of Hastelloy N in steam at 538°C results in the loss of less than 0.25 mpy of metal (Fig. 3–9). The facility at Bull Run is being modified to allow the test specimens to be dynamically stressed (Fig. 3–10).

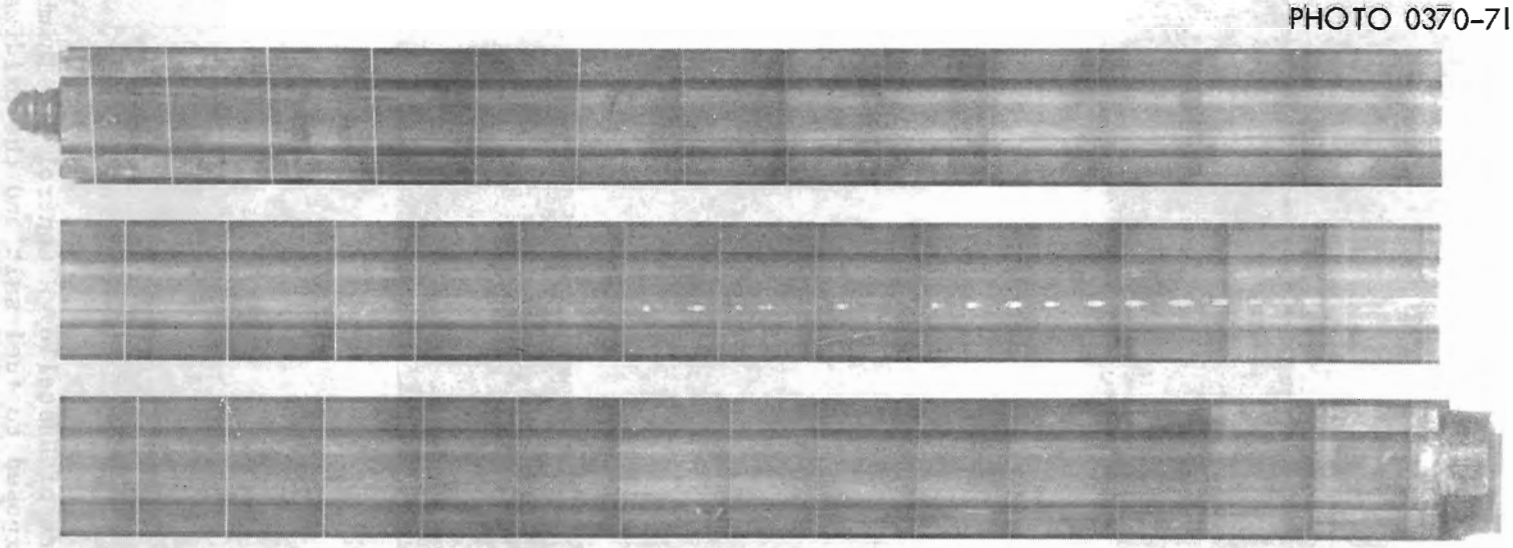

Fig. 3-1. Panoramic View of Graphite Moderator Element.

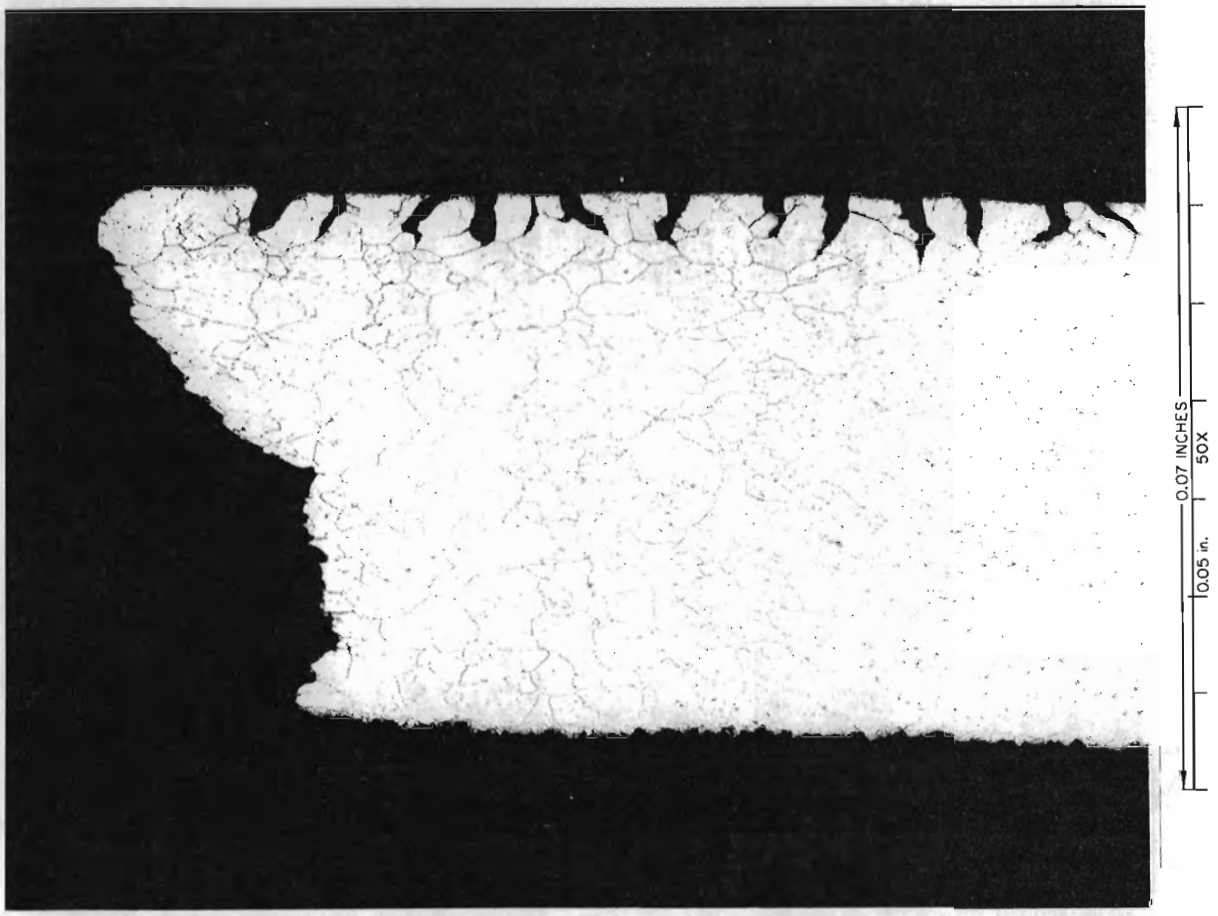

Fig. 3-2. Fracture of Hastelloy N Control Rod Thimble Tested at 25°C. The cracked side was exposed to fuel salt and the oxidized side was exposed to the cell atmosphere of N_2 plus 2 to 5% O_2.

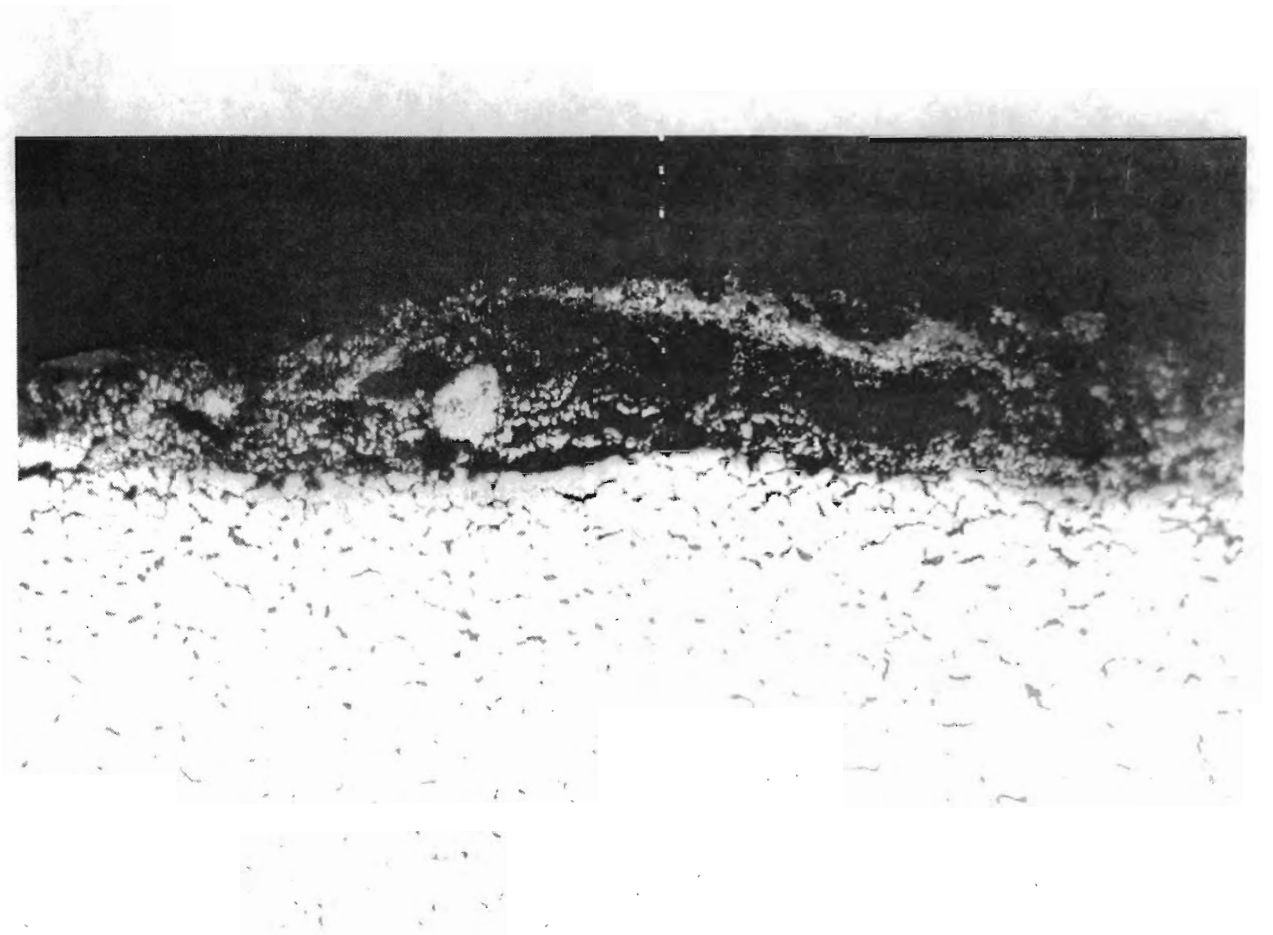

Fig. 3-3. Outside Diameter of Copper Capsule Exposed to Fuel Salt in MSRE Pump Bowl.

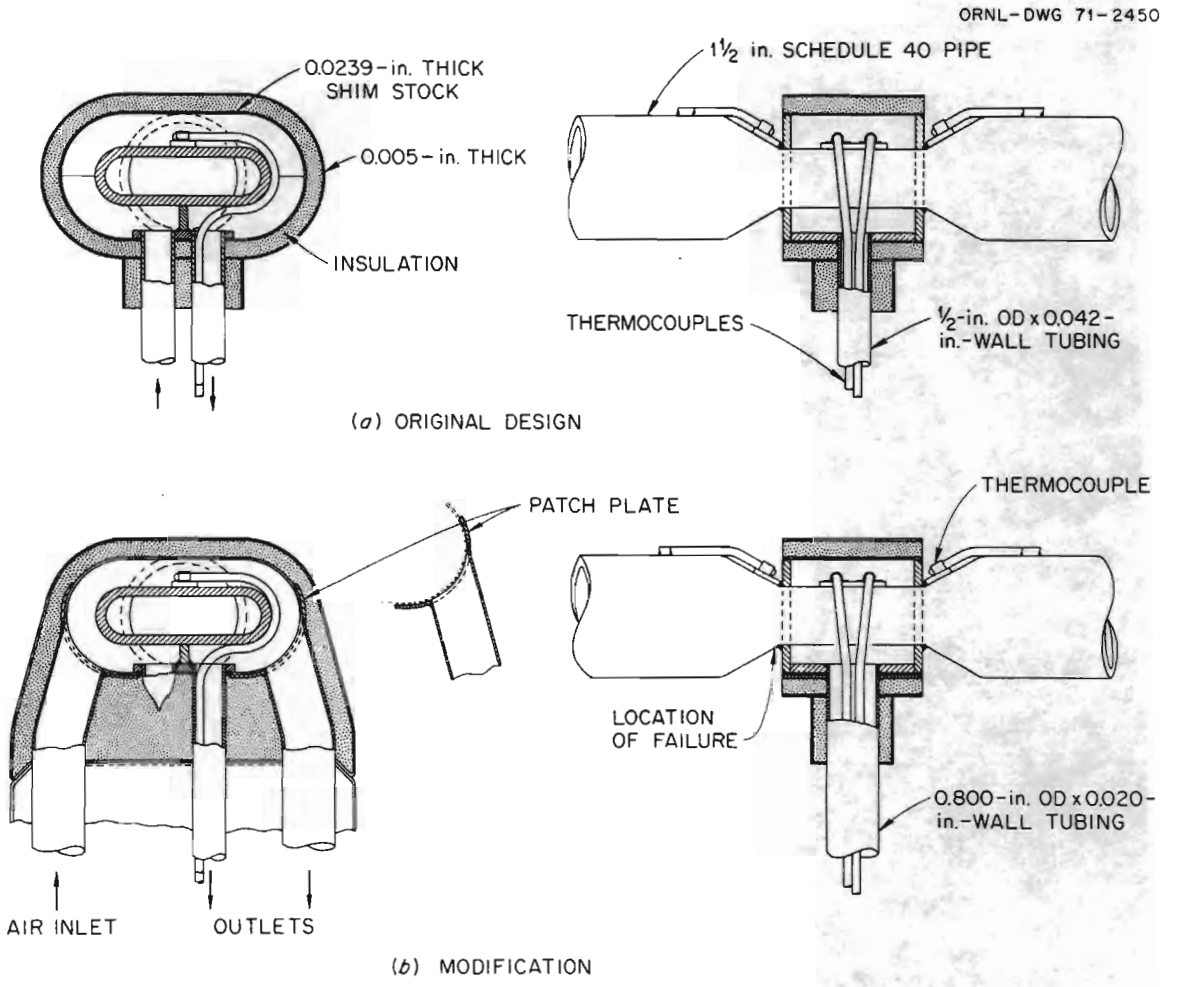

Fig. 3-4. Diagram Showing Possible Cause of Freeze-Valve Failure After Modification.

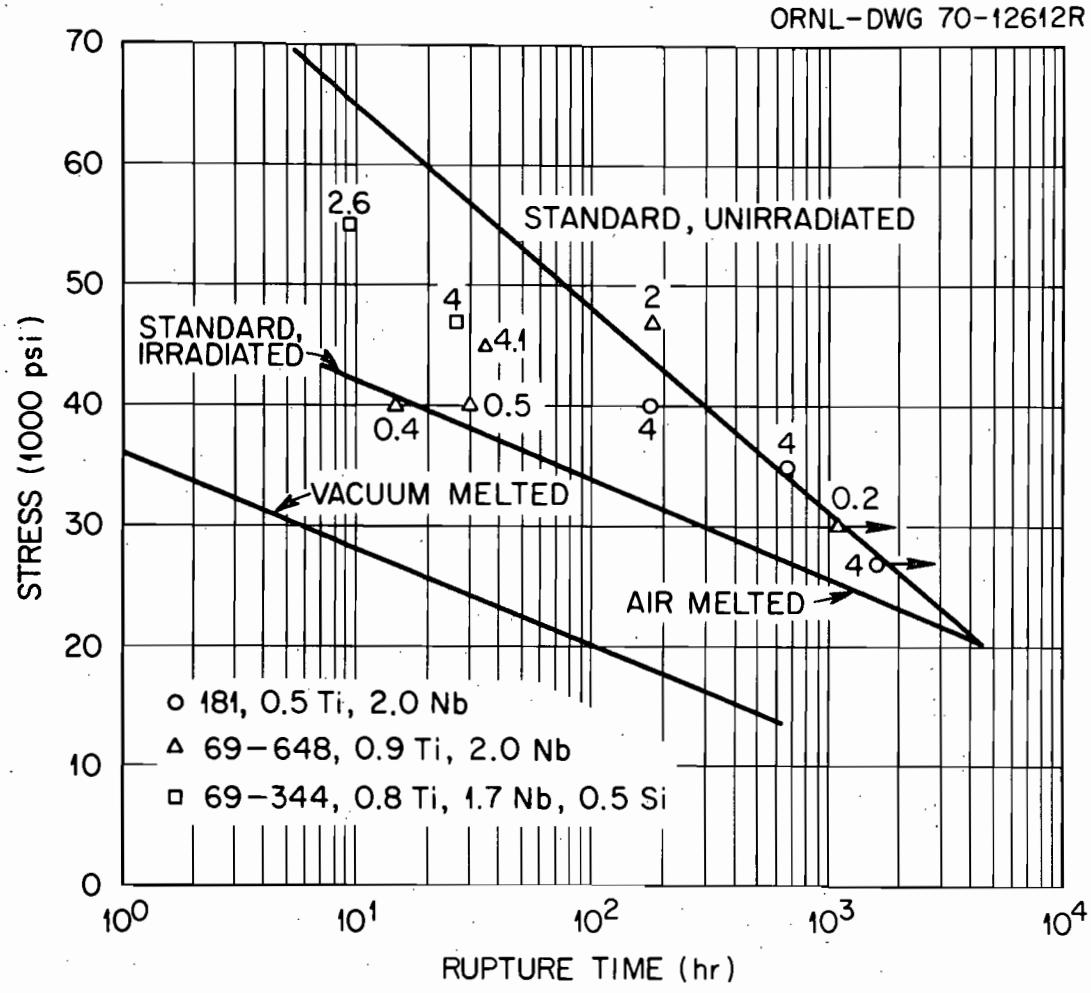

Fig. 3-5. Comparison of Stress-Rupture Properties at 650°C of Modified Hastelloy N Irradiated at 760°C to a Thermal Fluence of 3×10^{20} neutrons/cm^2.

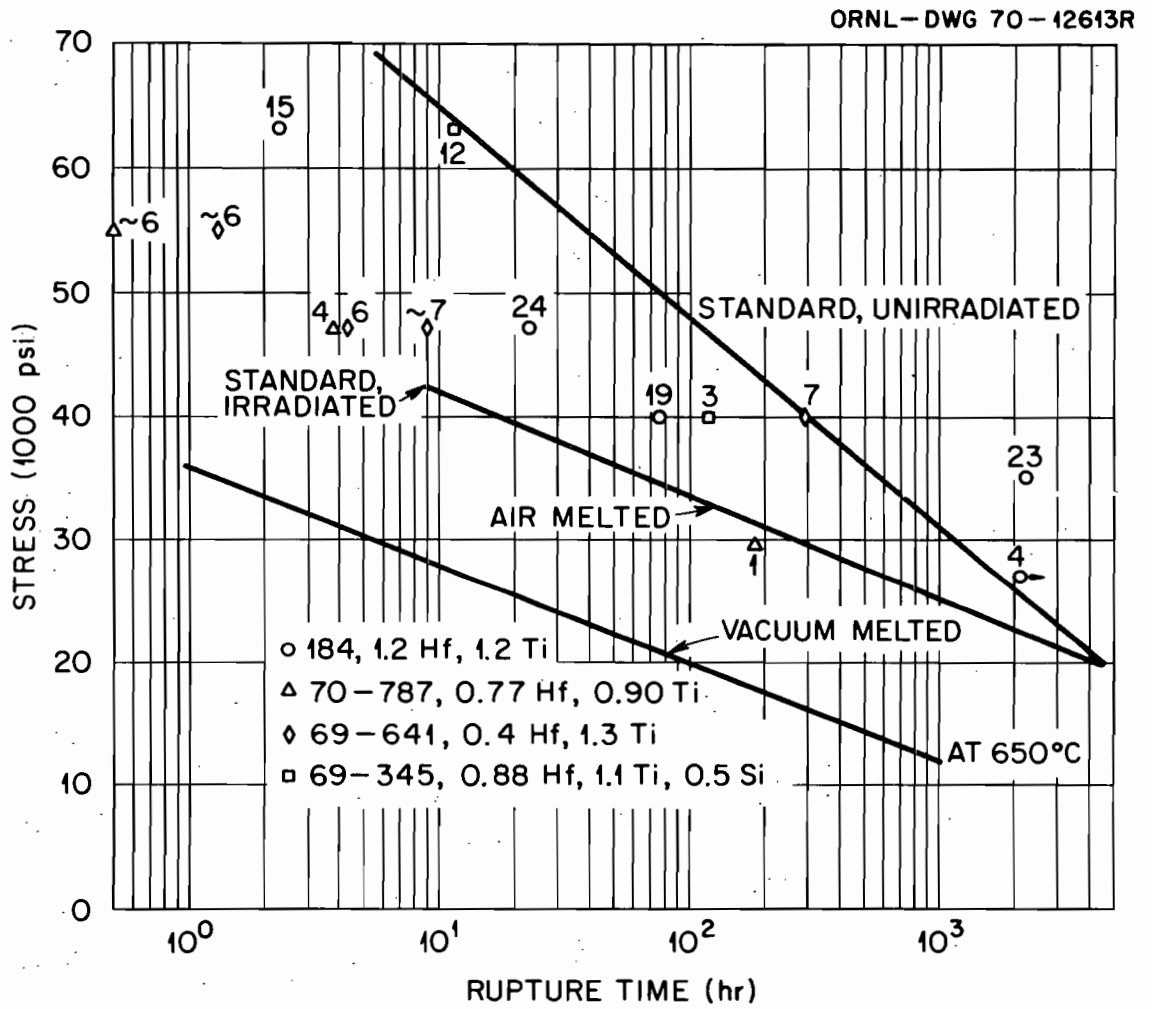

Fig. 3-6. Comparison of Stress-Rupture Properties at 650°C of Modified Hastelloy N Irradiated at 760°C to a Thermal Fluence of 3×10^{20} neutrons/cm^2.

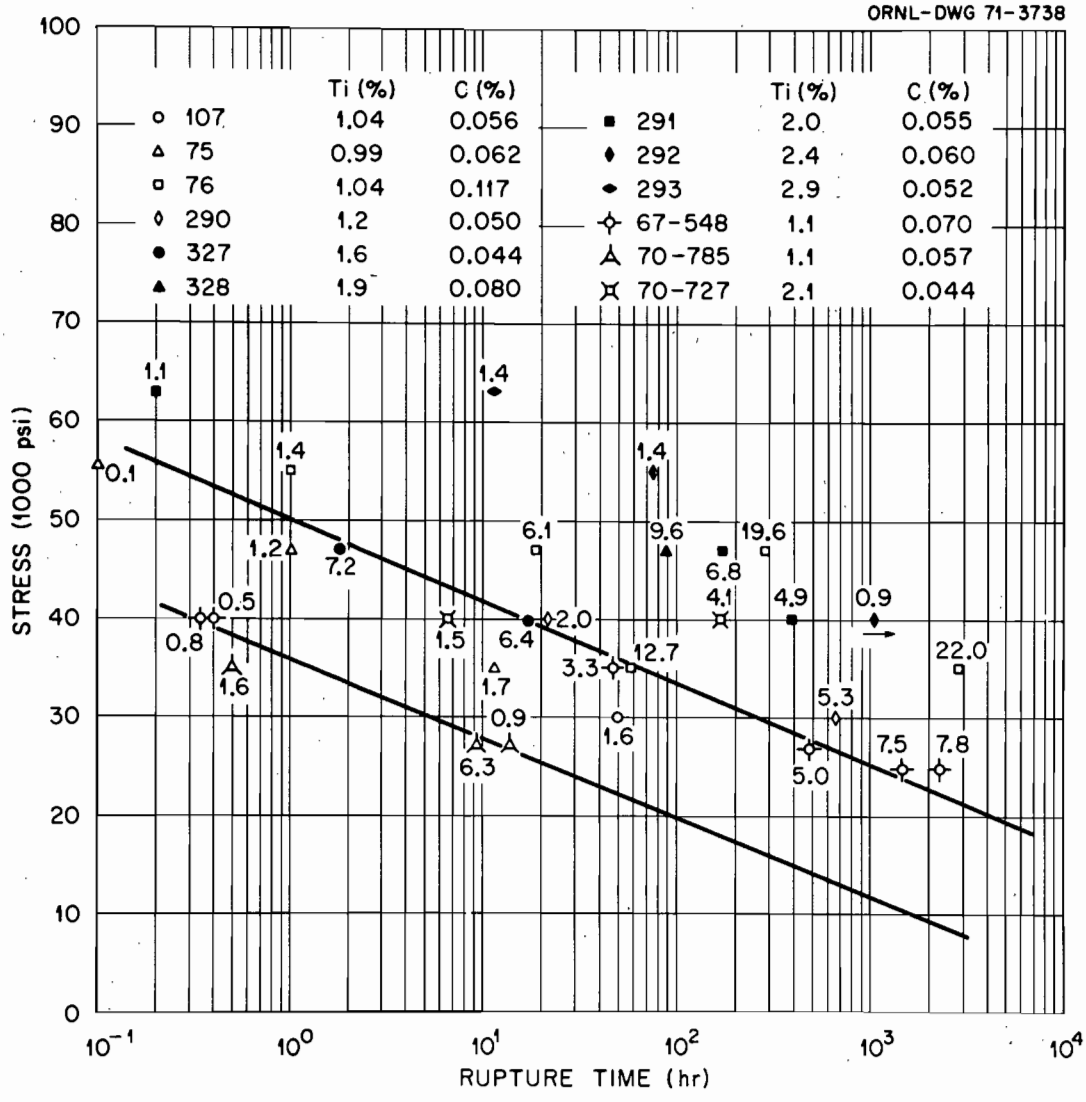

Fig. 3-7. Stress-Rupture Properties of Ti-Modified Hastelloy N at 650°C After Irradiation to a Thermal Fluence of 3 x 10^{20} neutrons/cm^2.

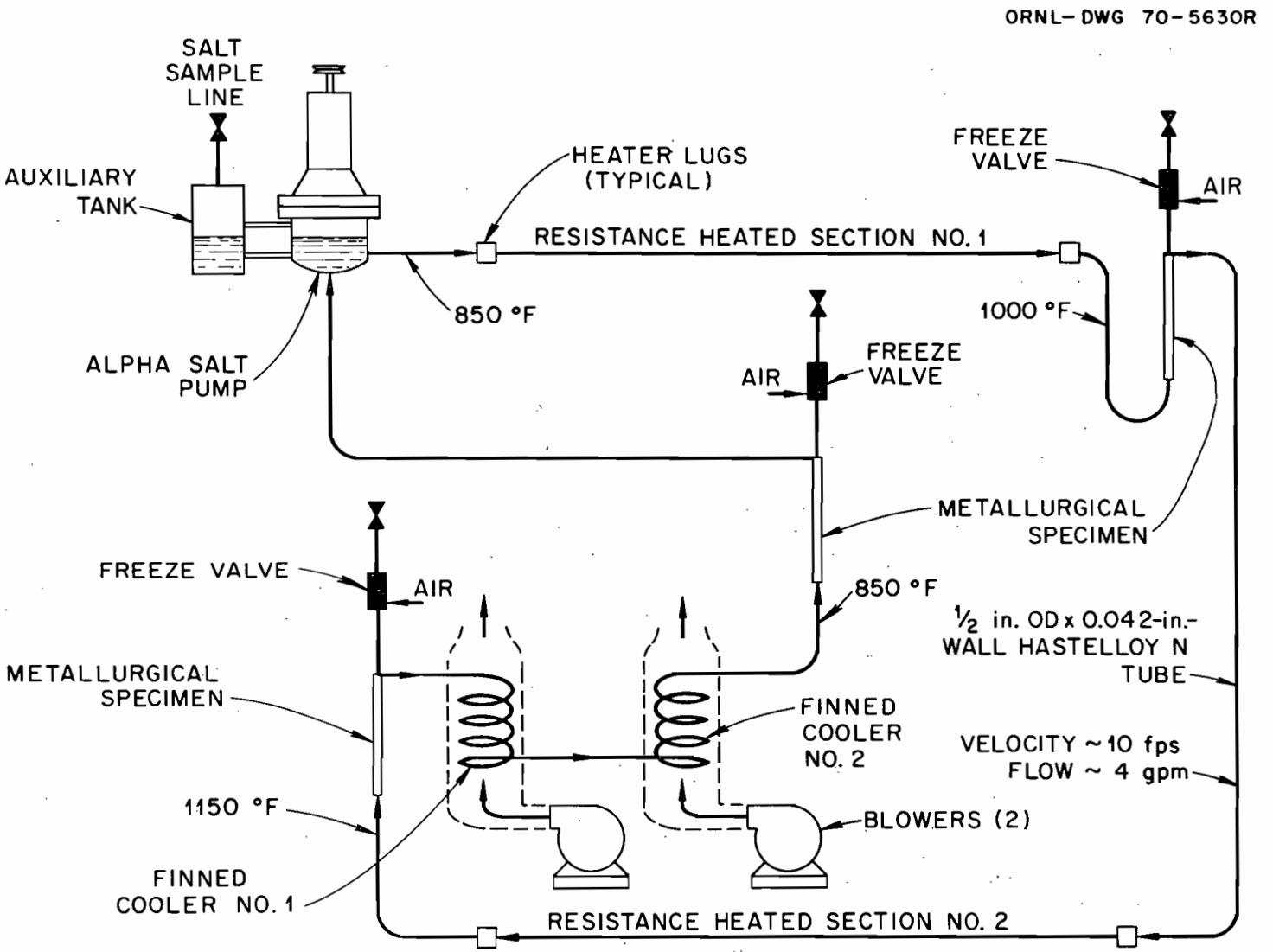

Fig. 3-8. Molten-Salt Forced Convection Corrosion Loop, MSR-FCL-2, Simplified Flow Diagram.

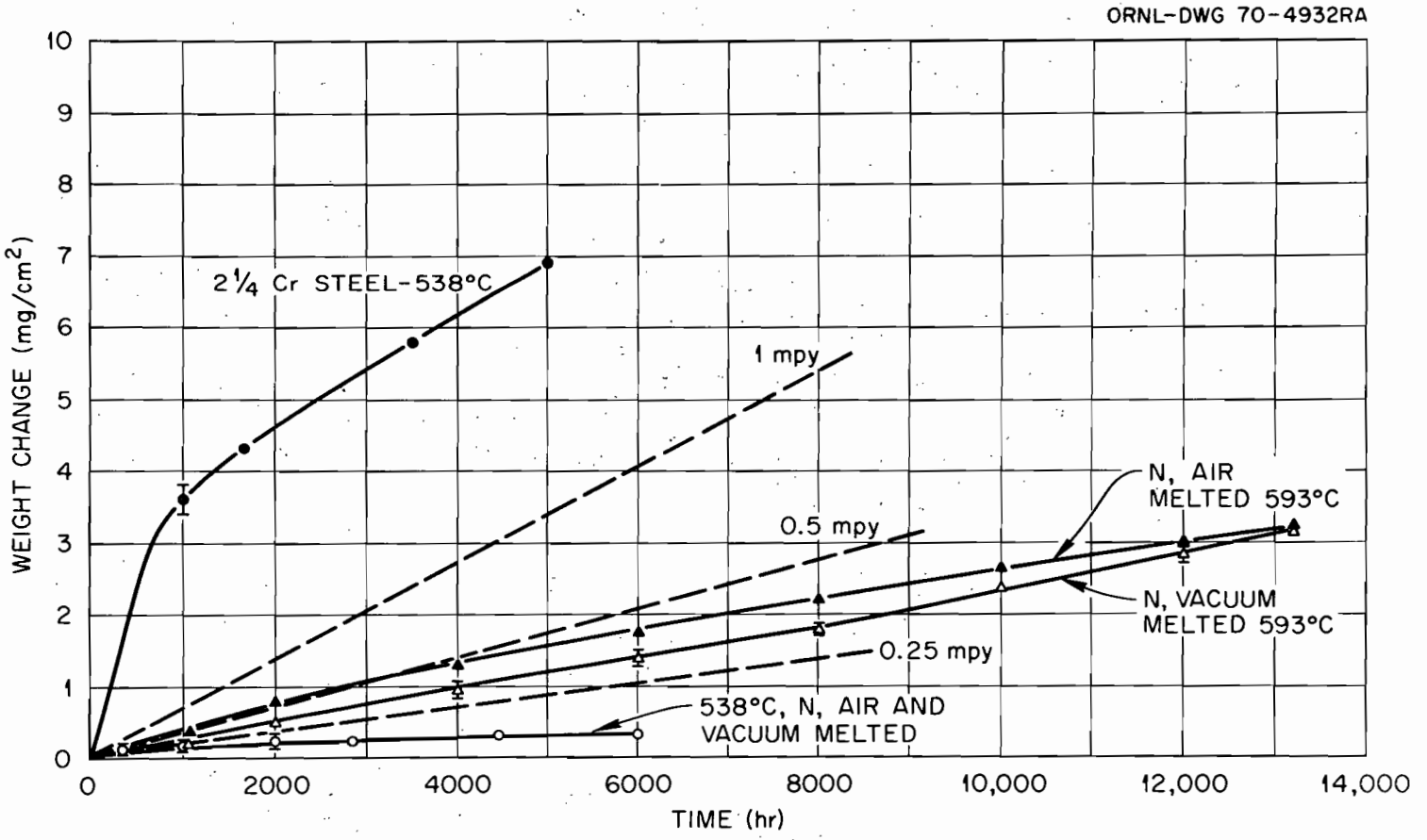

Fig. 3-9. Corrosion of Hastelloy N in Steam.

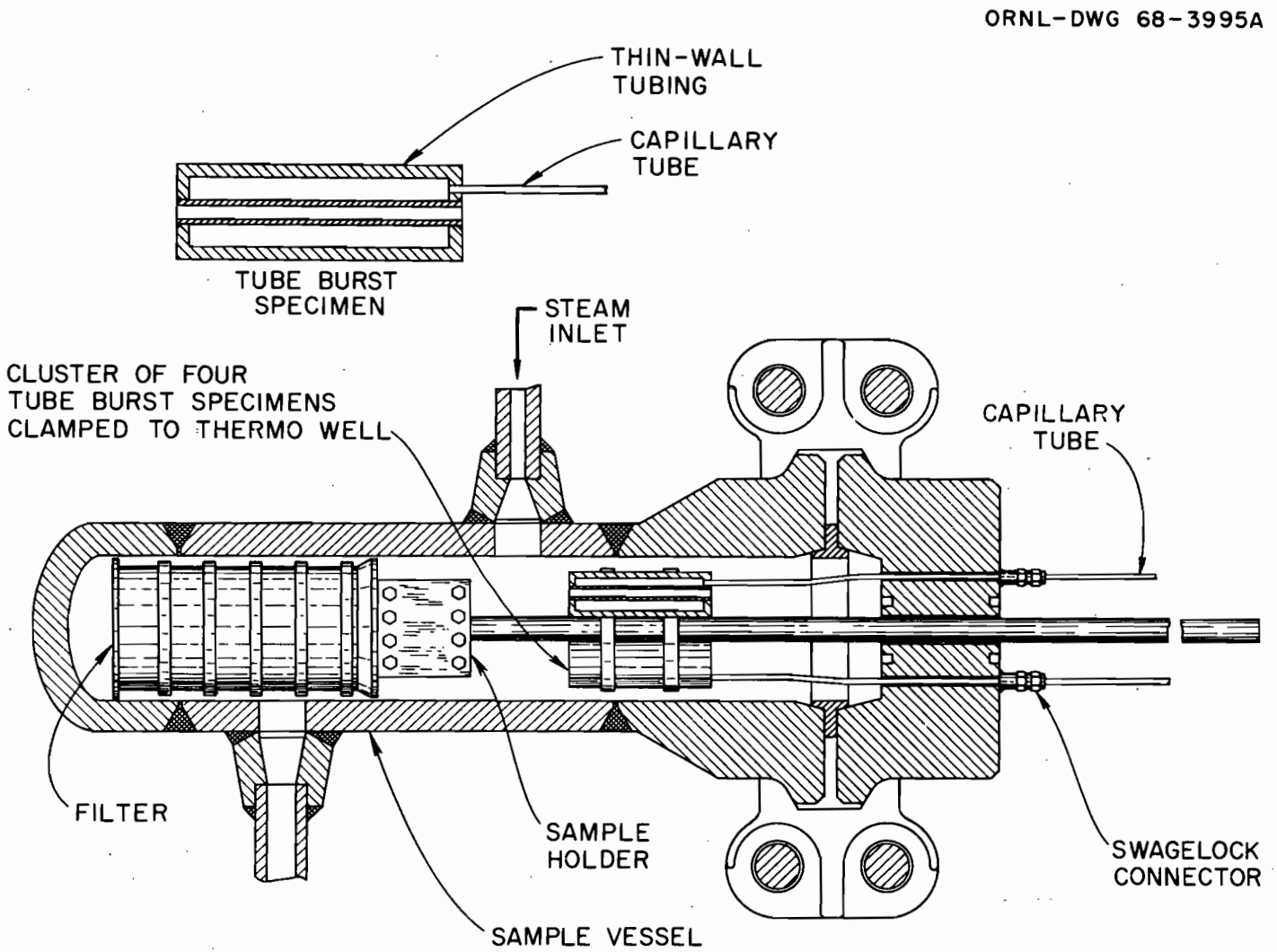

Fig. 3-10. Schematic of Corrosion Facility in Bull Run Steam Plant.

4. Chemical Studies Involving Control of Tritium in Molten-Salt Reactors

Stanley Cantor

The MSBR (reference design, 1000 Mw(e)) will create tritium at a rate of 2400 curies/day, almost all of this originating with the lithium and beryllium in the fuel salt (see Fig. 4-1). Both of these constituents would have to be replaced to effectively limit tritium production; such replacement would adversely affect breeding performance. Rather than averting tritium production, we are seeking methods for preventing tritium from eventually passing into the steam system of the reactor.

One general method is to impede the transport of tritium sufficiently so that it can be purged from the primary and secondary salt systems by gas stripping techniques. Two chemical studies in support of this approach are measurement of hydrogen gas solubility in molten salts, and determination of how steam-deposited oxide coatings on metals affect permeation of hydrogen.

A second general approach is to cause tritium to react chemically in such a way as to "fix" the tritium within the fuel or coolant circuits until it can be removed either by processing of the salt or by purging with an inert gas. For instance, in a coolant composed of molten alkali nitrate-nitrite, gaseous tritium reacts to form tritiated water vapor: $(Na,K)NO_3 + HT \rightarrow (Na,K)NO_2 + HTO$. The tritiated water vapor would then be removed continuously by purging with helium. Because of the consequences which might occur if the nitrate reached the moderator, this particular method for sequestering tritium would require interposing an additional circuit between the primary and nitrate-containing systems.

Thus far most of our experimental study pertains to using isotope exchange reactions to trap tritium in the fluoroborate coolant (92-8 mole % $NaBF_4$-NaF). A consideration of free energies of formation of hydrogen compounds (Fig. 4-2) leads to the selection of protonic compounds as the most attractive additives to the coolant. In a series of experiments, nickel capsules containing coolant salt (with hydroxide impurity or additive) and metal coupons were heated between 450-600°C within an evacuated silica vessel (Fig. 4-3). In contact with chromium coupons, the chemically-bound hydrogen in the salt was completely converted to hydrogen gas. In contact with nickel alone, a small but significant concentration of bound hydrogen remained with the salt. Since low concentrations of OH^- and OD^- in fluoroborate can be readily detected by infra-red spectroscopy, this tool has been frequently used to investigate retention and exchange of hydrogen in fluoroborate. Although the reasons are not entirely clear, infra-red studies indicate that, in fluoroborate, higher hydroxide concentrations are retained than can be accounted for in the capsule experiments. Rather low concentrations of OH^- in fluoroborate may suffice for isotope exchange in an MSBR since a

huge volume of coolant is available to sequester the relatively small quantities of tritium (see Fig. 4-4).

ORNL DWG. 71-4557

Reactor:

1000 Mw(e) – 2250 Mw(th)

$LiF - BeF_2 - ThF_4 - UF_4$ 72 – 16 – 12 – .232 mole %

99.995% ^{7}Li

Salt Replacement Life – 9.4 years

Distribution:

	$^{6}Li(n,\alpha)T$	710 Ci/day
$^{9}Be(n,\alpha)$	$^{6}Li(n,\alpha)T$	500
	$^{7}Li(n,\alpha n)T$	1170
	$^{19}F(n,^{17}O)T$	9
	Fission	31
		2420 Ci/day

2420 Ci = 0.0837 g-atoms = 0.252 g

Fig. 4-1. DISTRIBUTION AND DIMENSIONS OF MSBR TRITIUM PRODUCTION.

ORNL DWG. 71-3457

Standard Free Energies of Formation of Hydrogenous Compounds

	$\Delta G^f_{700(800°F)}$	$\Delta G^f_{1000(1341°F)}$
$LiH(\ell)$	−6.7	−2.9
$CaH_2(\alpha)$	−20.2	−10.8
$CH_4(g)$	−3.0	4.6
$NH_3(g)$	6.5	14.9
$H_2O(g)$	−49.9	−46.0
$HF(g)$	−65.9	−66.2

Fig. 4-2. FREE ENERGIES OF FORMATION (IN KCAL/MOLE) OF SOME HYDROGEN COMPOUNDS

ORNL-DWG 70-6766R

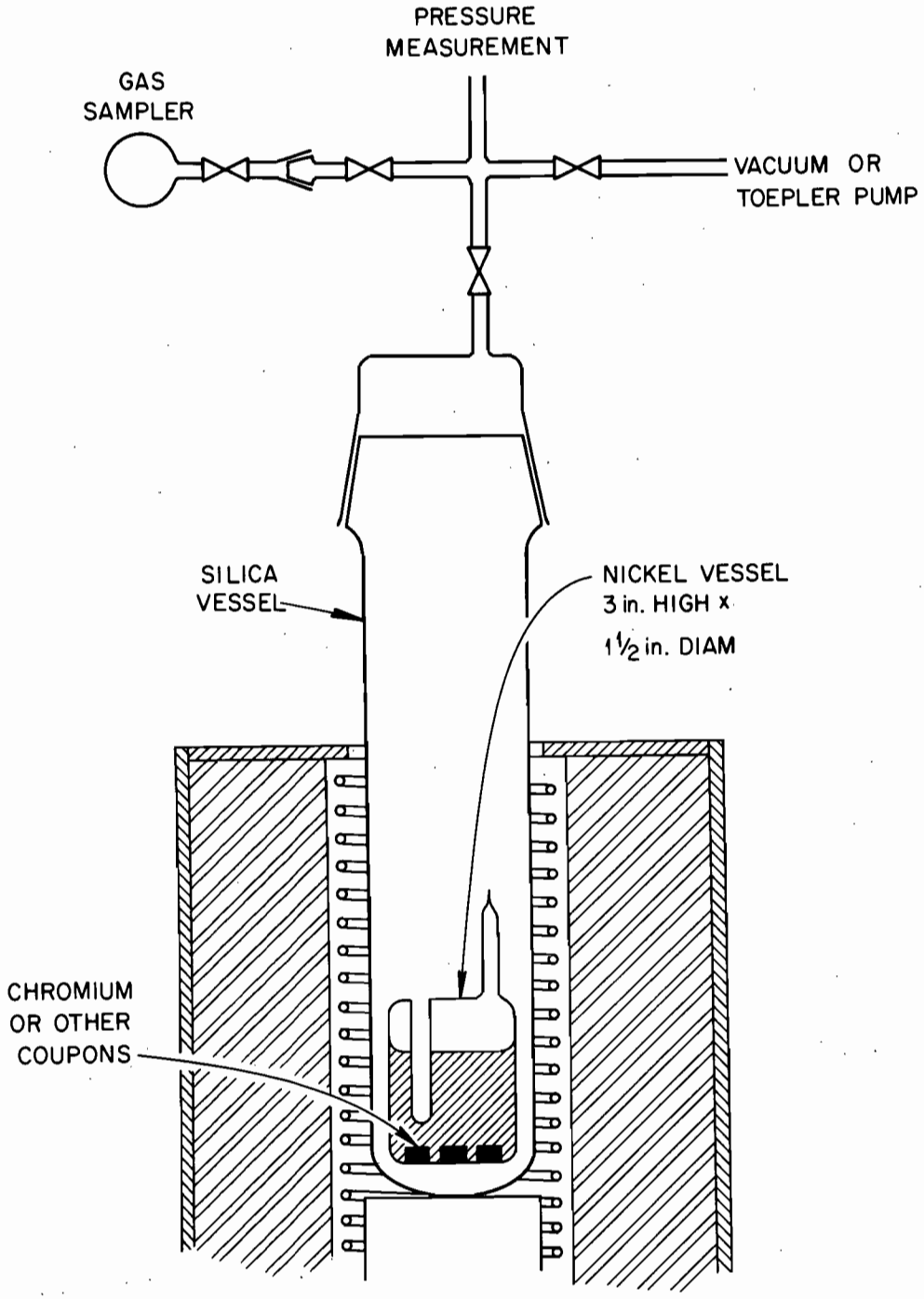

Fig. 4-3. APPARATUS FOR STUDYING HYDROGEN EVOLUTION AND TRITIUM EXCHANGE IN FLUOROBORATES.

ORNL-DWG 71-3499

$$HT\,(g) + OH^-(d) \rightleftharpoons H_2\,(g) + OT^-(d) \qquad K_{eq} = 1$$

$$\therefore \quad \frac{P_{HT}}{P_{H_2}} = \frac{OT^-}{OH^-}$$

ASSUME 1 ppm OH^- IN 4.44×10^8 g OF COOLANT

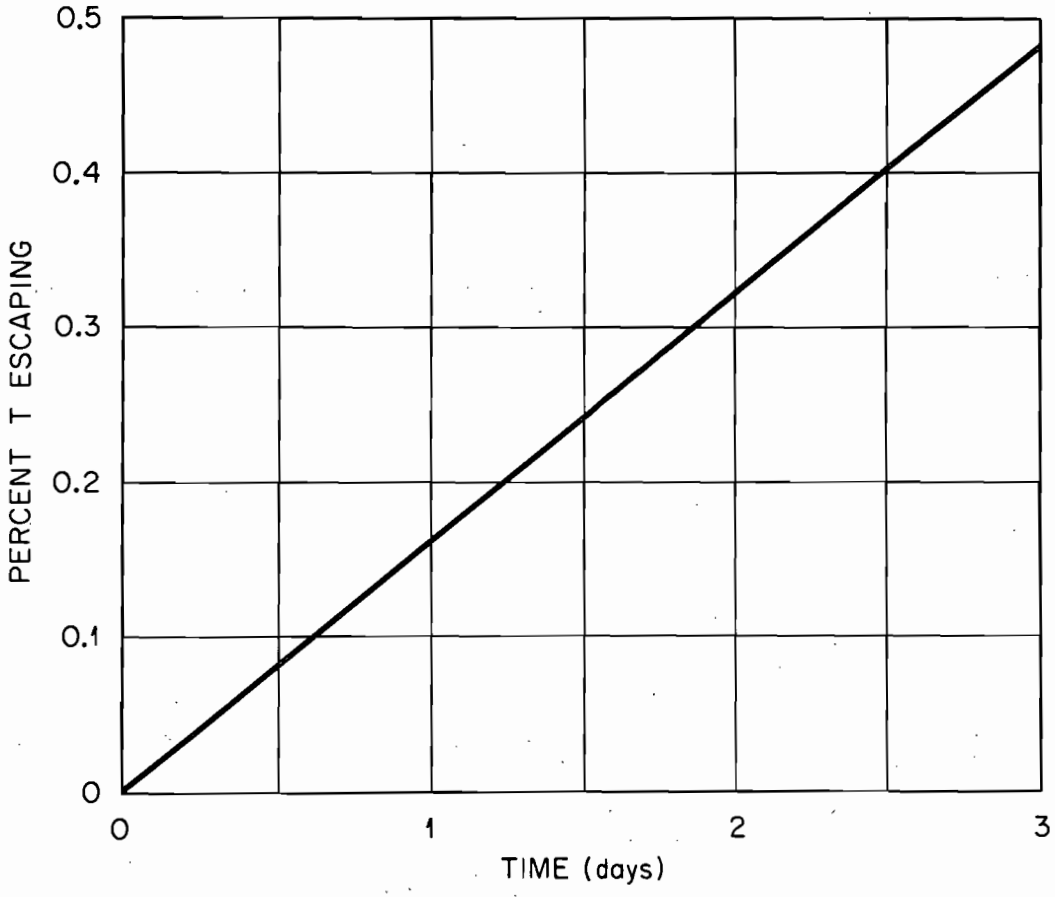

Fig. 4-4. CAPACITY OF THE COOLANT FOR TRAPPING TRITIUM IN AN MSBR.

The graph illustrates how much tritium would be retained under equilibrium conditions, if at time zero the coolant contained 1 ppm hydroxide ion. For higher concentrations of hydroxide, the slope of the line is less.

5. Chemical Processing Development for Molten-Salt Breeder Reactors

L. M. Ferris

An improved method for removing protactinium from the fuel salt of an MSBR was developed in which the protactinium is held for decay in a secondary salt that is physically and chemically isolated from the reactor. A processing flowsheet (Fig. 5-1) based on this development and the metal transfer process for rare earth removal has been adopted. A method for combining and fluorinating the various waste streams from the flowsheet was developed (Fig. 5-2) which will eliminate several potential routes for loss of fissile material from the system.

Data on the extraction of uranium from molten salt by countercurrent contact with bismuth containing reductant in a packed column were correlated by an HTU model based on the assumption that the uranium transfer rate was controlled entirely by the diffusive resistance in the salt phase (Fig. 5-3). Flooding data obtained during countercurrent flow of the salt and bismuth in a packed column are in good agreement with predictions based on studies with a mercury-water system (Fig. 5-4).

The second engineering experiment on the metal transfer process for the removal of rare earths was completed (Fig. 5-5 through 5-9). More than 85% of the lanthanum and more than 50% of the neodymium originally in the fuel carrier salt were removed and deposited in a lithium-bismuth solution with no measurable accumulation of thorium. The thorium-lanthanum decontamination factor was greater than 10^5 which demonstrates that the rare earths can be removed without significant removal of thorium. The third engineering experiment for development of the metal transfer process was designed (Fig. 5-10). The experiment uses flow rates that are 1% of the estimated flow rates for a 1000-MW(e) reactor. Mechanical agitators will be used to promote efficient contacting of the salt and metal phases.

Experiments with a simulated continuous fluorinator (Fig. 5-11) have demonstrated that radio-frequency induction heating can be used to simulate heat generation in molten salt resulting from decay of fission products in a continuous fluorinator having frozen wall corrosion protection.

Oxide precipitation is being considered as an alternative to the fluorination-reductive extraction method for isolating protactinium and for subsequently removing uranium from the fuel salt of an MSBR. The solubility of Pa_2O_5 was measured at various temperatures in MSBR fuel salt that was saturated with ThO_2 (Fig. 5-12). The results, which are in general agreement with previous data obtained with a UF_4 concentration in the salt of 0.0022 mole fraction, show that the solubility of Pa_2O_5 at 550°C and ThO_2 saturation is quite low (less than 0.01 wt ppm). The solubility product for Pa_2O_5 appears to be much lower than that for UO_2; hence, Pa_2O_5 can be precipitated in preference to UO_2. An engineering experiment to study the precipitation of uranium oxide from MSBR fuel salt from which the protactinium has been previously removed was designed (Fig. 5-13). Uranium oxide will be precipitated from 2 liters of fuel salt in a single-stage batch operation by contacting the salt with an argon-steam mixture.

ORNL DWG 70-2811R1

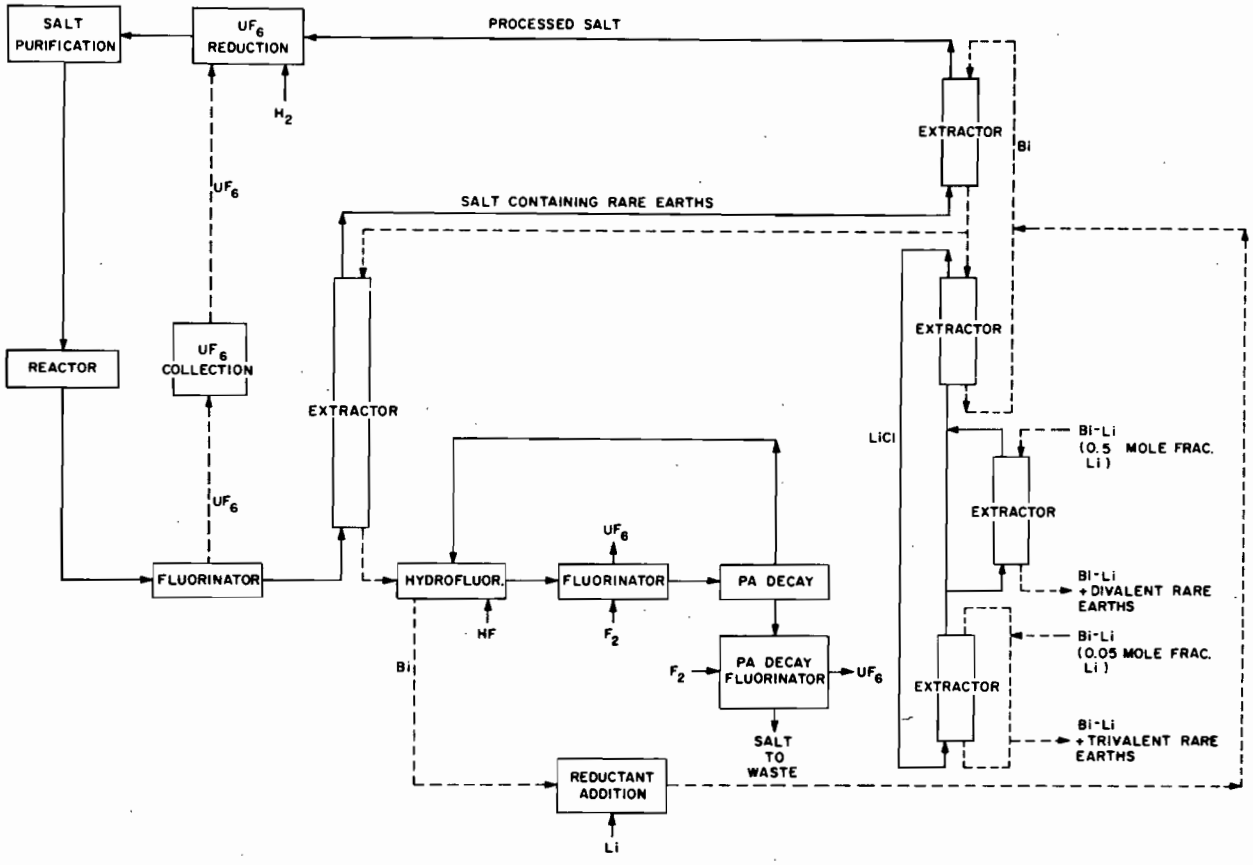

Fig. 5-1. This figure shows the flowsheet for processing a single-fluid MSBR by fluorination-reductive extraction and the metal transfer process. About 99% of the uranium is removed from the fuel salt leaving the reactor by fluorination. The protactinium and remaining uranium are then extracted into a bismuth stream containing reductant. The extracted materials are transferred to a seconary salt by hydrofluorination of the bismuth in the presence of the salt. The secondary salt flows to a fluorinator where uranium is removed and through a tank where most of the protactinium is held. Lithium is added to the recovered bismuth and the solution is returned to the top of the protactinium extraction column. Rare earths are removed from the salt leaving the extraction column by the metal transfer process.

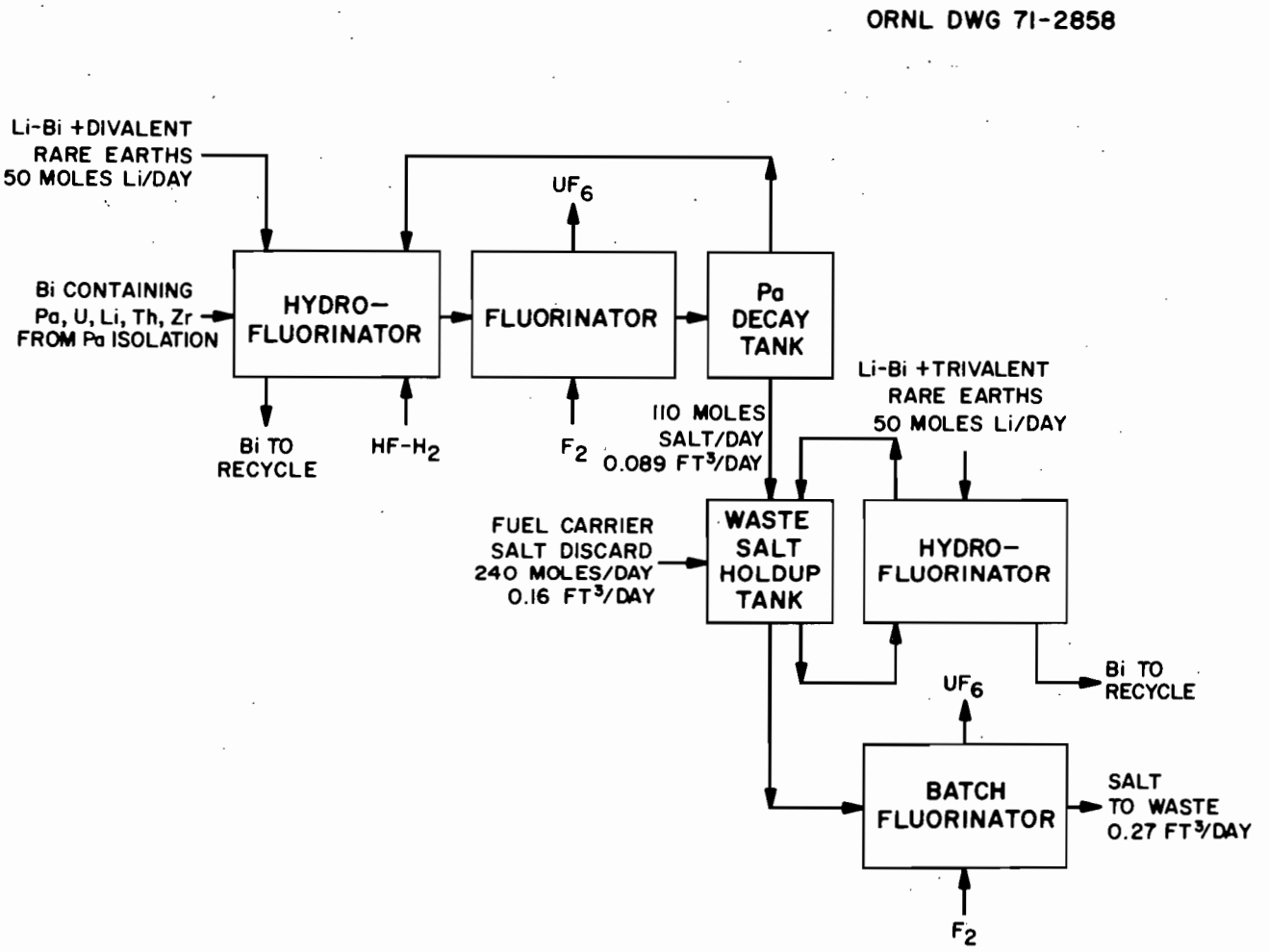

Fig. 5-2. This figure shows a method for combining and fluorinating the various waste streams from the metal transfer process and the protactinium isolation system. This eliminates several potential routes for loss of fissile materials from the system. The flow rates shown are for an assumed uranium removal efficiency in the primary fluorinator of 99%.

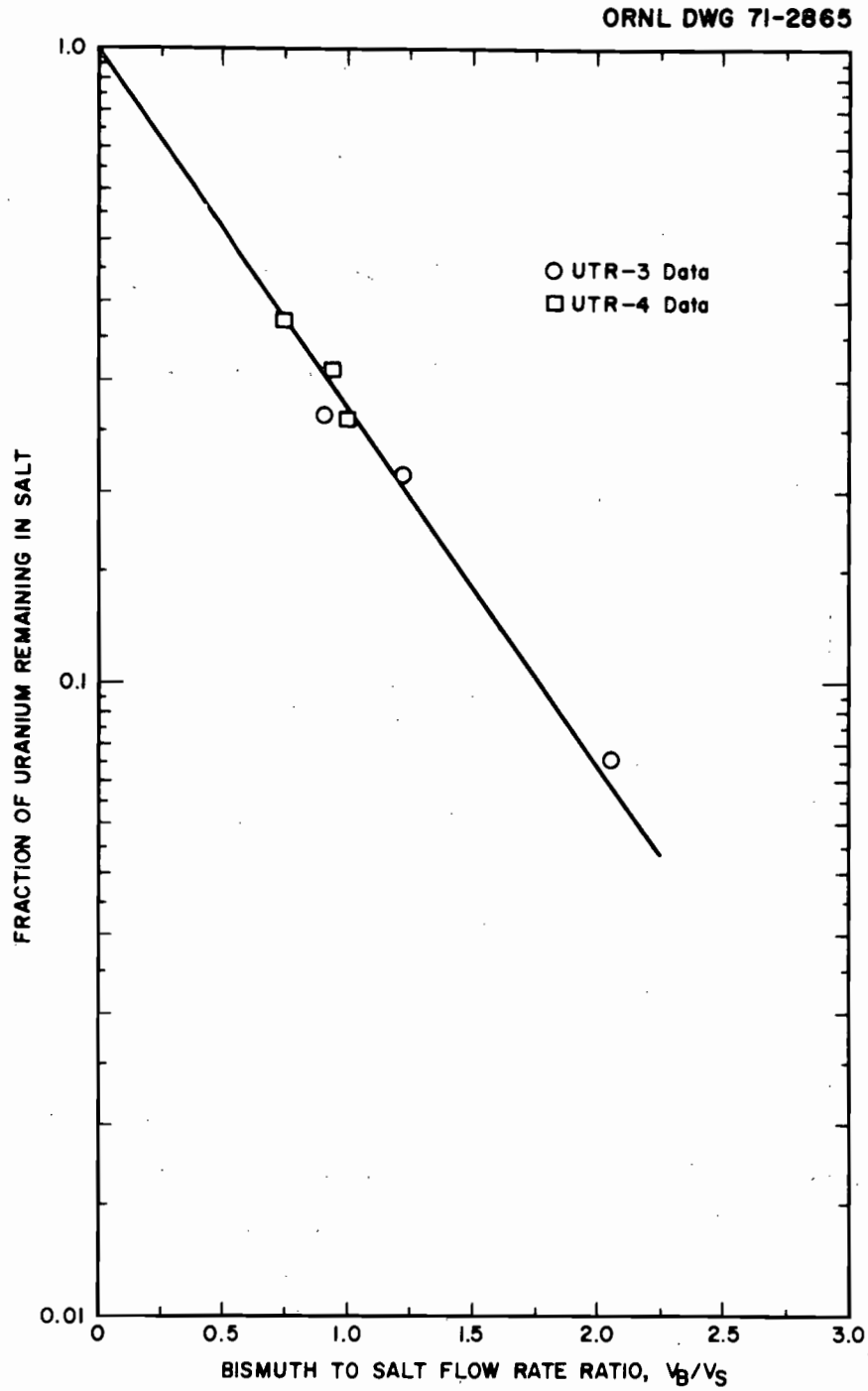

Fig. 5-3. This figure shows data on the extraction of uranium from molten $LiF-BeF_2-ThF_4$ (72-16-12 mole %) to bismuth containing reductant at 600°C in a 0.82-in.-diam, 24-in.-long column packed with 1/4-in. Raschig rings. The data are consistent with an HTU model based on the assumption that the uranium transfer rate is controlled entirely by the diffusive resistance in the salt phase.

ORNL DWG 71-2840R1

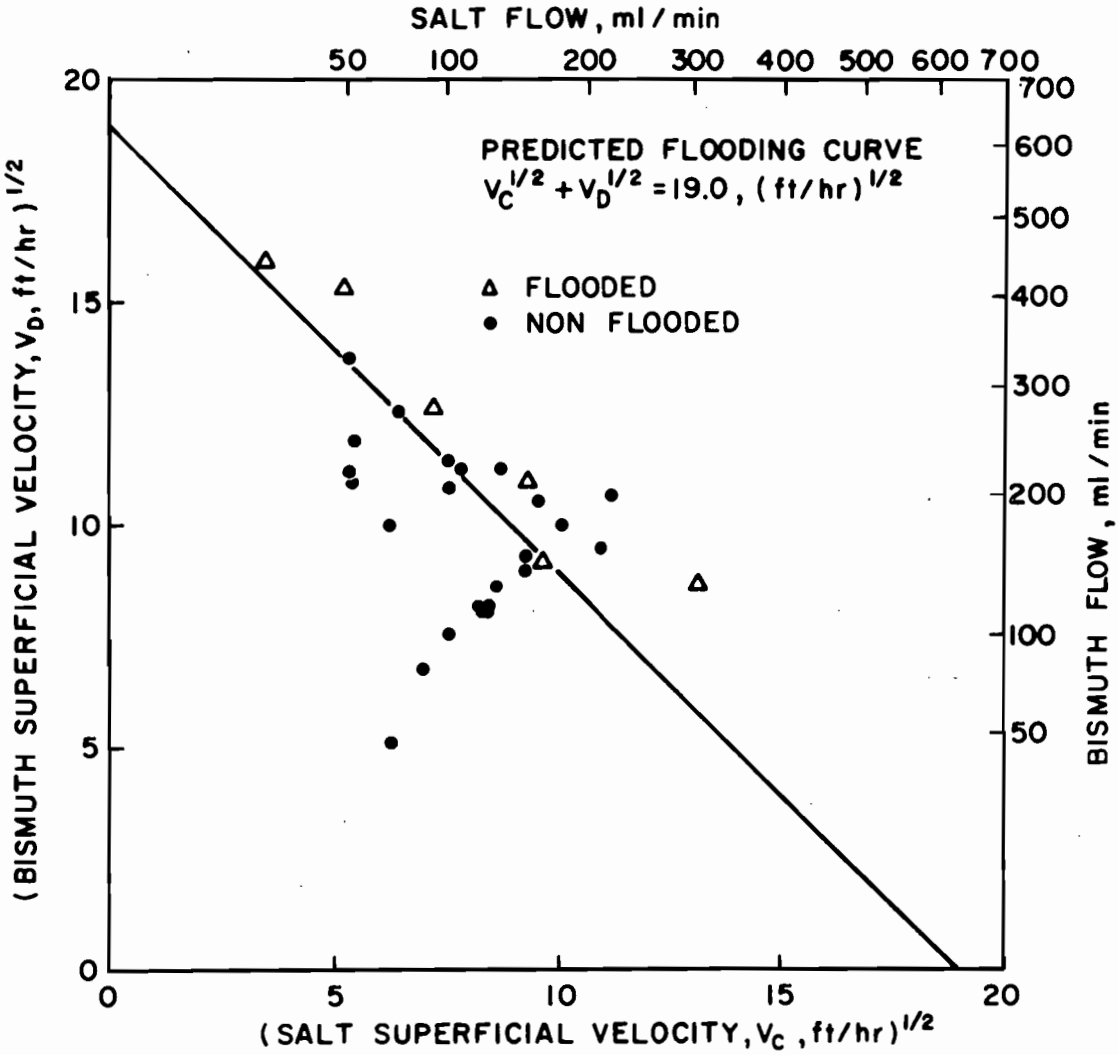

Fig. 5-4. This figure summarizes flooding data obtained during countercurrent flow of molten salt and bismuth in a 0.82-in.-diam, 24-in.-long column packed with 1/4-in. Raschig rings. The data are in good agreement with the predicted flooding line which is based on measurements during countercurrent flow of mercury and aqueous solutions in packed columns.

ORNL DWG 70-12503-R1

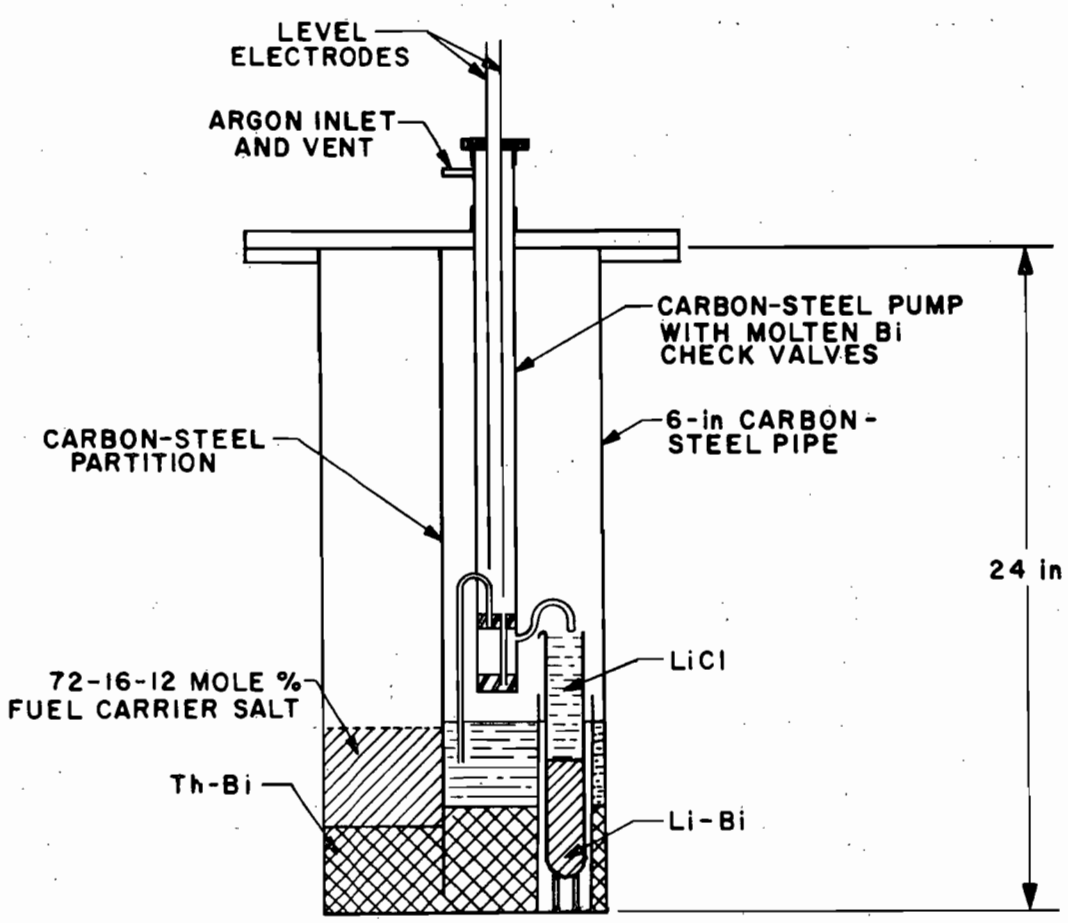

Fig. 5-5. This figure shows the carbon steel vessel used in metal transfer experiment MTE-2. The vessel had two compartments that were interconnected at the bottom by a pool of bismuth saturated with thorium. One compartment contained fluoride salt (71.7-16-12-0.3 mole % $LiF-BeF_2-ThF_4-LaF_3$) to which 7 mCi of ^{147}Nd had been added. The other compartment contained lithium chloride as well as a cup containing a 35 at. % lithium-bismuth solution. During operation lithium chloride was circulated through the lithium-bismuth cup at the rate of about 25 cm^3/min.

ORNL DWG 71-2926

MATERIALS USED IN METAL TRANSFER EXPERIMENT MTE-2

	VOLUME (cm^3)	MOLES (g)
FLUORIDE SALT ($LiF-BeF_2-ThF_4-LaF_3$, 72-15.7-12-0.3 mole %; 7 mCi $^{147}NdF_3$)	789	40.7
BISMUTH SATURATED WITH THORIUM	799	36.9
LiCl	1,042	36.6
Li-Bi (35 at. % LITHIUM)	164	9.5

Fig. 5-6. This figure shows the quantities of materials used in metal transfer experiment MTE-2.

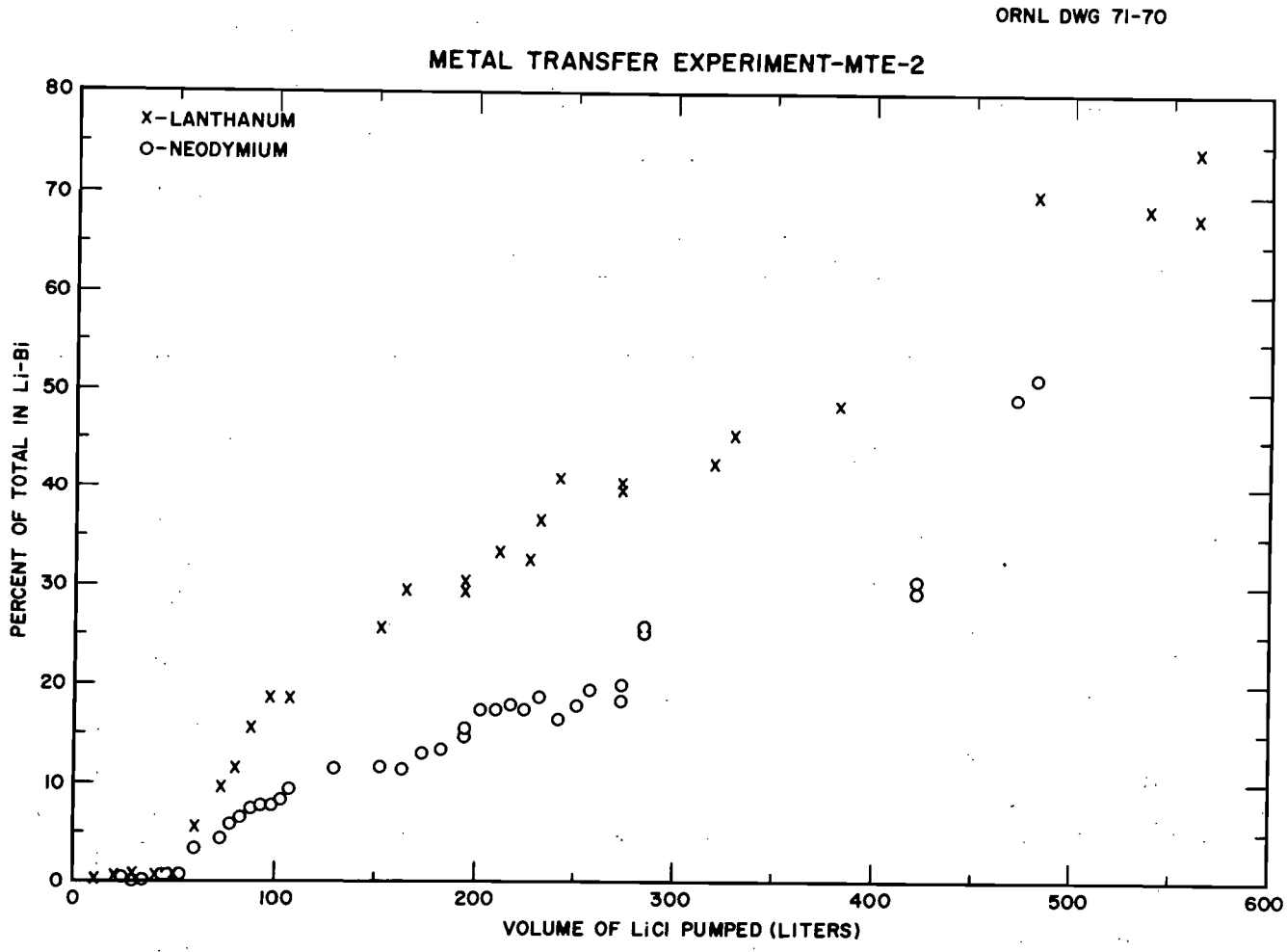

Fig. 5-7. This figure shows the rate of accumulation of lanthanum and neodymium in the lithium-bismuth solution during experiment MTE-2. There was essentially no accumulation until operation of a gas-lift sparge tube in the cup was initiated after about 50 liters of lithium chloride had been circulated through the lithium-bismuth compartment. After 400 liters of lithium chloride had been circulated (about two thirds through the run), about 50% of the lanthanum and 30% of the neodymium originally in the fluoride salt was found to be in the lithium-bismuth solution. During the last third of the run, the rare earths continued to accumulate, however, the rate of accumulation could not be determined accurately because a leak developed in the lithium-bismuth cup allowing about 30% of the solution to flow into the area between the cup and the holder.

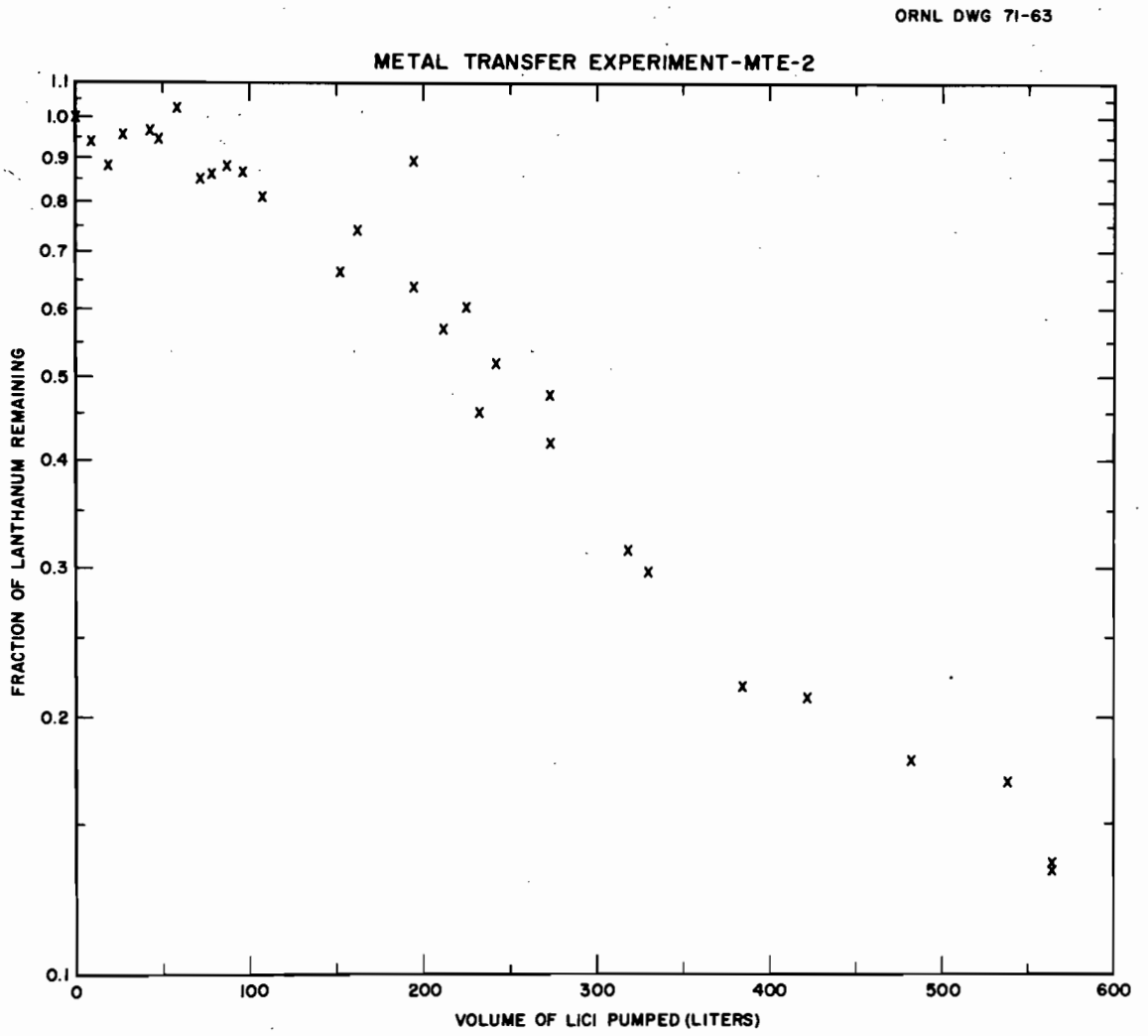

Fig. 5-8. This figure shows the rate of removal of lanthanum from the fluoride salt during metal transfer experiment MTE-2. More than 85% of the lanthanum had been removed at the end of the experiment. There was no measurable accumulation of thorium in the lithium-bismuth solution, thus demonstrating that the rare earths can be removed from MSBR fuel carrier salt without removal of significant quantities of thorium.

VARIATION OF BERYLLIUM, THORIUM, AND FLUORIDE CONCENTRATIONS IN THE LiCl AFTER ADDITION OF 1 vol % FUEL CARRIER SALT

TIME AFTER ADDITION (hr)	PUMPING TIME (hr)	FLUORIDE (wt %)	BERYLLIUM (ppm)	THORIUM (ppm)
0	0	0.98[a]	490[a]	9,480[a]
19.8	0	1.49	490	7,200
45.4	0	1.08	500	1,100
69.7	0	1.81	320	-
93	0	2.03	490	644
115.9	5.9	2.34	470	-
163.9	20.3	1.07	120	1,400
188.8	27.4	0.91	-	350
188.8	27.4	1.7[b]	135[b]	171[b]

[a] CALCULATED VALUES BASED ON THE AMOUNT OF FLUORIDE SALT ADDED.

[b] SALT TAKEN FROM VESSEL AFTER EXPERIMENT WAS CONCLUDED.

Fig. 5-9. This figure shows the variation of beryllium, thorium, and fluoride concentration in the lithium chloride in experiment MTE-2 after the simulated entrainment of 1 vol % of fuel carrier salt into the lithium chloride. During the 93-hr period in which the lithium chloride was not circulated through the lithium-bismuth container, the beryllium concentration remained constant at the initial value of 490 ppm, and the thorium concentration decreased as expected from the initial value of 9480 ppm to a value of 644 ppm because of transfer of thorium into the thorium-bismuth solution. When circulation of the lithium chloride was resumed, the beryllium concentration began to decrease, probably because of reduction of the Be^{2+} by the lithium-bismuth solution. After 27 hr of LiCl circulation, a beryllium concentration of 135 ppm and a thorium concentration of 171 ppm were observed.

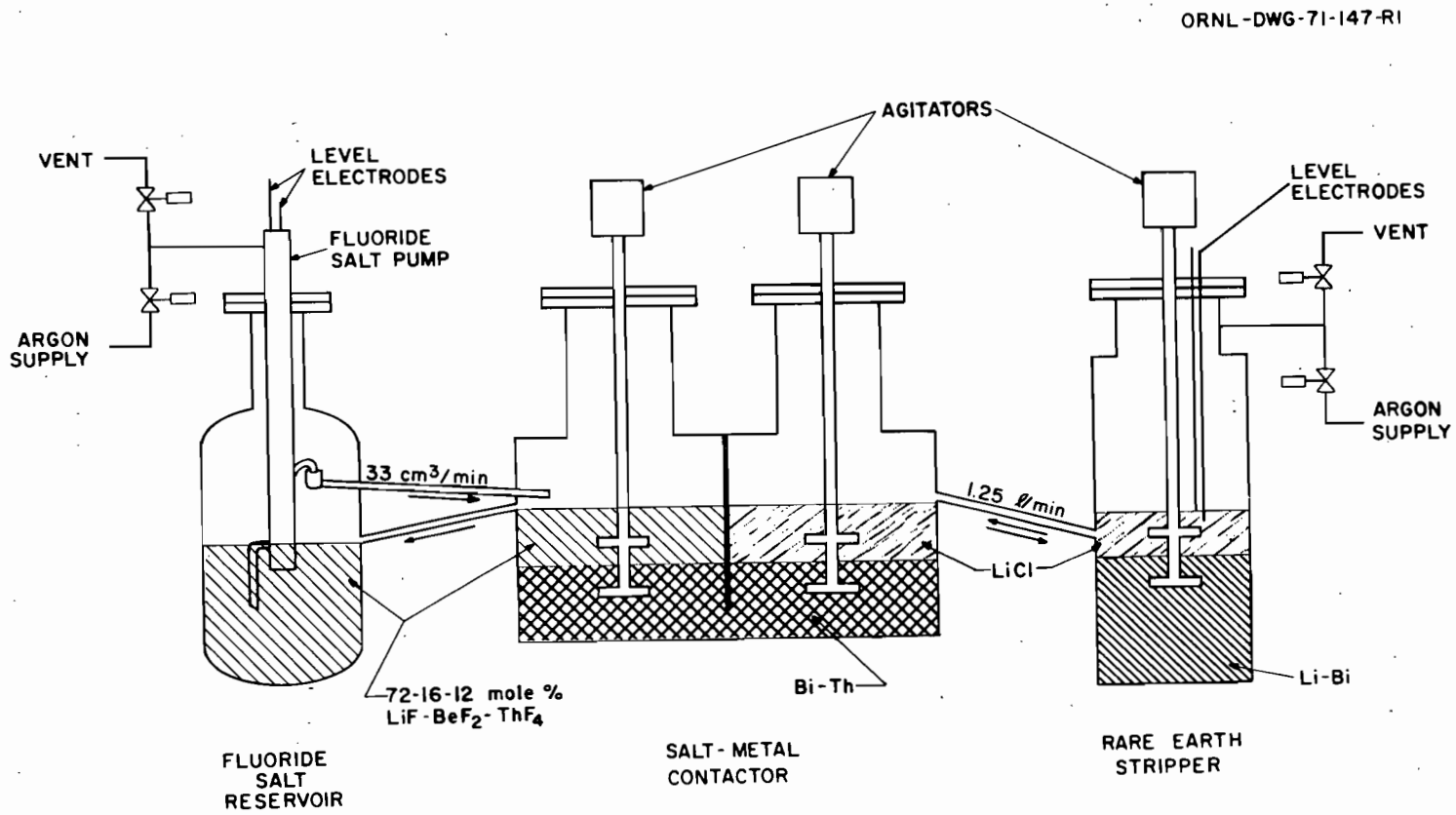

Fig. 5-10. This figure is a schematic representation of the third engineering experiment for development of the metal transfer process. The experiment will use flow rates that are 1% of the estimated flow rates for a 1000-MW(e) reactor. Mechanical agitators will be used to promote efficient contacting of the salt and metal phases.

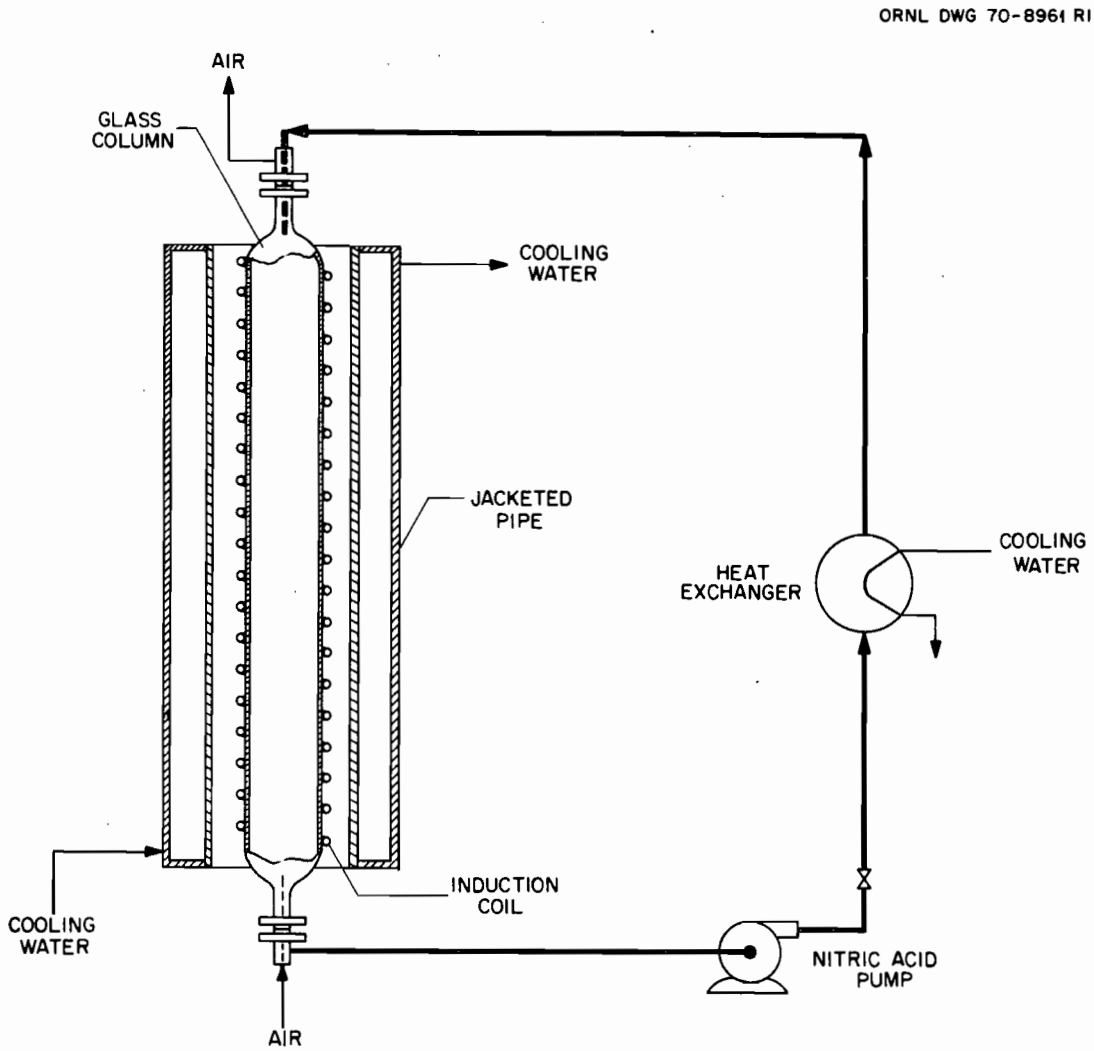

Fig. 5-11. This figure shows a simulated continuous fluorinator used for studies of radio-frequency induction heating. Measurements were made of heat generation rates in a column of nitric acid (used as a stand-in for molten salt), in the pipe surrounding the acid column (representing the fluorinator wall), and in induction coils of several designs. Air was bubbled through the nitric acid, resulting in bubble fractions as high as 18%, to determine the effect of bubbles on the heat generation rate in the acid. Efficiencies predicted for heating molten salt in a fluorinator ranged from 37% with no bubbles to 33% with a bubble fraction of 15%. These efficiencies are sufficiently high to allow operation of a continuous fluorinator having frozen-wall corrosion protection.

ORNL-DWG-71-2920

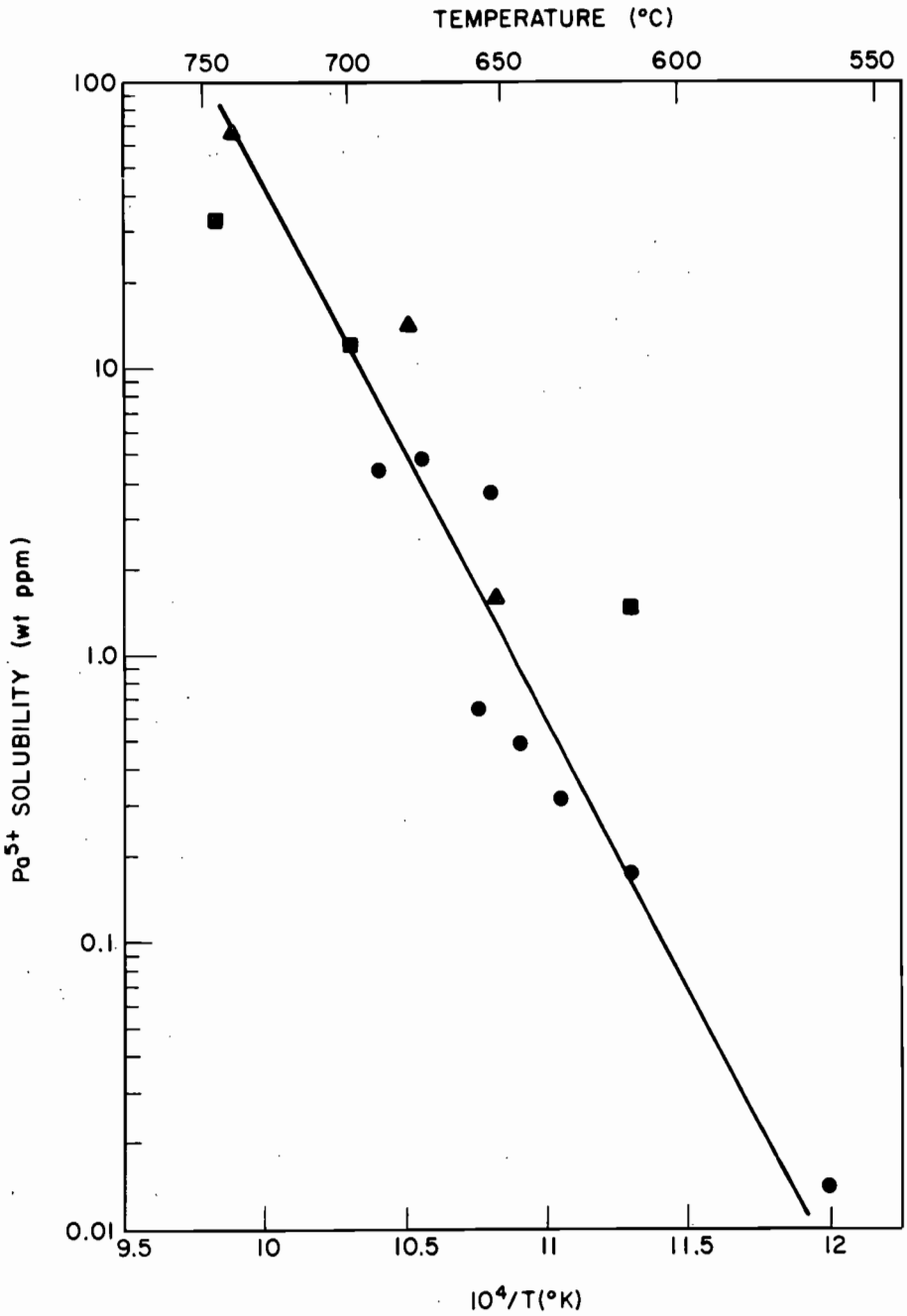

Fig. 5-12. This figure shows measured values of the solubility of Pa_2O_5 at various temperatures in MSBR fuel salt that was saturated with ThO_2. The results, which are in general agreement with previous data obtained with a UF_4 concentration in the salt of 0.0022 mole fraction, show that the solubility of Pa_2O_5 at 550°C and ThO_2 saturation is quite low. The solubility product for Pa_2O_5 appears to be much lower than that for UO_2; hence, Pa_2O_5 can be precipitated in preference to UO_2.

ORNL DWG 71-2871

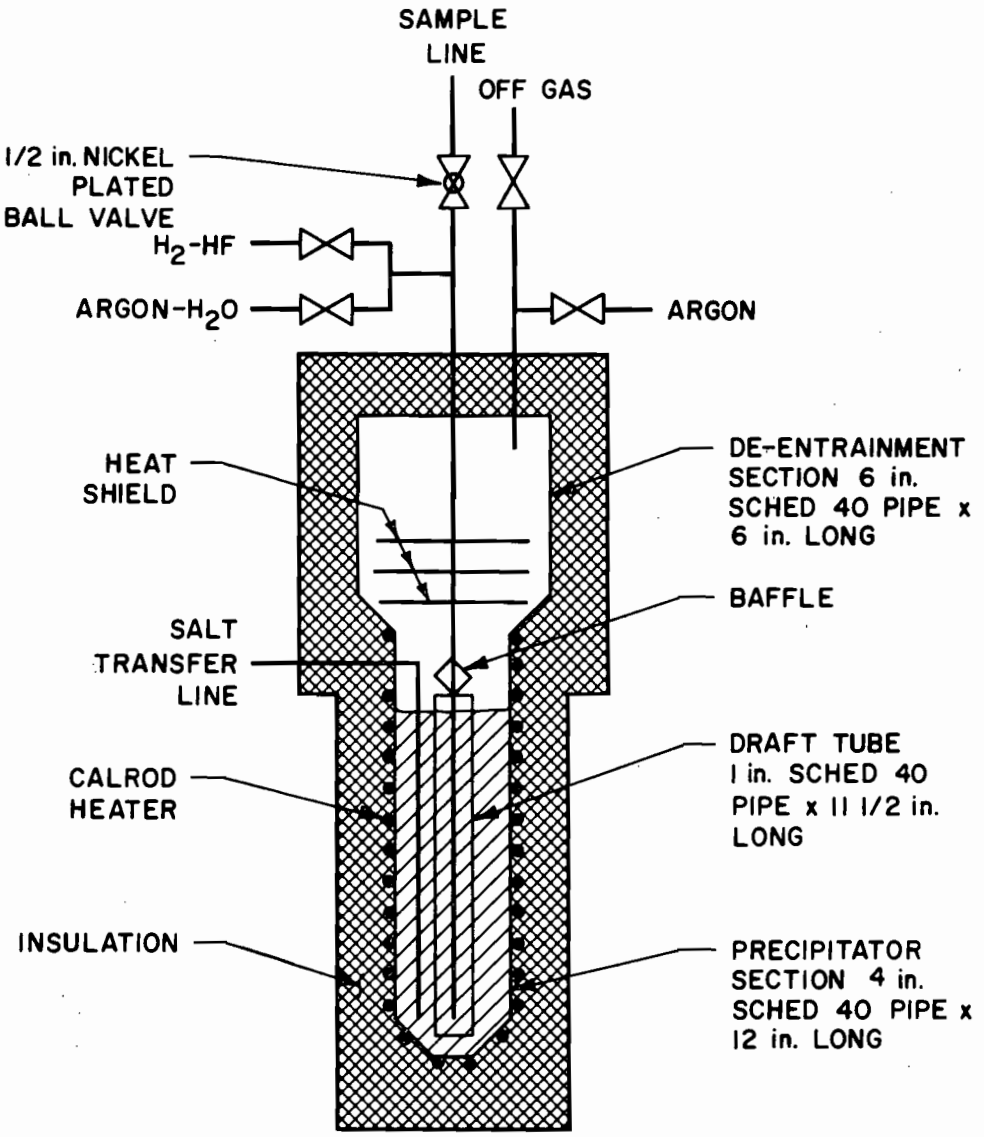

Fig. 5-13. This figure is a schematic diagram of a precipitator vessel for the first engineering experiment on uranium oxide precipitation. Uranium oxide will be precipitated from 2 liters of fuel salt in a single-stage batch operation by contacting the salt with an argon-steam mixture.

6. Development of Processing Plant Materials

J. R. DiStefano

We have continued to concentrate our efforts on materials that appear promising for the containment of liquid bismuth in the range 500–700°C. On the basis of solubility and other compatibility data in both bismuth and molten fluoride salts, we are investigating molybdenum, graphite and tantalum. Our present materials program is summarized in Fig. 6-1. The program is divided into two main areas. One is the fabrication of a molybdenum test stand to be used for determining hydrodynamic data relating to the reductive-extractive process. The other area is research to study the compatibility of molybdenum, TZM, graphite, tantalum, and recently developed iron-base brazing alloys with liquid bismuth and Bi-Li solutions. Also included is the development of techniques for coating iron and nickel-base alloys with tungsten or molybdenum.

A schematic drawing of the molybdenum loop is shown in Fig. 6-2. It consists of a 5 ft long, 1 1/8 in. OD packed column through which bismuth and salt will countercurrently circulate. Two 3 7/8 in. diam head pots will feed bismuth and salt to the column and two 3 7/8 in. diam containers will serve as the end sections of the column where bismuth and salt will be separated.

We are using a back-extrusion technique to fabricate the 3 7/8 in. OD closed-end containers with integral bosses for joining (Fig. 6-3). Test pieces have been back-extruded at 1300–1500°C and machined for welding studies (Fig. 6-4). The maximum inside length we have been able to back-extrude in a single step is about 4 in. under these conditions. We have back-extruded longer lengths at 1650°C, however, reaction with the steel tooling causes OD surface tears and cracks. Figure 6-5 shows the excellent internal surface produced by back extruding over a ZrO_2-coated plunger and the rough external surface. With a ZrO_2-coated liner we have now produced containers with smooth inside and outside diameter surfaces.

We have developed procedures for electron beam welding a girth joint between two of the 3 7/8 OD x 0.125 in. wall molybdenum headers (Fig. 6-6) and tube-to-header joints between 1/4, 3/8, 1/2, 7/8 and 1 1/8 in. OD tubes and the 3 7/8 in. OD headers. For field welding molybdenum we have modified a commercial orbiting-arc welding head and developed procedures for making tube-to-tube welds in 1/4, 3/8 and 1/2 in. OD tubing (Fig. 6-7).

We continued to evaluate the compatibility of several container materials and brazing alloys in pure bismuth and bismuth-lithium solutions (Fig. 6-8). In a quartz thermal convection loop test (700°C max temperature, 100°C temperature difference) three grades of graphite showed no significant attack but the more open grades contained bismuth in their pores. Four iron base filler metals (Fe-C-B) that contained 0, 15 or 25% Mo, and, in one case 5% Ge, were also tested in pure bismuth under similar conditions. No increase in the iron content of the bismuth was found, but the braze alloys picked up significant amounts of bismuth and showed surface layers that were all rich in iron (Fig. 6.9). Molybdenum and TZM have been tested in Bi–100 ppm Li and only slight attack of the fine grains along the surface of the molybdenum was noted. A number of tests that are being fabricated or in progress are shown in Fig. 6-10.

We have continued to coat stainless steels and nickel-base alloys with tungsten and molybdenum by hydrogen reduction of WF_6 and MoF_6. A number of significant accomplishments are listed in Fig. 6-11. Objects of various size and shapes, including equipment now being used in chemical processing experiments, have been coated with tungsten. We have been able to coat cylindrical shapes up to 4 1/2 in. in diam and 48 in. long with little difficulty. We are currently coating a Hastelloy N loop with tungsten for subsequent test in flowing bismuth (Fig. 6-12). Since the nickel-base alloy substrate would be readily attacked by bismuth, a severe test of the coating will be obtained.

Y-105476

CHEMICAL PROCESSING MATERIALS RESEARCH

Fabrication of Molybdenum Components by Back Extrusion

Welding of Molybdenum
- EB and TIG welding in atmosphere chamber
- TIG field welding

Brazing of Molybdenum
- Evaluation of properties of Fe-base filler alloys for brazing Mo to Mo
- Braze joint design
- Field brazing
- Molybdenum to stainless steel braze joints

Evaluation of Some Commercial Mechanical Couplings of Mo

Compatibility
- Static tests in Bi and molten salts
- Quartz loop tests: Bi and Bi + 100 ppm Li
- Mo, T-111, graphite TCL: Bi + 2.5% Li

Chemically Vapor Deposited Tungsten and Molybdenum Coatings

Fig. 6-1. Summary of Chemical Processing Materials Program.

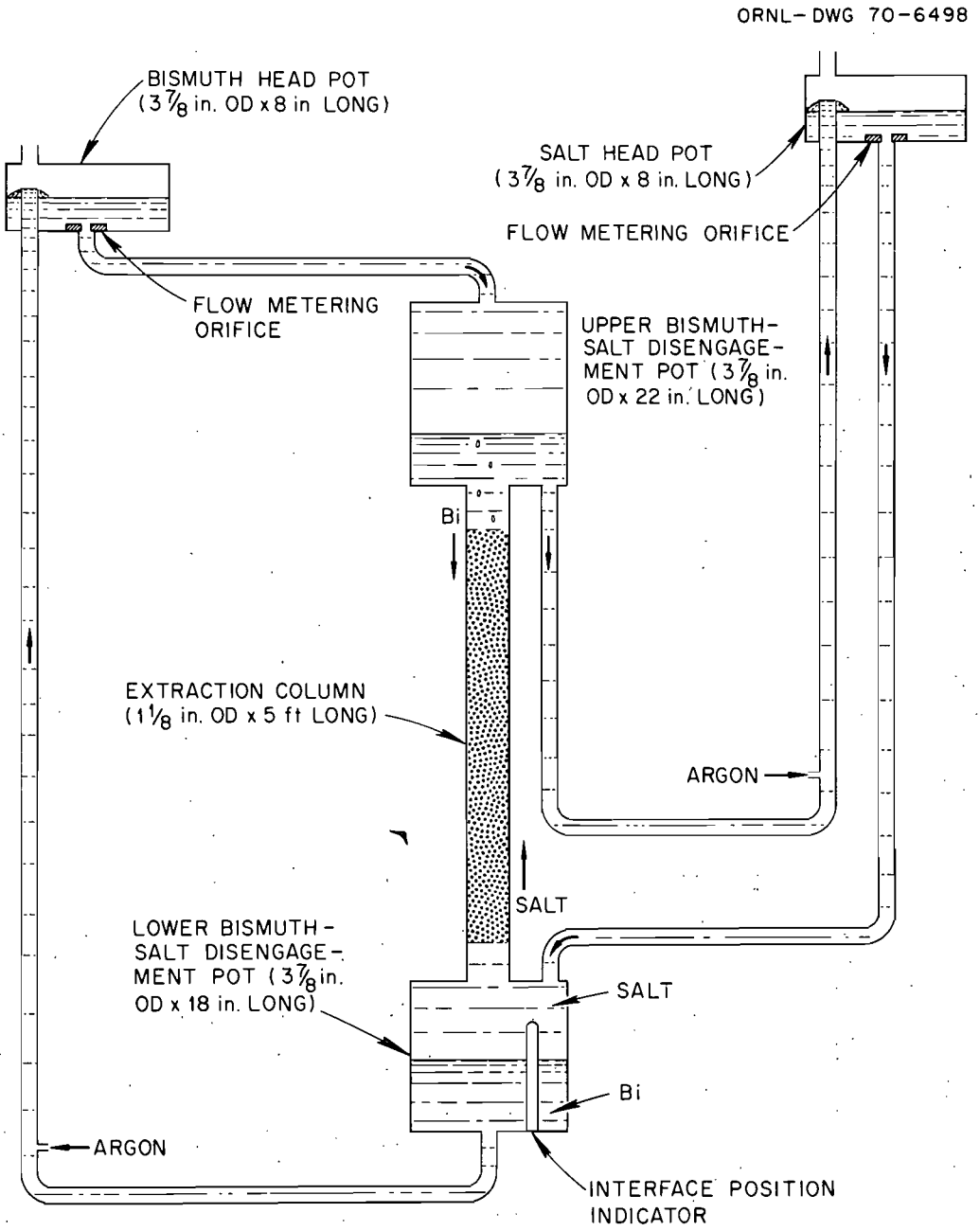

Schematic of Molybdenum Loop
for Chemical Processing Studies.

Fig. 6-2. Schematic of Molybdenum Loop for Chemical Processing Studies.

PHOTO 100969

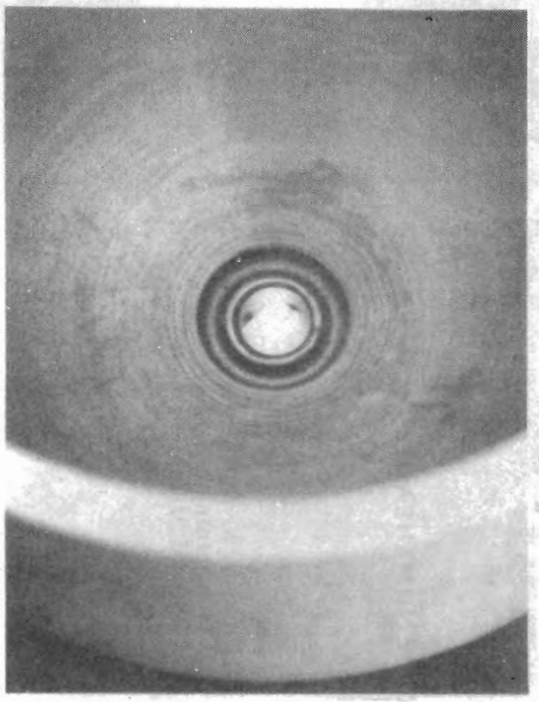

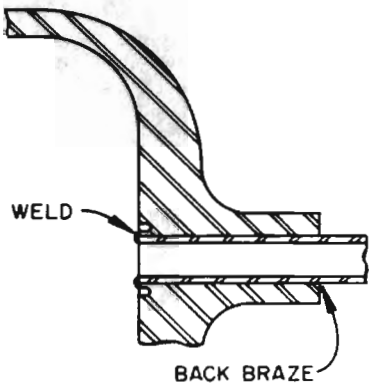

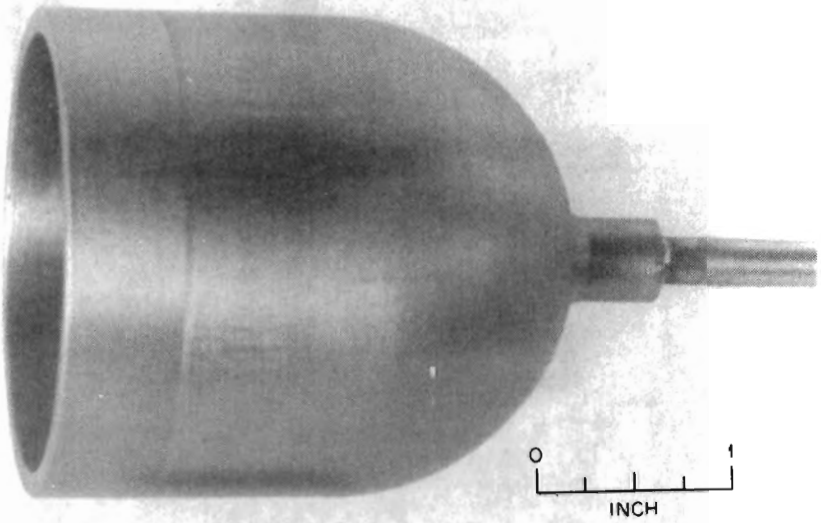

Electron-Beam Welded Back-Extruded Header.

Fig. 6-3. Back-Extruded Closed-End Container. Boss is provided to make tube-to-header joint by electron beam welding. Back-brazing provides back-up seal and further strengthens joint.

Y-103350

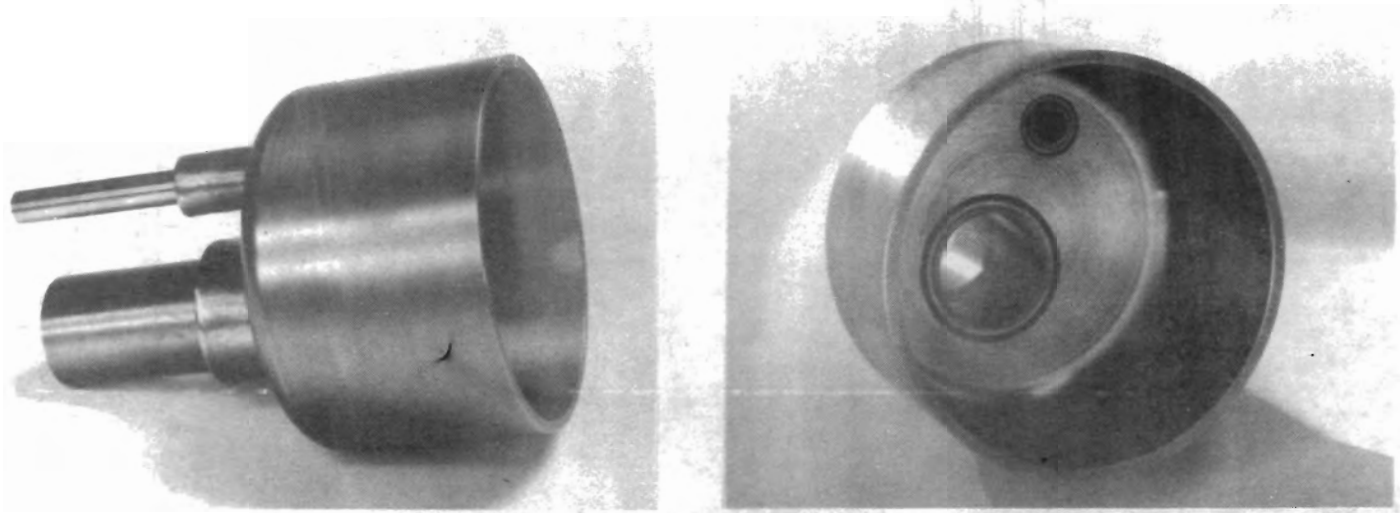

[redacted]

BACK-EXTRUDED MOLYBDENUM HEADER

Fig. 6-4. Molybdenum Back Extrusion After Machining. Tube-to-header electron beam welds have been made with 1 1/8 in. and 3/8 in. OD tubing.

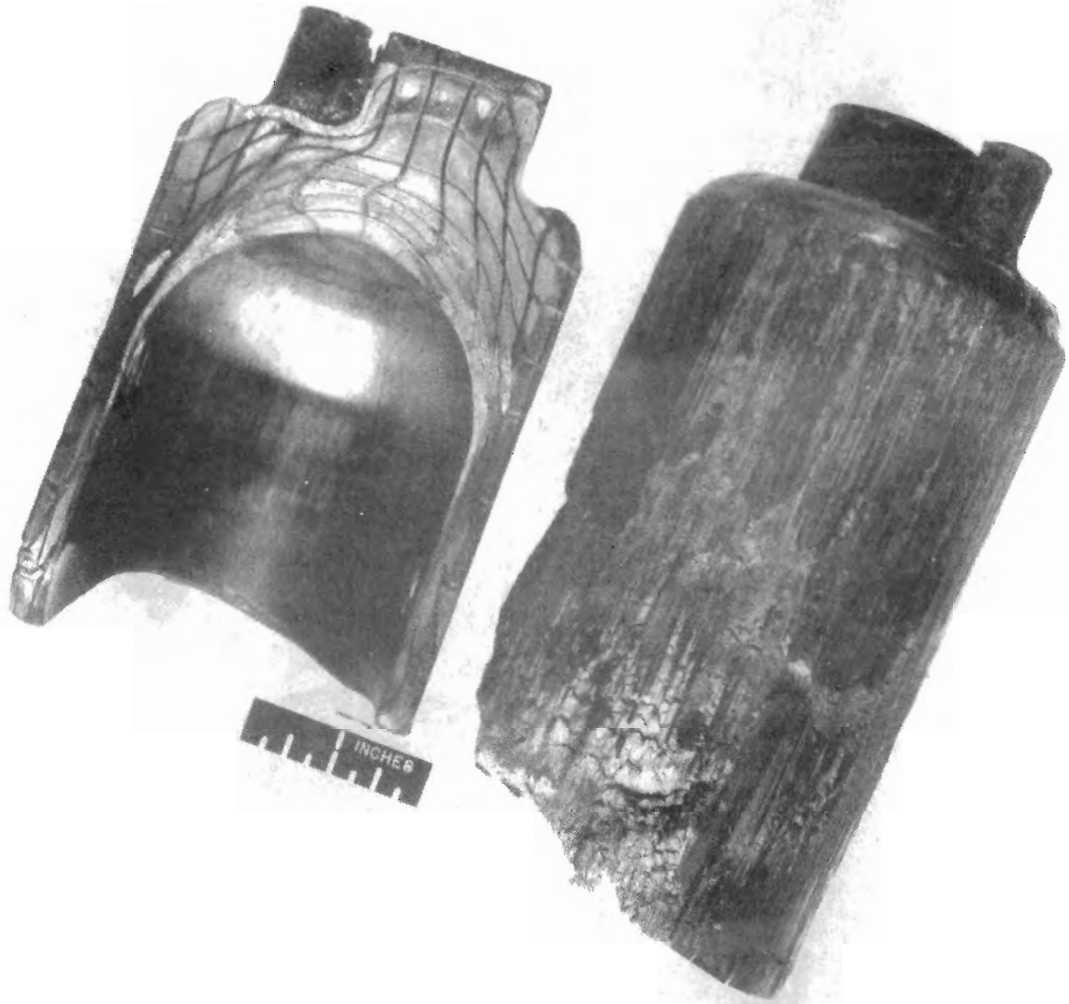

Fig. 6-5. Molybdenum Back Extrusion Illustrating Smooth Inside Surface and Rough Outside Surface. (Metal flow during extrusion indicated by wire grids on inside.)

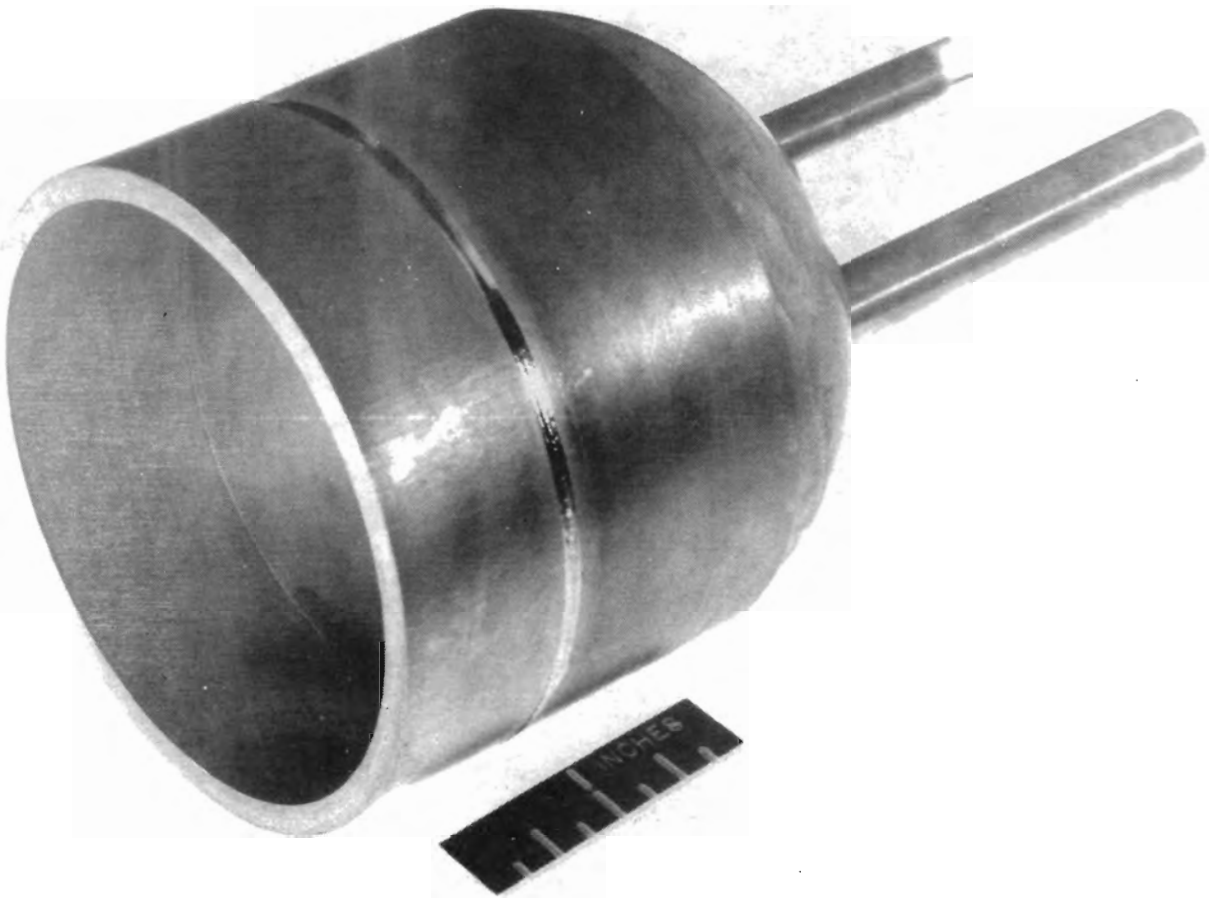

Fig. 6-6. Electron Beam Girth Weld in Molybdenum Back Extrusion.

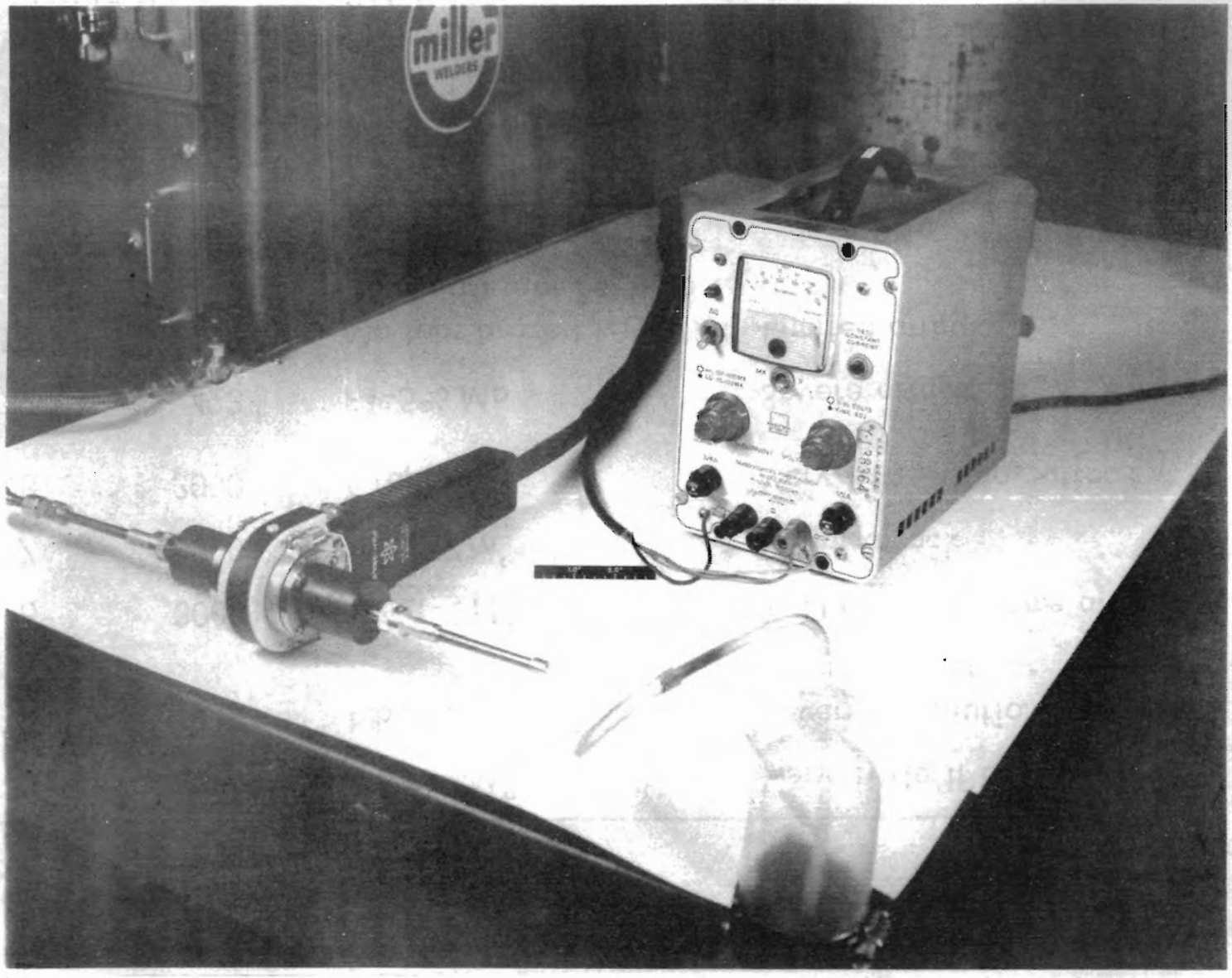

Fig. 6-7. Modified Astro Arc Welder for Field Welding Molybdenum Tubes.

QUARTZ THERMAL CONVECTION LOOP RESULTS

Loop No.	Operating Time (hr)	Samples Tested	Results
3	3024	Mo, TZM[a]	Very little if any attack
4	115	Nb, Nb-1 Zr	Severe dissolution and mass transfer
6	3000	Ta, T-111[b]	T-111 brittle, some attack
7	3000	Mo. TZM[c]	Slight attack
8	3000	Graphite	Very little if any attack
9	423[d]	Fe-5% Mo	Severe attack
10	2112	Mo tabs brazed with four different Fe-base braze alloys	Limited attack

[a]TZM: Mo-0.5% Ti-1% Zr alloy.
[b]T-111: Ta-8% W-2% Hf alloy.
[c]Bi contained 100 ppm Li.
[d]Power failure terminated test, one sample in hot leg came loose and floated to the top after 216 hr.

Fig. 6-8. Summary of Results After Exposure to Bismuth in Quartz Thermal Convection Loops.

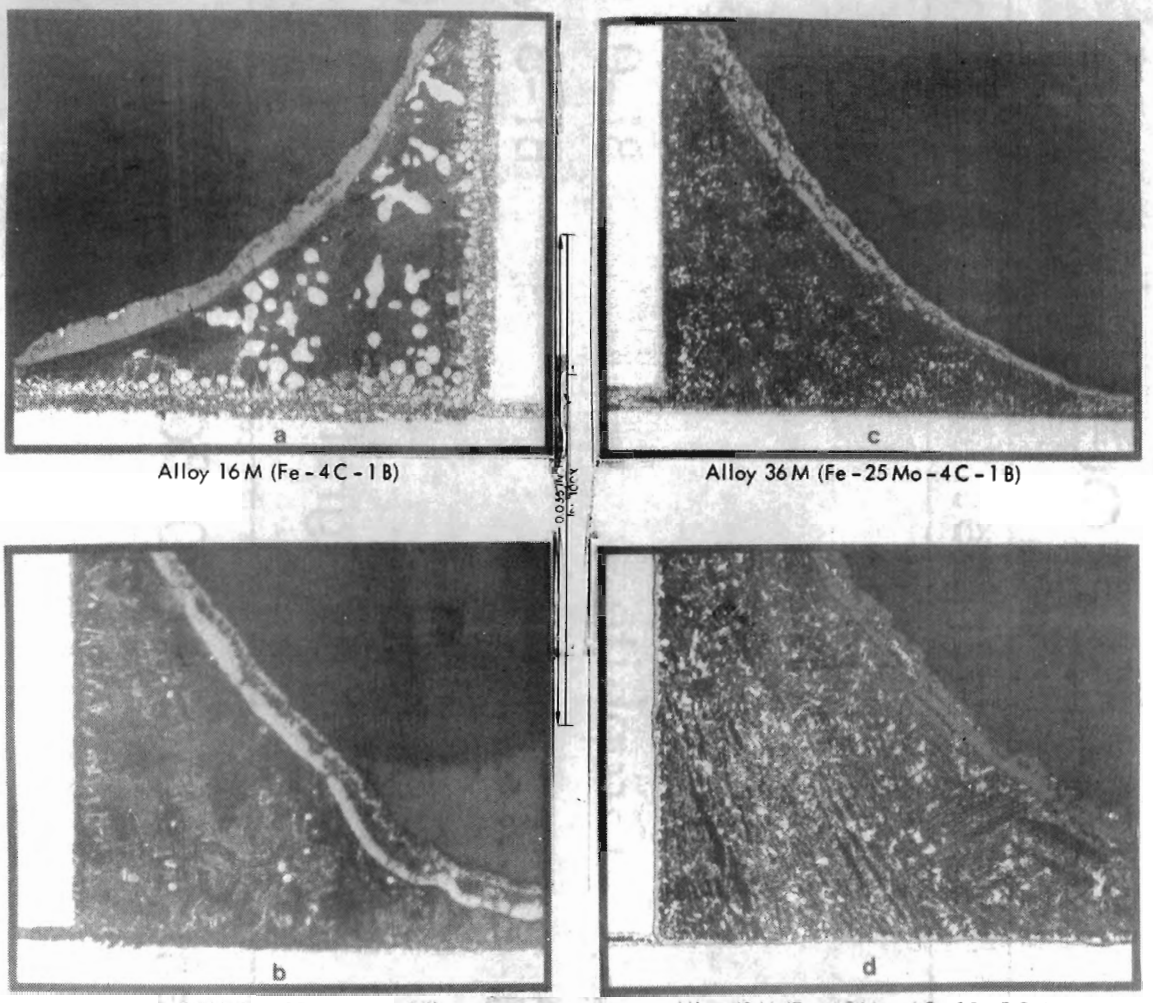

Alloy 16 M (Fe - 4 C - 1 B)

Alloy 36 M (Fe - 25 Mo - 4 C - 1 B)

Alloy 35 M (Fe - 15 Mo - 4 C - 1 B)

Alloy 42 M (Fe - 15 Mo - 4 C - 1 B - 5 Ge)

IRON-BASE BRAZE ALLOYS AFTER TESTING IN FLOWING BISMUTH AT 610-700°C

Fig. 6-9. Four Iron Base Brazing Alloys After 2000 Hr Exposure to Bismuth in Quartz Thermal Convection Loop.

Y-105623

TESTS IN PROGRESS

Test	Samples	Conditions[a]
All metal loops	Mo, T-111	Bi-2$\frac{1}{2}$ wt % Li
Graphite loops	Graphite	Bi-2$\frac{1}{2}$ wt % Li
Capsule tests	Graphite	Bi-0.5 wt % Li Bi-3 wt % Li
Quartz loops	Ta, T-111 Graphite, grafoil	Bi-100 ppm Li

[a] Maximum temperature of 700°C.

Fig. 6-10. Summary of Compatibility Tests Currently in Progress.

Y-105624

SCOPE OF COATING STUDIES

Coating: W, Mo

Application: CVD by H_2 reduction of WF_6 and MoF_6

Substrates: Fe- and Ni-base alloys

Accomplishments:

- Applied adherent W and Mo coatings to Ni-base alloys and to Fe-base alloys electroplated with Ni
- Coated Ni vessels with W and Mo for static corrosion testing of the coating in liquid bismuth
- Demonstrated that adherent W coatings can be applied to hardware of practical size and interest
  - $\frac{1}{2}$-in.-OD tubing, 5 to 10 ft long
  - $4\frac{1}{2}$-in.-OD vessels, 2 and 3 ft long

Current Work:

- Evaluating electroless Ni coatings as a substitute for electroplated Ni on Fe-base alloys
- Coating a Hastelloy N convection loop with W for testing in flowing bismuth
- Coating with W of a low carbon steel vessel for a metal transport experiment

Fig. 6-11. Summary of CVD Studies Aimed at Depositing Tungsten on Molybdenum on Iron and Nickel-Base Alloy Substrates

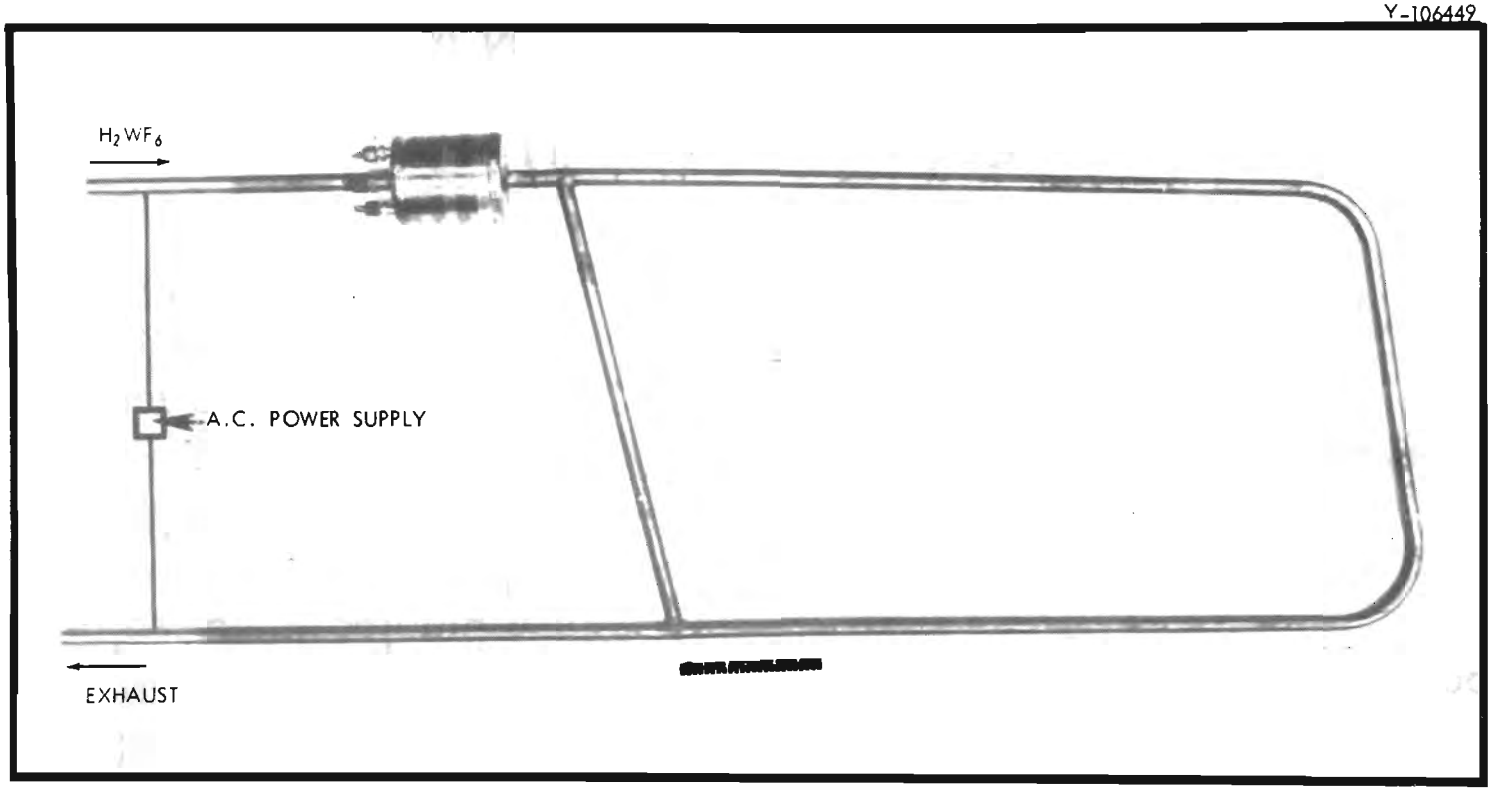

Fig. 6-12. Hastelloy N Thermal Convection Loop Coated with Tungsten for Testing with Bismuth.

7. Graphite Development

W. P. Eatherly

In recent months our attention on graphite has focused on materials based on blacks and on raw cokes. It will be recalled that black-based graphites were found to be quite sensitive to radiation damage at temperatures of 500°C and lower and appeared also to be a deleterious additive to coke-based graphites. In earlier irradiations at 715°C in HFIR, graphites with blacks as additives were found to behave as well as their counterparts without blacks, which encouraged us to look again at graphites based entirely on blacks.

A number of grades were obtained both from commercial vendors and from the graphite group in Y-12 development, and their behavior is shown in Fig. 7.1. Grades A-680 and 681 were obtained from Stackpole and differ only in that A-680 is carbonized, whereas A-681 is graphitized. Grade SA-45 is a Union Carbide product. Grades T/ITX and T/V are graphitized Thermax bonded with isotruxene and Varcum, respectively, and fabricated at Y-12.

The most interesting behavior of these materials is, first, their immediate response at low damage levels, and second, their relatively slow rate of expansion at high fluences. For comparison, the behavior of POCO grade AXF, the most damage resistant material observed to date, is shown by the dotted curve. The POCO material also shows the quadratic expansion at high fluences, which is typical of all the previously studied graphites. In contrast, the black-based materials behave in a linear fashion at high fluences.

It will be noted the entire set of black-based materials has essentially the same slopes but differ in maximum densification. This latter appears to be a function of both binder type and heat-treatment temperature. An experiment was therefore initiated by taking the A-680 material and heat treating it to various temperatures between 1000°C and 2800°C. The results are shown in Fig. 7.2, and there is indeed a continuing decrease in maximum densification as the heat-treatment temperature increases.

The data on these black-based materials is still being taken, and their analysis is obviously incomplete. However, we obviously are dealing with a new class of radiation behavior, and one which looks most promising for potential reactor application.

In our own fabrication program we have employed two types of uncalcined isotropic cokes. The first of these is an experimental material obtained from Union Carbide which is derived from air-blown asphaltines. The second is obtained from Collier Coke and derived from crudes obtained from the Santa Maria field in California. The use of raw cokes is dictated by the desire to obtain a monolithic structure; the still chemically active coke reacts with the binder to yield essentially a single-phase graphite.

The technique being used is to dry blend milled pitch and the sized coke flour, and slurry mix these with benzene to disperse the pitch. The benzene is then largely evaporated before forming, baking, and graphitizing. The resultant structures are quite good, particularly with the Santa Maria coke. Samples have recently been inserted into HFIR for irradiation testing.

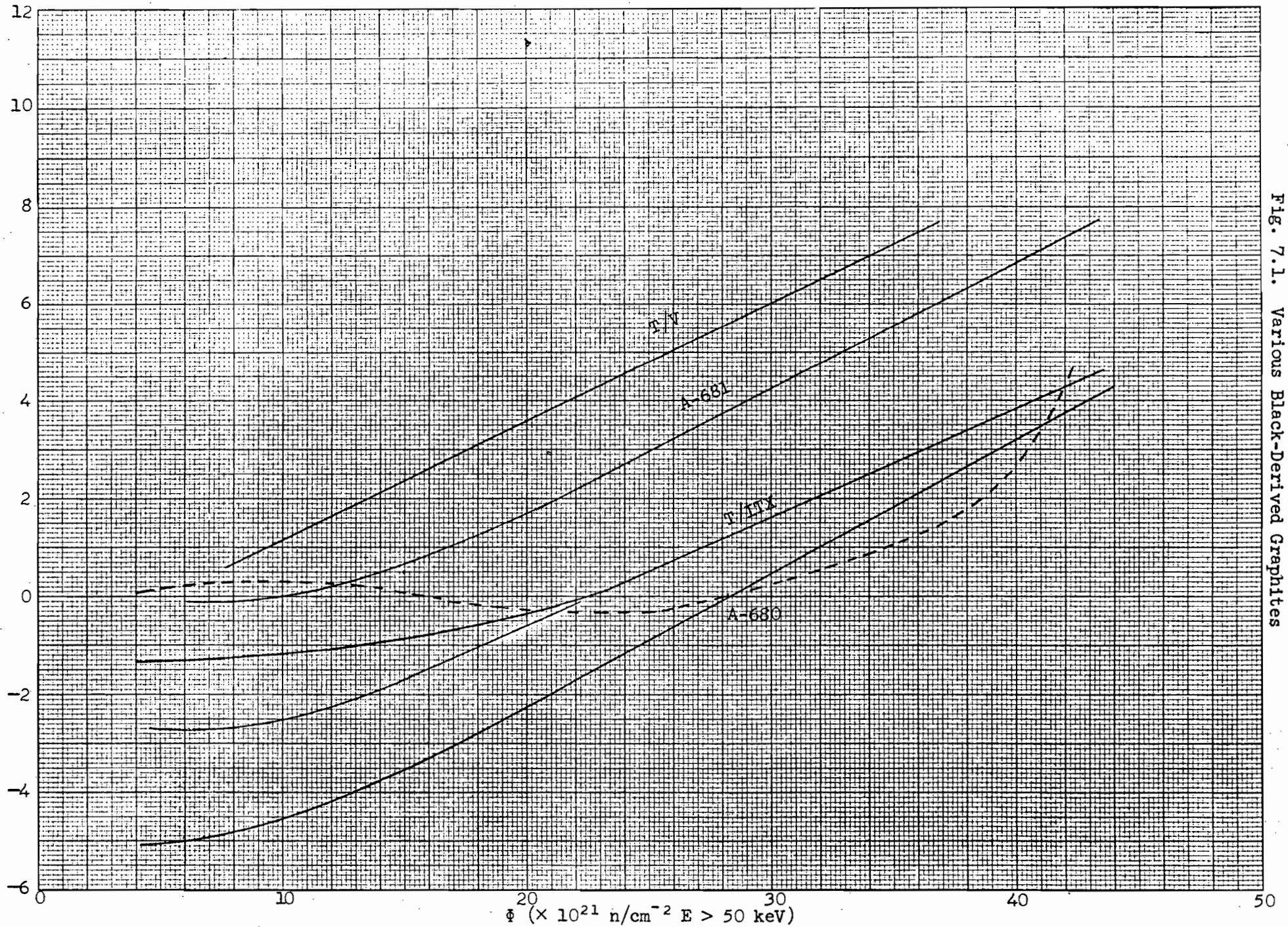

Fig. 7.1. Various Black-Derived Graphites

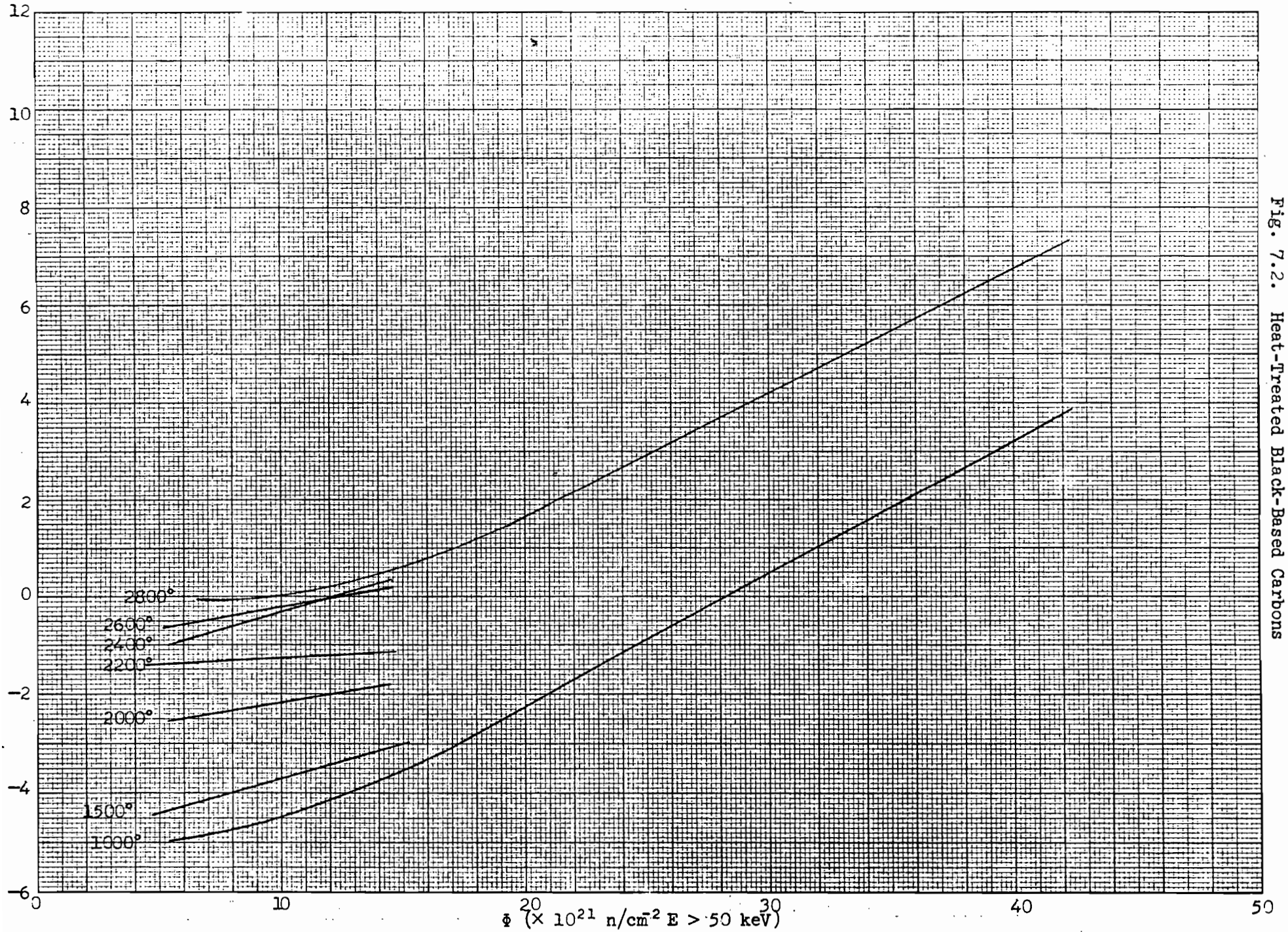

Fig. 7.2. Heat-Treated Black-Based Carbons

8. Status and Plans for the Engineering Technology Program

Dunlap Scott

Our present development program is limited to the investigation of basic technology problems of the components and systems of Molten Salt Reactors. We are preparing reviews of the state of the technology for each area, defining problems which need further study and then surveying related programs for information which might be applicable to our problems. We are using the reference design of the MSBR and the design of the Molten Salt Breeder Experiment to help define the problems and new data that are needed and to establish the scale of some experiments.

The major areas of interest are listed in Table 8-1. In the noble gas handling system we are concerned primarily with the rapid removal of Xe-135 and other noble gases from the circulating salt and then the safe removal and disposal of these gases in the off-gas system. We are preparing design bases reports for these two sub-systems which will serve to describe the tests needed to establish the designs. Tests are underway to determine the characteristics of the bubble generator and separator. After it is shown that these components perform satisfactorily in water, we will proceed with tests in salt in the Gas System Technology Facility.

In the steam generator program we are preparing a technology report on steam generators in preparation for some small tests we plan for studying the mechanisms for generating steam with molten salt. In parallel with this work we are proceeding with plans to procure conceptual designs of systems which industrial firms would propose and would later build for use in the MSBE.

Under secondary coolant technology we are modifying an existing loop which will be used for tests to help us establish the requirements for components and for their operation with sodium fluoroborate.

We are preparing a report listing the requirements for valves for MSR's and the status of the technology of high temperature valves which meet these requirements. We expect to build a throttling valve for use in the technology loops described below, however, most of the valve design and development work will be accomplished through an industrial participation program.

The Gas System Technology Facility (Fig. 8.1) will be used to test the bubble generator and separator in salt. The modifications make use of the existing spare pump and the coolant salt piping and other material salvaged from the MSRE. There are provisions for attaching equipment for heat transfer, tritium migration, and chemical process studies. The experimental program for the GSTF is given in Table 8-2. During the

operation of the MSRE, there appeared to be much interaction between the bubble dynamics and the oxidation state of the fuel salt. We plan to evaluate the performance of several of the components while operating with varying chemical states of the salt.

We have divided the steam generator program into three phases as shown in Table 8-3. Presently our plans are to complete Phase I by the end of FY-1973 and to start Phase II in FY-1974. Phase III is given here only to indicate the logical progression of the program.

The parts of the Industrial Conceptual Design Study are given in Table 8-4. In Tasks I and II we will get conceptual designs of steam generators for 1000-Mw(e) plants. After a choice is made, the designer will proceed to show how he would propose to scale this design for use with a Molten Salt Reactor of about 150 Mw(t) and will describe an R and D program for producing such a steam generator.

A schematic diagram of the Coolant Salt Technology Facility is shown in Fig. 8-2. Here we use the coolant salt pump and piping from the MSRE and much of the service equipment from the original loop. We will install a tank near the pump which will provide access to the surface of a flowing stream of salt for studying methods of monitoring the chemical state of the salt. There are nozzles to which we will attach equipment to make the studies shown in Table 8-5. We will use the loop to evaluate the importance of interactions between the corrosion rate of the loop, tritium migration, and the chemical condition of the salt.

We expect that the completion of the program described briefly here will develop much of the background for proceeding with a detailed design of an MSBE or first demonstrator plant.

ORNL DWG. 71-3456

MOLTEN SALT REACTOR TECHNOLOGY DEVELOPMENT PROGRAM

NOBLE GAS HANDLING SYSTEM
- XENON REMOVAL SYSTEM
- OFF-GAS SYSTEM

STEAM GENERATOR
- TECHNOLOGY DEVELOPMENT
- INDUSTRIAL DESIGN

SECONDARY COOLANT TECHNOLOGY

VALVES FOR SALT SERVICE

Table 8-1. This table lists the major parts of the technology development program.

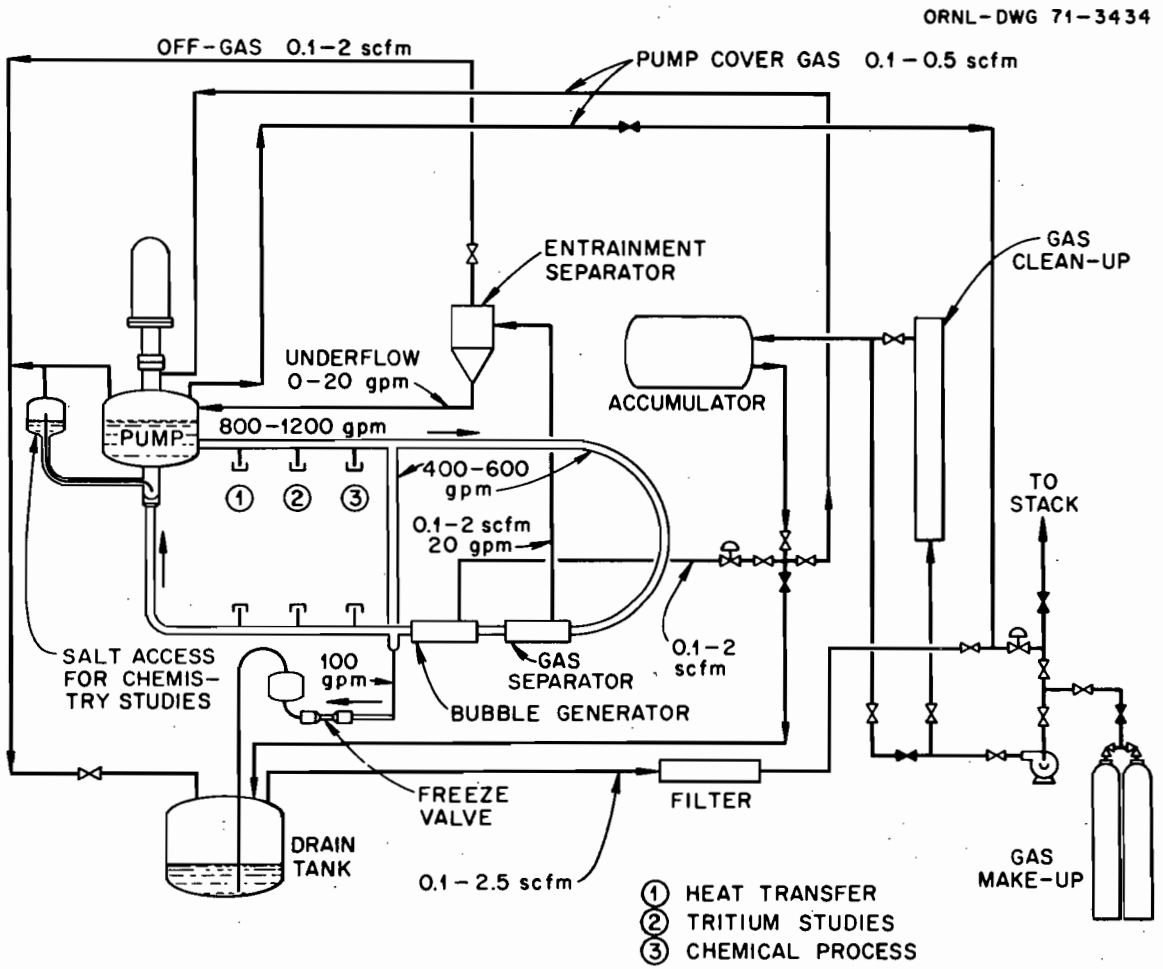

Schematic Diagram of Gas-System Technology Facility

Figure 8-1.

ORNL DWG. 71-3455

EXPERIMENTAL PROGRAM
GAS-SYSTEM TECHNOLOGY FACILITY

Study and Evaluate

1. Bubble Generator and Gas Separator
2. Off-Gas Components
3. Mass Transfer
4. Bubble Dynamics
5. Chemical Variables
6. Noble Metal Distribution
7. Heat Transfer
8. ^{3}H Distribution

Table 8-2. This table lists the studies to be made in the GSTF. The equipment for items 1 and 2 will be installed in the loop during construction.

MOLTEN-SALT STEAM GENERATOR PROGRAM PLAN

Phase I Preliminary Development of Technology
- Industrial Design Study - Conceptual
- Development Basis Report
- Small Tests

Phase II Engineering Design and Development
- Industrial Design Study - Preliminary
- Engineering Tests
- Steam-Generator Tube Test Stand

Phase III Design, Fabrication and Tests
- of Steam Generators for Use With a
- Molten-Salt Demonstration Plant

Table 8-3. This table lists the three phases of the Steam Generator Program Plan. We are presently concerned only with Phast I.

STEAM GENERATOR PROGRAM

Industrial Design Study - Conceptual

Task I - Conceptual Design of a Steam Generator for the ORNL - 1000 Mw(e) MSBR Reference Steam Cycle

Task II - Feasibility Study and Conceptual Design of Steam Generators Using Lower Feedwater Temperature

Task III - Conceptual Design of a Steam Generator for a Molten Salt Reactor of about 150 Mw(t)

Task IV - Description of a Research and Development Program for Task III Steam Generator

Table 8-4. This table lists the four tasks of the industrial conceptual design study of Phase I of the Steam Generator Program Plan.

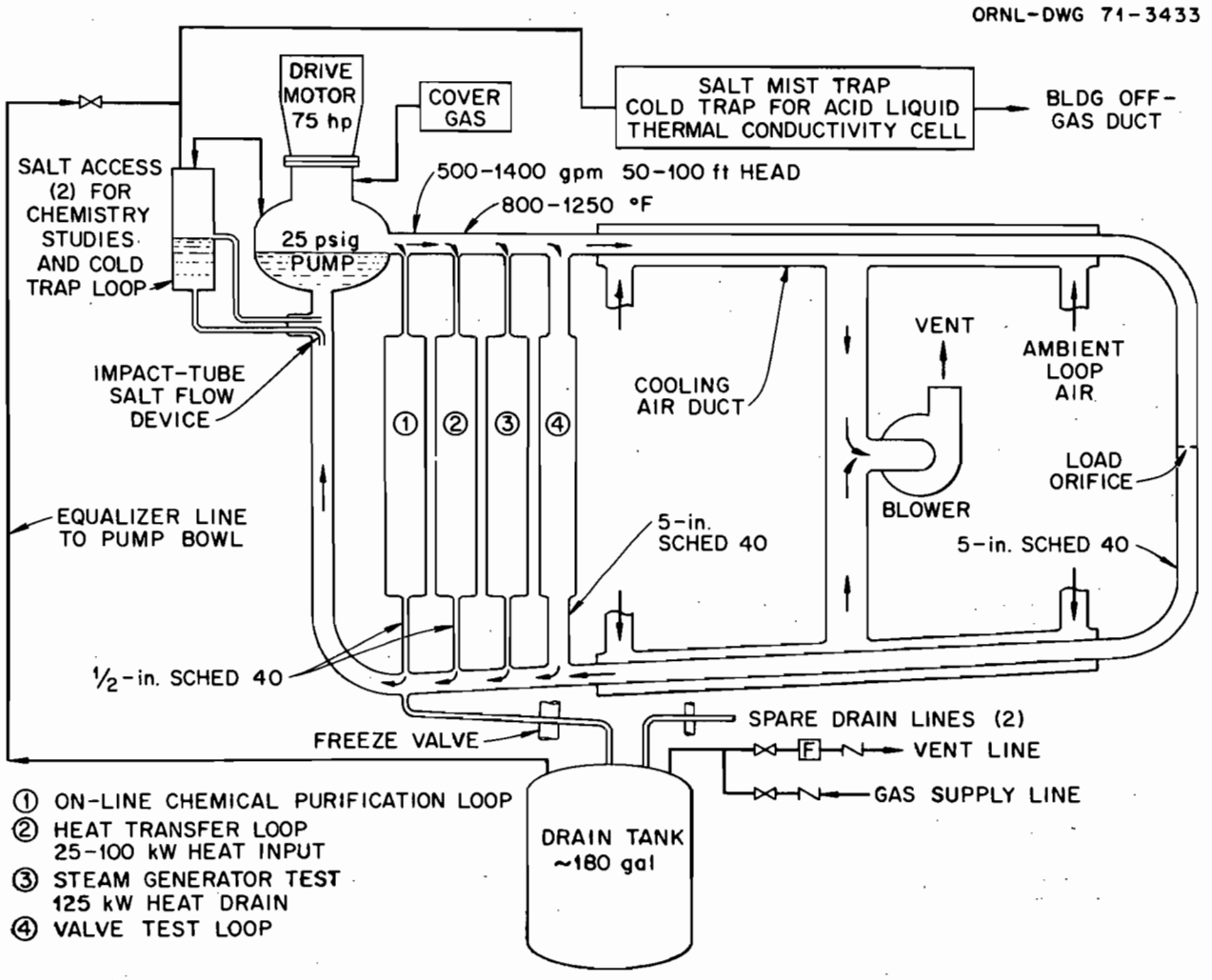

Schematic Diagram of Coolant Salt Technology Facility.

Figure 8-2.

ORNL DWG. 71-3454

EXPERIMENTAL PROGRAM
COOLANT-SALT TECHNOLOGY FACILITY

Study and Evaluate:

1. Engineering-scale operation with sodium fluoroborate and its cover gas.
2. Detecting and removal of corrosion products resulting from small steam leaks into the salt.
3. Heat and mass transfer near the liquidus salt temperature.
4. Tritium containment by control of salt chemistry.
5. Salt purification by on-line chemical means.
6. Molten-salt-heated steam generation.
7. Operation of valves in molten salts.

Table 8-5. This table lists the studies to be made in the CSTF described in Figure 8-2.

9. Development of MSBR Bubble Generator and Bubble Separator

C. H. Gabbard

The continuous removal of ^{135}Xe has been shown to be a necessary requirement for a MSBR. Figure 9.1 shows the results of calculations that have formed the bases of the ^{135}Xe removal system. The proposed removal system consists of helium sparging the fuel salt to maintain a 0.2 to 1% average void fraction and stripping the helium from a 10% bypass stream of the fuel salt. This ^{135}Xe removal system, together with low permeability coated graphite, would reduce the Xe poison fraction to the target 0.5%.

The target requirements for the bubble generator are:

1. A uniform dispersion of bubbles over the cross section of pipe.

2. A bubble size of about 0.020 in. to provide adequate surface area for mass transfer of Xe.

3. Pressure drop consistent with the available pump head and compatible with available pressure from the gas system.

Figure 9.2 shows the venturi type bubble injector that is being developed for this purpose. Because of its simplicity while still meeting the requirements, this design was selected for final development over previously proposed "tear drop" and "multivane" designs.

The requirements for the gas separator are:

1. The separator should be capable of operating at relatively high efficiency over a wide range of gas flows.

2. Should be capable of completely degassing the circulating loop.

3. Pressure drops must be compatible with the available pump head and the gas system.

4. The liquid entrained in the gas removal stream should not be excessive.

The gas separator being developed for this application was originally designed during the Aqueous Homogeneous Reactor Program and is shown in Figure 9.3.

The development testing of the gas injector and separator has consisted of operation with demineralized water and with a 41.5% glycerin-water mixture which simulates MSBE fuel salt in respect to kinematic viscosity. The water tests of the bubble injector indicated that the bubbles were satisfactorily dispersed through the fluid and that the bubble size was determined mainly by the flow rate or velocity. Figure 9.4

shows the approximate bubble size as a function of flow rate. The bubble size was also affected by the fluid properties and was reduced somewhat by additives of sodium oleate and n-butyl alcohol and by the 41.5% glycerin mixture.

Figure 9.5 shows the removal efficiency of the original design as compared to that of the revised annular takeoff design while operating on demineralized water. The liquid flow rate from the gas takeoff was increased from a range of about 1.5 - 0.5 gpm in the original design to a range of about 9 - 6.5 gpm. The separator was found to have excellent performance over a wide range of liquid and gas flows while operating on demineralized water.

When the loop fluid was changed to the 41.5% glycerin-water mixture, the gas bubbles going through the pump were sheared to a smaller size range (0.001 to 0.003 in. in diameter) and as a result were not effectively removed at the separator. The bubble size produced by the pump was found to be dependent on the pump speed (or head). Figures 9.6 and 9.7 show the degradation of the bubbles at 875 and 1750 rpm, respectively. At the present time we are unable to measure the removal efficiency in the present loop, and additional instrumentation is being obtained to permit these measurements.

Calculations have been completed indicating that the length required to separate the gas is about a factor of 2 greater in salt than in water and that the length increases rapidly at smaller bubble sizes. The results of these calculations are shown on Figures 9.8 and 9.9.

The current development efforts are:

1. To determine the gas removal efficiency in the 41.5% glycerin mixture and to determine the void fraction associated with the very small bubbles.

2. To select a fluid for simulating the fuel salt which does not stabilize the very small bubbles.

3. To obtain a comparison of bubble size in salt with that in water, the glycerin mixture, and in other fluids of interest.

The present evidence leads us to believe that the small bubbles are not stable in salt, but the final proof of this will be obtained from tests with fuel salt in the Gas System Test Facility which is in the beginning design stage.

ORNL-DWG 68-13037R

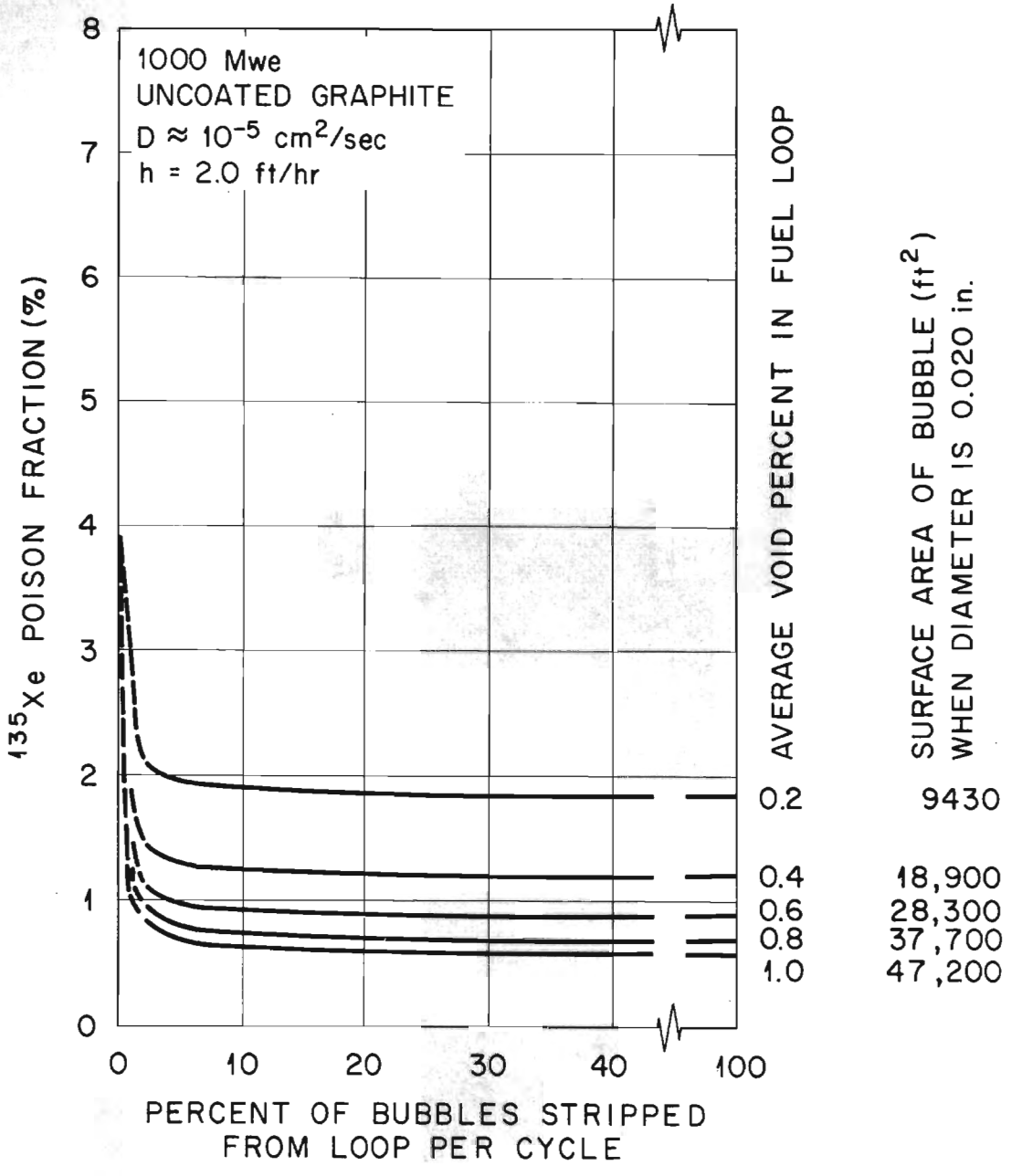

Fig. 9.1. Xe-135 poison fraction as a function of the fraction of the bubbles removed from the fuel salt per loop cycle. The curves illustrate the effect of void fraction and show that there is no advantage to a stripping cycle greater than 10%.

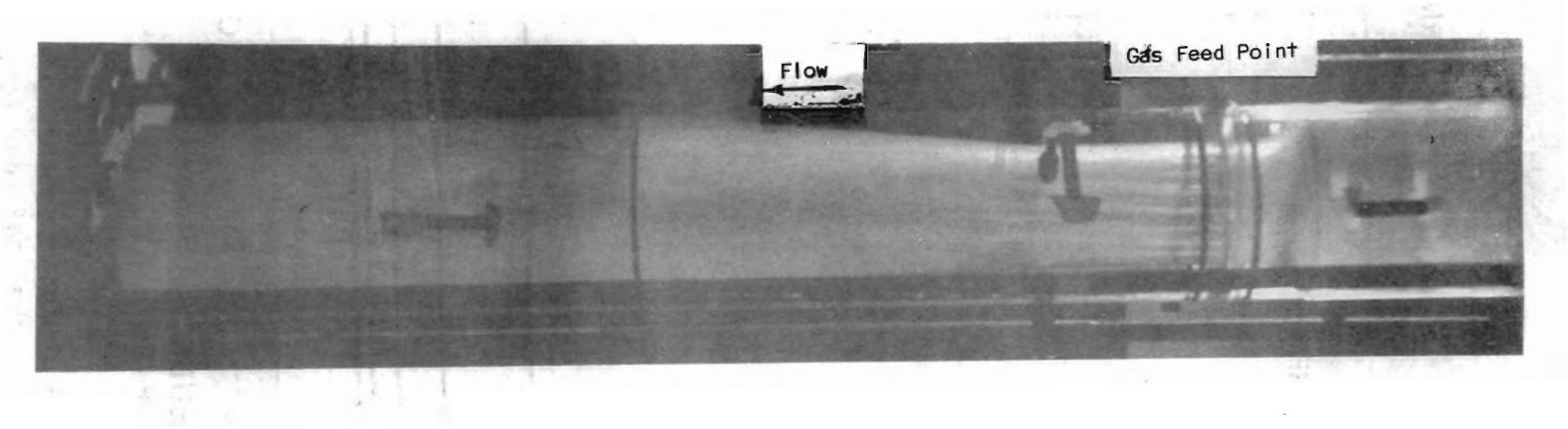

Fig. 9.2 Venturi type bubble generator operating on demineralized water.

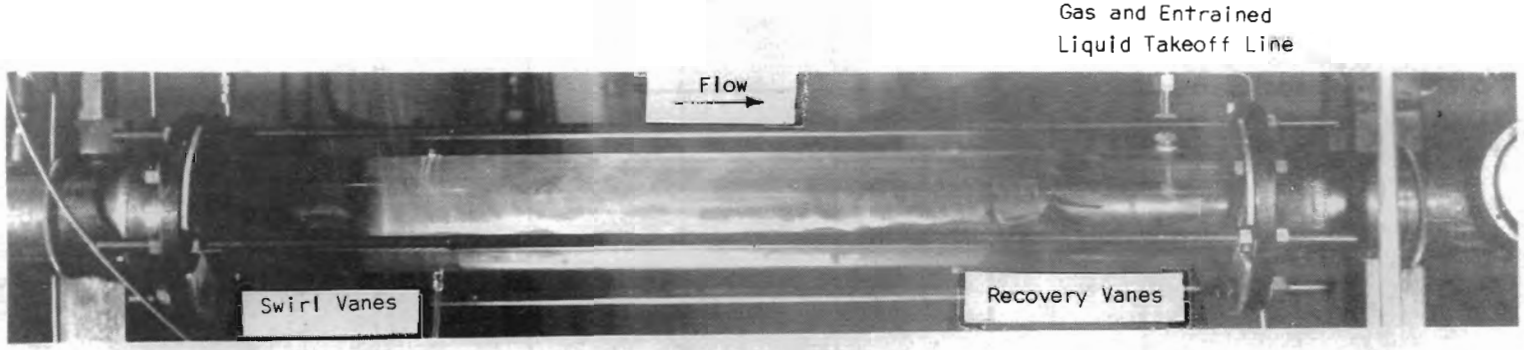

Fig. 9.3. Pipeline bubble separator operating on demineralized water with inlet void fraction = 0.3%.

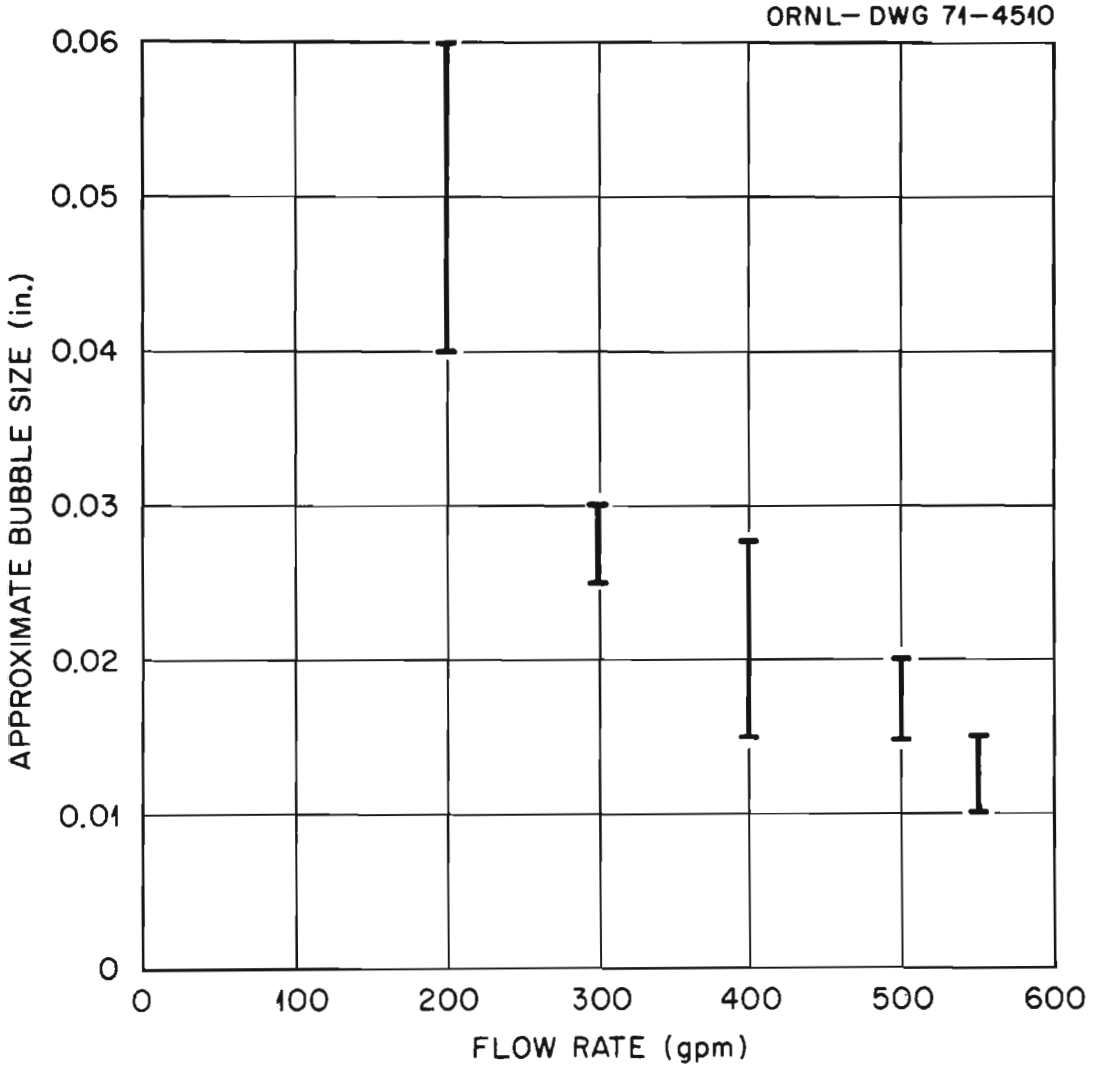

Fig. 9.4. Approximate bubble diameter produced by the bubble generator as a function of liquid flow rate.

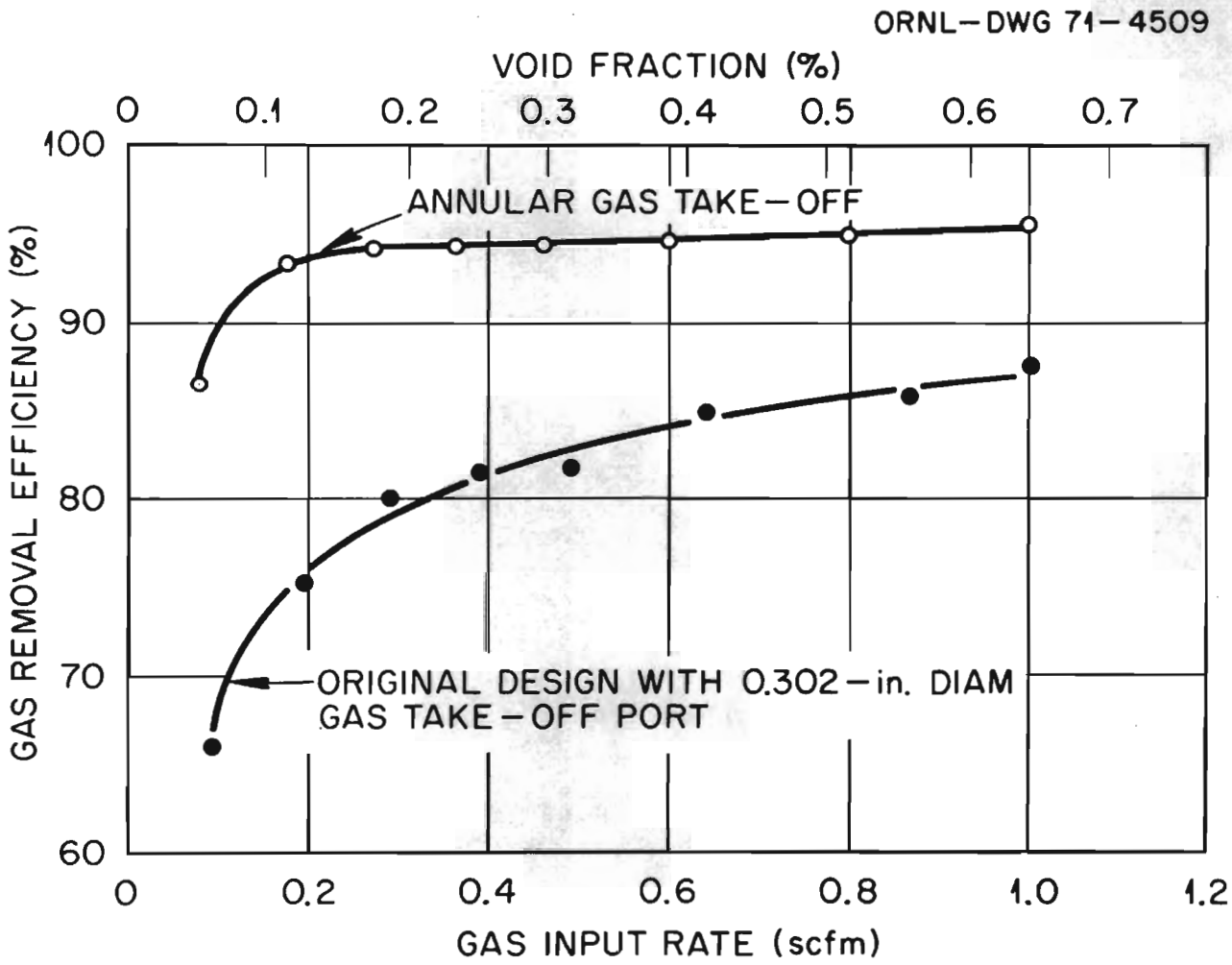

Fig. 9.5. Performance of gas separator with revised annular takeoff as compared to the original design. Inlet void fraction is shown at top of figure.

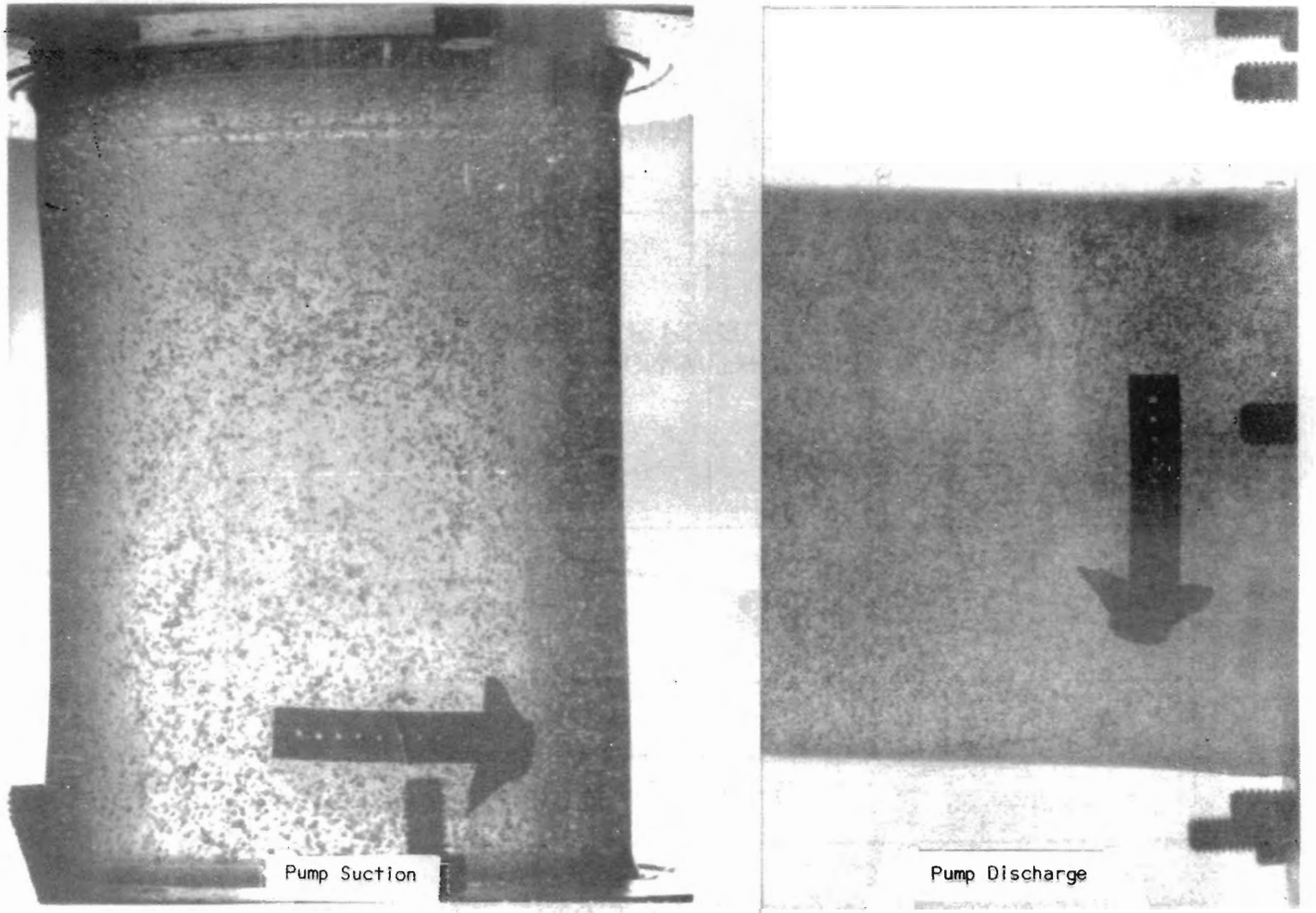

Fig. 9.6. Bubble degradation in 41.5% glycerin mixture by centrifugal pump at 875 rpm. Flow = 290 gpm, Head = 32 ft.

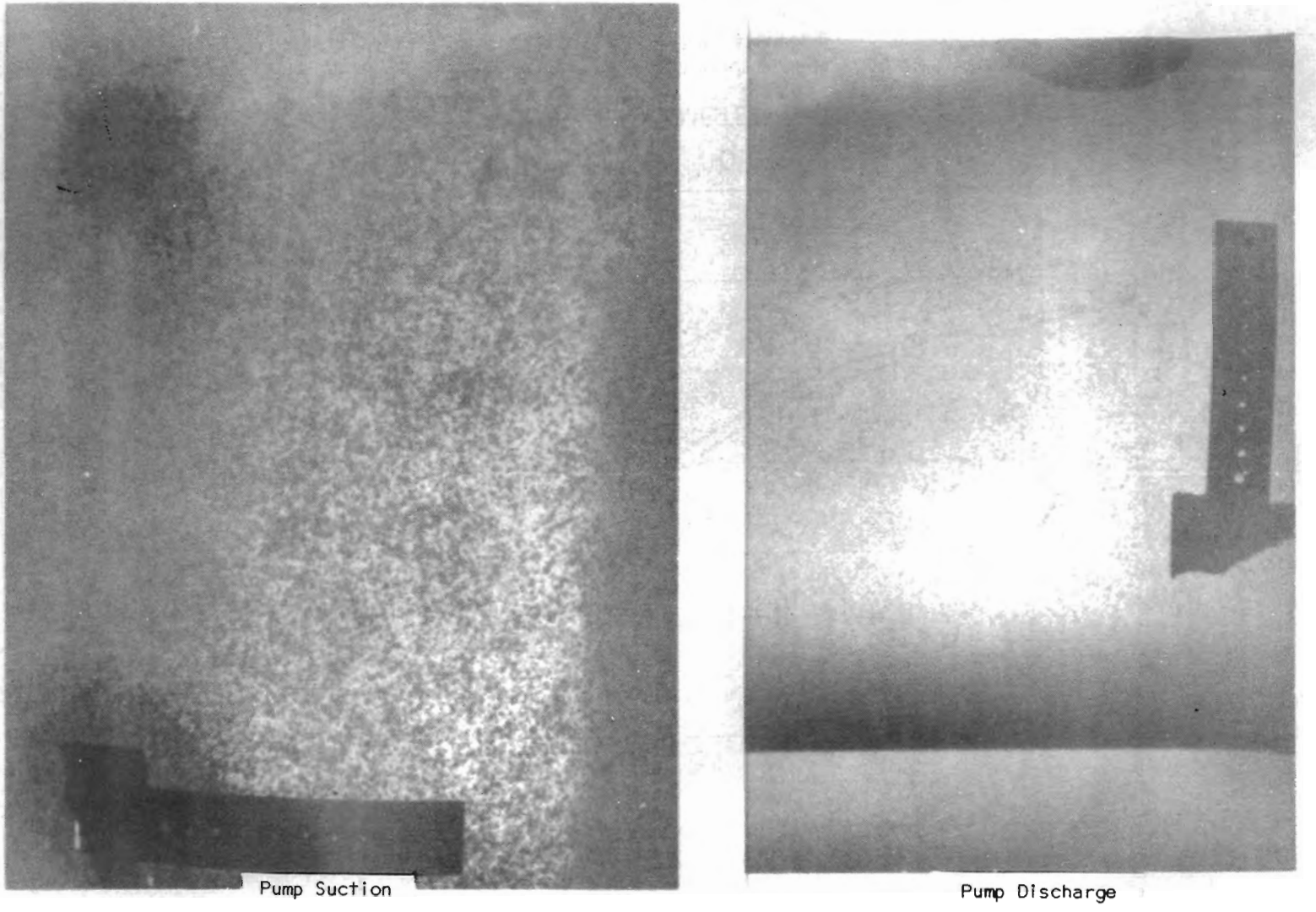

Fig. 9.7. Bubble degradation in 41.5% glycerin mixture by centrifugal pump at 1750 rpm. Flow = 480 gpm, Head = 125 ft.

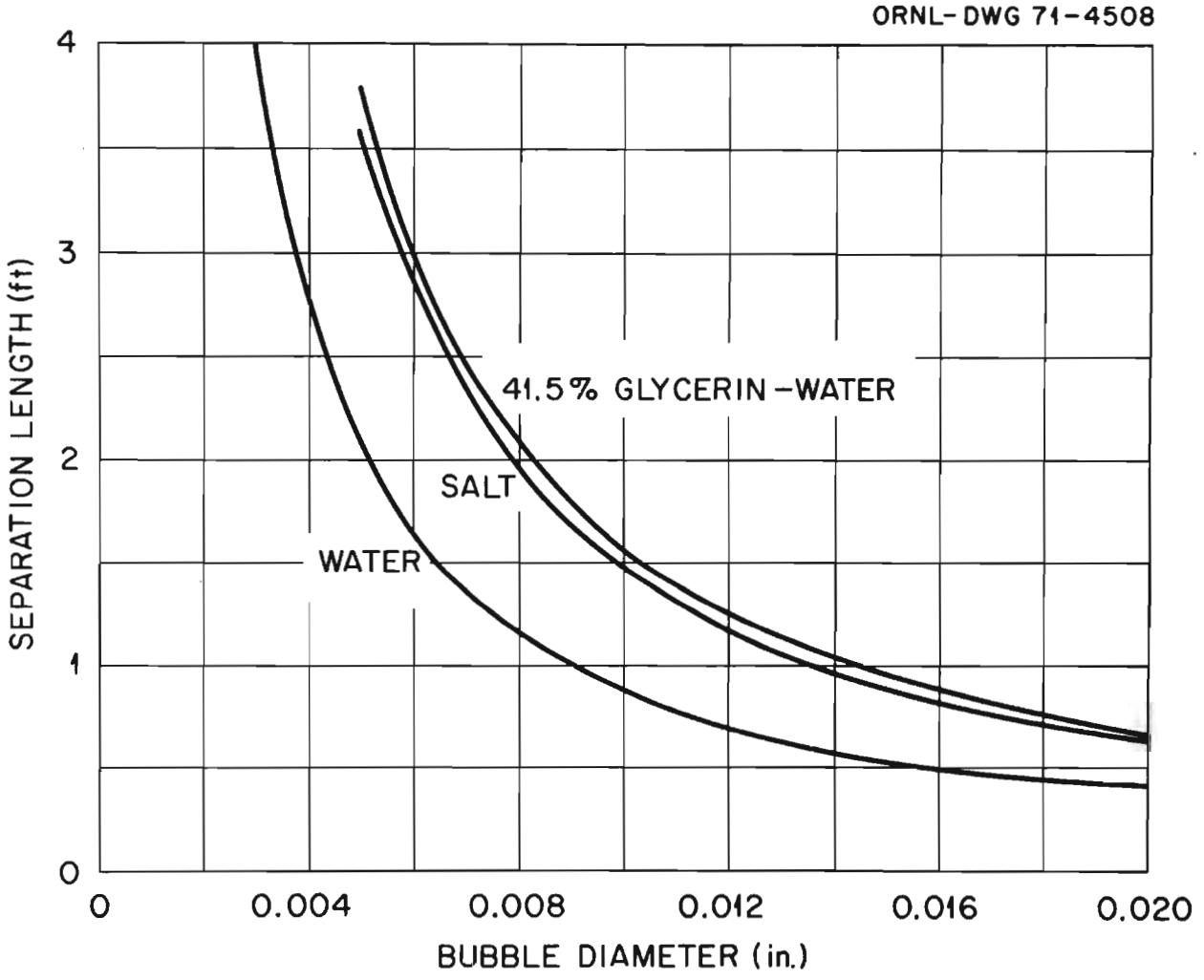

Fig. 9.8. Calculated length required for 100% bubble separation for 4-in. ID pipeline separator at 400 gpm.

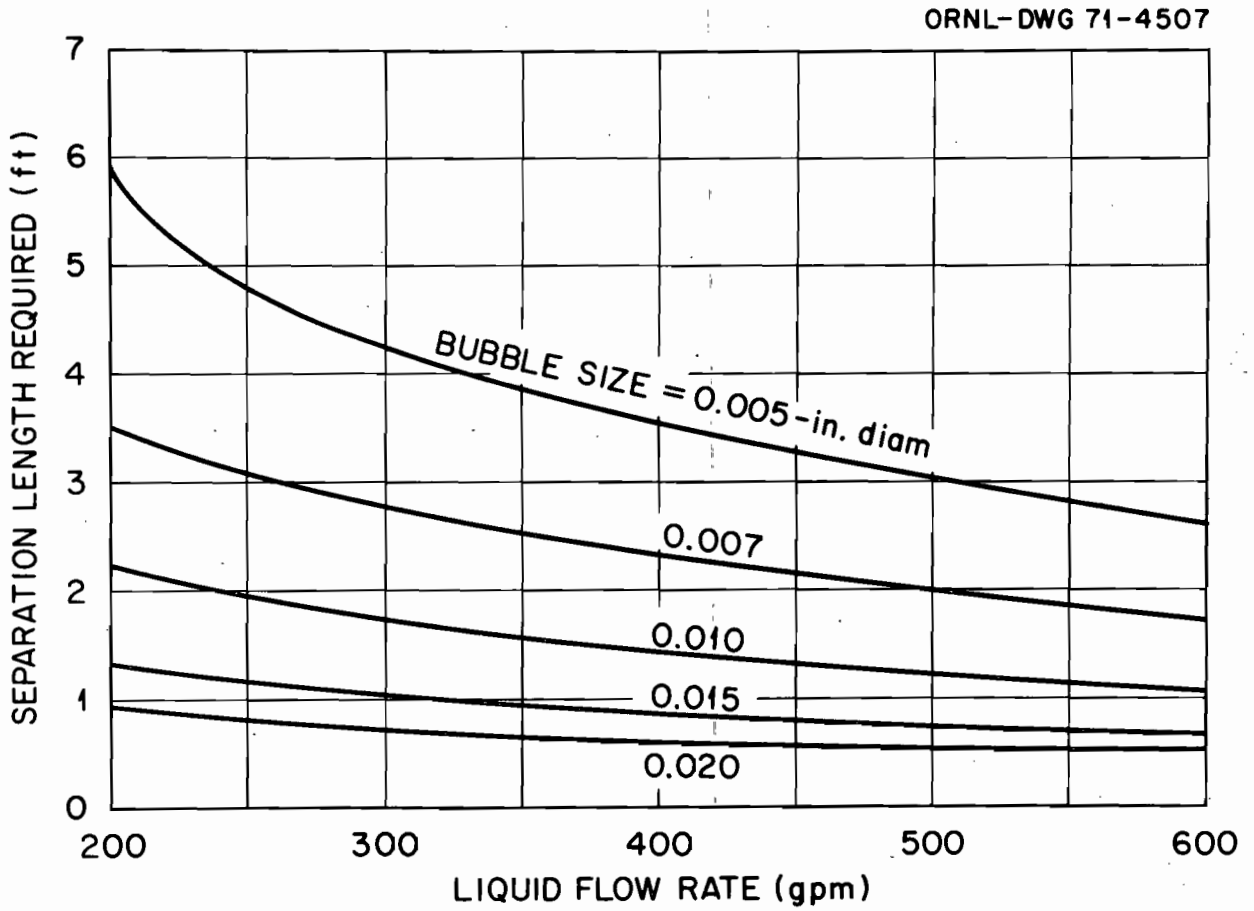

Fig. 9.9. Calculated separation length for a 4-in. ID pipeline separator as a function of the liquid flow rate.

10. Influence of Physical Properties and Entrance Region Conditions on Molten-Salt Heat Transfer

J. W. Cooke

Heat-transfer experiments employing a proposed MSBR fuel salt ($LiF-BeF_2-ThF_4-UF_4$; 67.5-20-12-0.5 mole %) flowing in a horizontal tube have shown that the local heat-transfer coefficient varies along the entire length of the tube in the range $2000 < N_{Re} < 4000$ for a heat flux range of 0.7×10^5 to 3.0×10^5 Btu/hr·ft^2. It has been hypothesized that a delay in transition to turbulent flow could result in such a variation for the transitional flow range.

To investigate the effect of flow development on heat transfer, a new test section was installed in the inert-gas-pressurized molten salt heat-transfer system shown in Fig. 10.1. The test section consists of a 48-in. length of 0.25-in.-OD X 0.035-in.-wall Hastelloy-N tubing. Three electrodes are welded to the test section so that either the left half, the right half, or the entire length can be resistance heated. For the initial studies, the left half was heated so that with flow to the left there would be a 24-in. entrance length and with flow to the right there would be a rounded-edge entrance.

Experimental results have been obtained at three temperature levels (~1070°F, ~1250°F, and ~1450°F) and three Reynolds moduli (~3500, ~7000, and ~12,000) over the heat flux range of 0.7×10^5 to 3.4×10^5 Btu/hr·ft^2. A representative sample of these results is tabulated in Table 10.2. The odd-numbered runs were without, and the even-numbered runs were with the 24-in. entrance length. Examining Runs 44, 45, 70, and 71 ($7000 < N_{Re} < 13,000$), one can see little variation in the heat-transfer function beyond that associated with variations in the Reynolds modulus. However, for the other runs shown ($3100 < N_{Re} < 3700$), the average heat-transfer function is 15% greater with a hydrodynamic entrance length.

Some indication of the consistency and precision of the experimental data can be gained from Figs. 10.3, 10.4, and 10.5, where local temperatures and heat-transfer coefficients are plotted as function of axial position along the test section. But the influence of the entrance region on the heat transfer can best be seen by comparing plots of the ratio of local-to-exit heat-transfer coefficients as function of the distance from the entrance to the heated section. (The exit heat-transfer coefficient with the entrance length was used for each of the pair of plots shown in Figs. 10.6 through 10.10). As can be seen in comparing these figures, the results obtained with an entrance region behave in a manner predicted by circular-tube thermal-entry-length theory; whereas those without the entrance length do not.

The abnormal behavior may be attributed to the existence of laminar flow at the test-section inlet for those runs at the lower Reynolds moduli ($3000 < N_{Re} < 4000$). With an unheated entrance length, a transition to developed turbulent flow can occur ahead of the heated section. Without an entrance length, the transition will be initiated in the heated section.

Furthermore, it is believed that the transition in the heated section will be delayed because of the stabilizing influence of heat transfer from the wall. Although there are no experimental data to confirm this, a published computer study of incompressible flow has indicated that the flow of a fluid whose viscosity has a large negative temperature dependence will be stabilized by heating. The present results tend to confirm this theoretical conclusion.

A summary of an analysis of the uncertainties influencing the subject heat-transfer study is presented in Table 10.11. The maximum uncertainty in the heat-transfer coefficient is within the normal range of ±10%; however, the uncertainty in the correlating function ($\overline{N}_{S-T}$) is close to ±55%. Most of this uncertainty is due to the uncertainty in the estimated value for the salt viscosity (no experimental measurements have been conducted for the subject salt mixture).

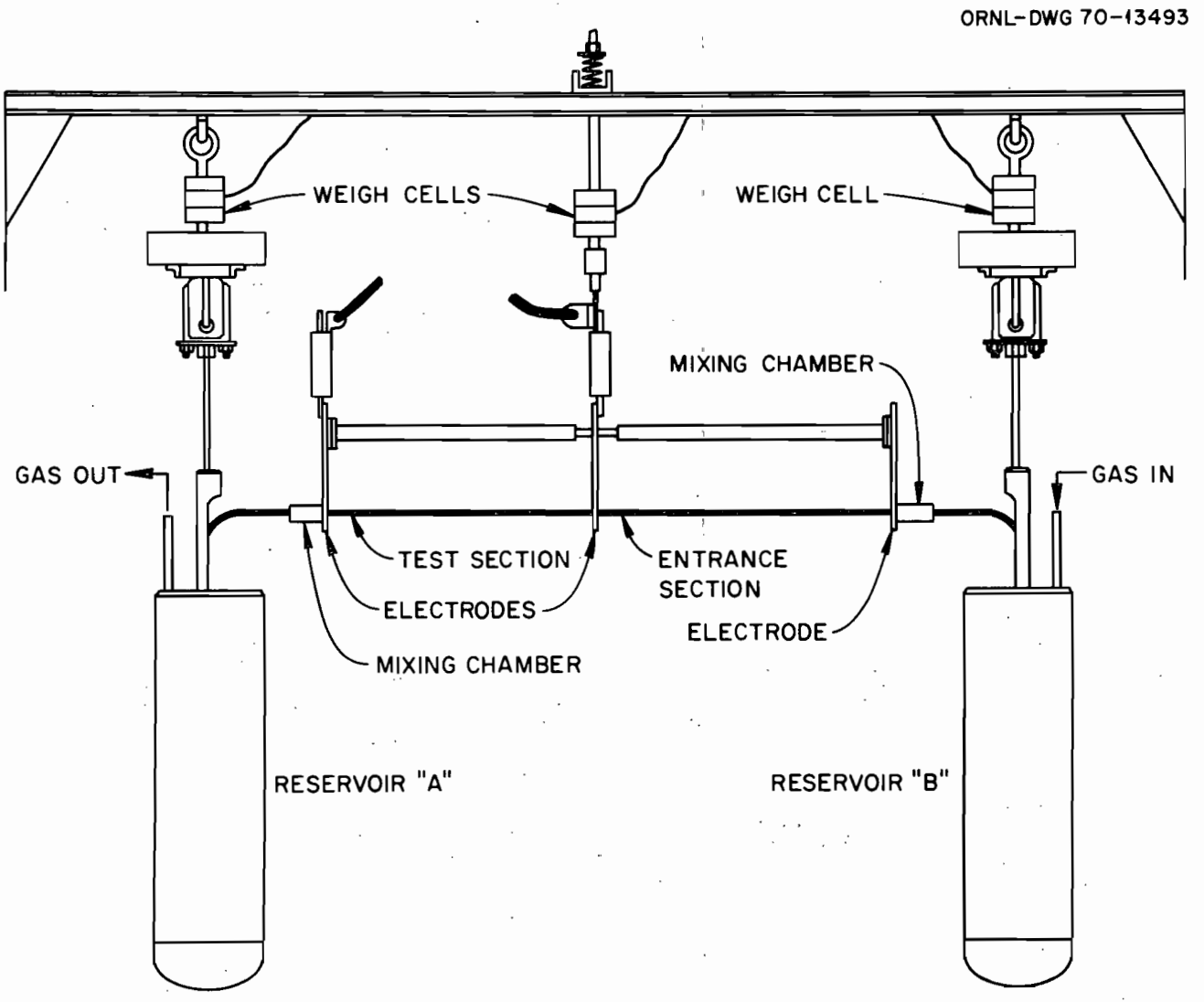

Fig. 10.1. Inert-Gas Pressurized, Molten-Salt Heat Transfer System.

Table 10.2. Experimental Data for Heat Transfer Studies Using the Salt Mixture $LiF-BeF_2-ThF_4-UF_4$ (67.5-20-12-0.5 Mole %)

Run No.	T_{in} (°F)	T_{out} (°F)	ΔT_f (°F)	q/A (Btu/hr·ft² x 10^{-5})	Heat Balance	$\bar{N}_{Re}$	$\bar{N}_{Pr}$	$\bar{N}_{Nu}$	$\bar{h}$ (Btu/hr·ft²·F)	$\bar{N}_{S-T}$ [a]
15	1077.2	1099.9	105.8	0.99	1.01	3370	15.0	20.4	937	7.96
16	1082.7	1106.6	85.8	0.99	1.08	3264	14.7	25.1	1153	9.94
22	1089.3	1135.5	170.7	2.0	1.13	3591	13.8	25.1	1157	9.87
23	1114.2	1163.6	189.8	2.0	1.09	3749	12.7	23.4	1076	9.40
44	1088.2	1117.9	89.3	2.7	1.08	7299	14.3	65.1	2997	26.1
45	1104.8	1135.0	85.6	2.7	1.03	7614	13.5	68.2	3136	27.8
70	1247.3	1265.5	41.1	1.78	1.06	12470	9.09	94.0	4324	44.69
71	1258.3	1276.2	39.47	1.77	1.03	12957	8.83	97.6	4490	46.89
94	1192.6	1216.1	59.8	0.79	1.00	3706	10.49	28.78	1324	12.94
97	1189.3	1212.9	60.7	0.78	1.00	3617	10.59	28.17	1296	12.62
100	1173.7	1237.0	184.5	2.00	1.09	3541	10.36	23.62	1086	10.21
103	1192.9	1259.6	220.1	2.02	1.13	3589	9.76	20.05	928	8.76
104	1399.5	1445.7	78.9	0.82	1.02	3260	6.00	20.22	930	10.93
105	1410.0	1459.0	99.3	0.82	1.04	3152	5.84	16.21	750	8.80
106	1390.6	1510.3	246.9	1.96	1.12	3409	5.56	17.28	795	9.17
107	1385.4	1506.3	272.8	2.02	1.10	3457	5.62	16.31	750	8.57

[a] $\bar{N}_{S-T} = \bar{N}_{Nu}/\bar{N}_{Pr}^{1/3}(\mu/\mu_S)^{0.14}$.

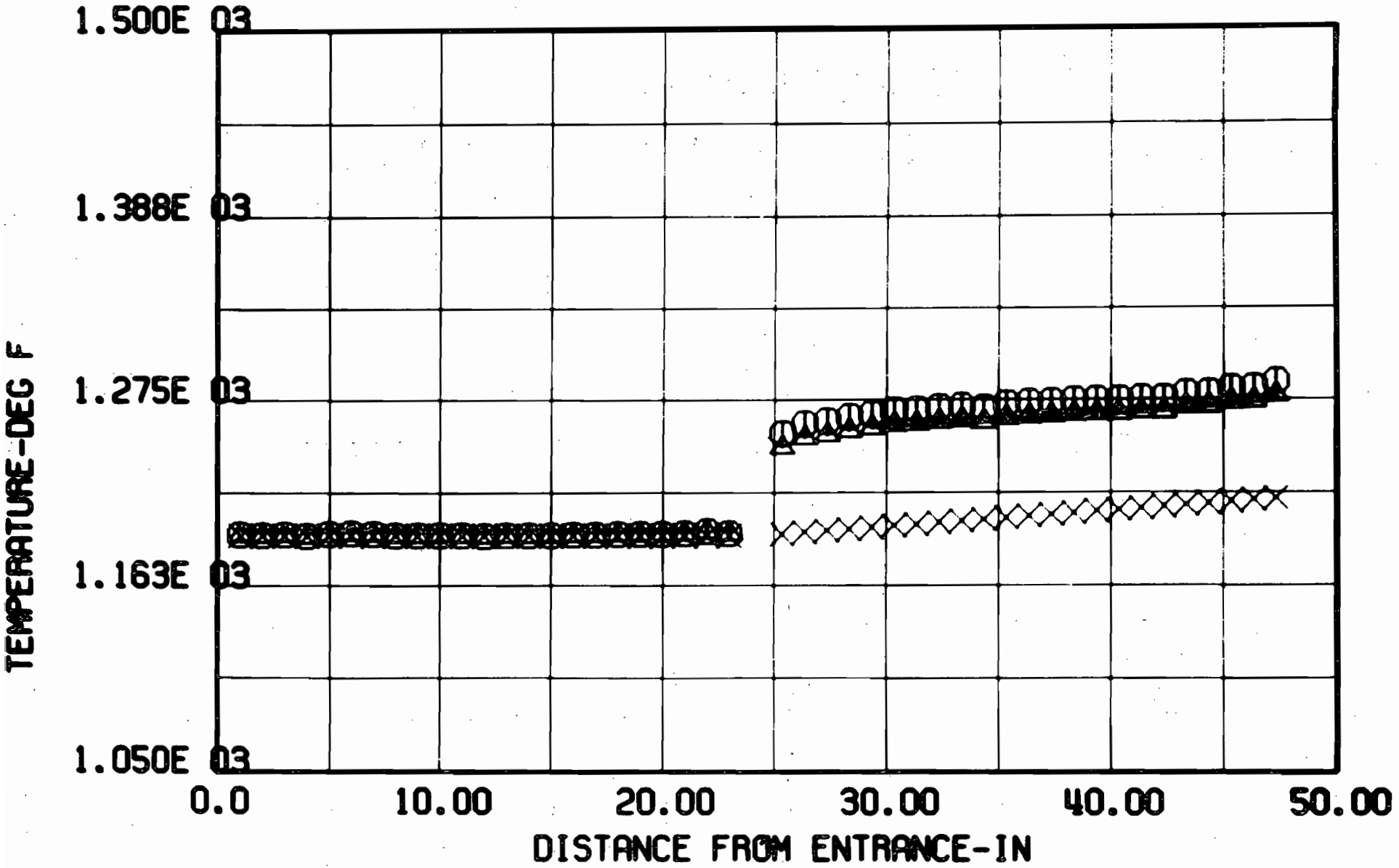

Fig. 10.3. Inside-Outside Wall and Fluid Temperatures for Run 94.

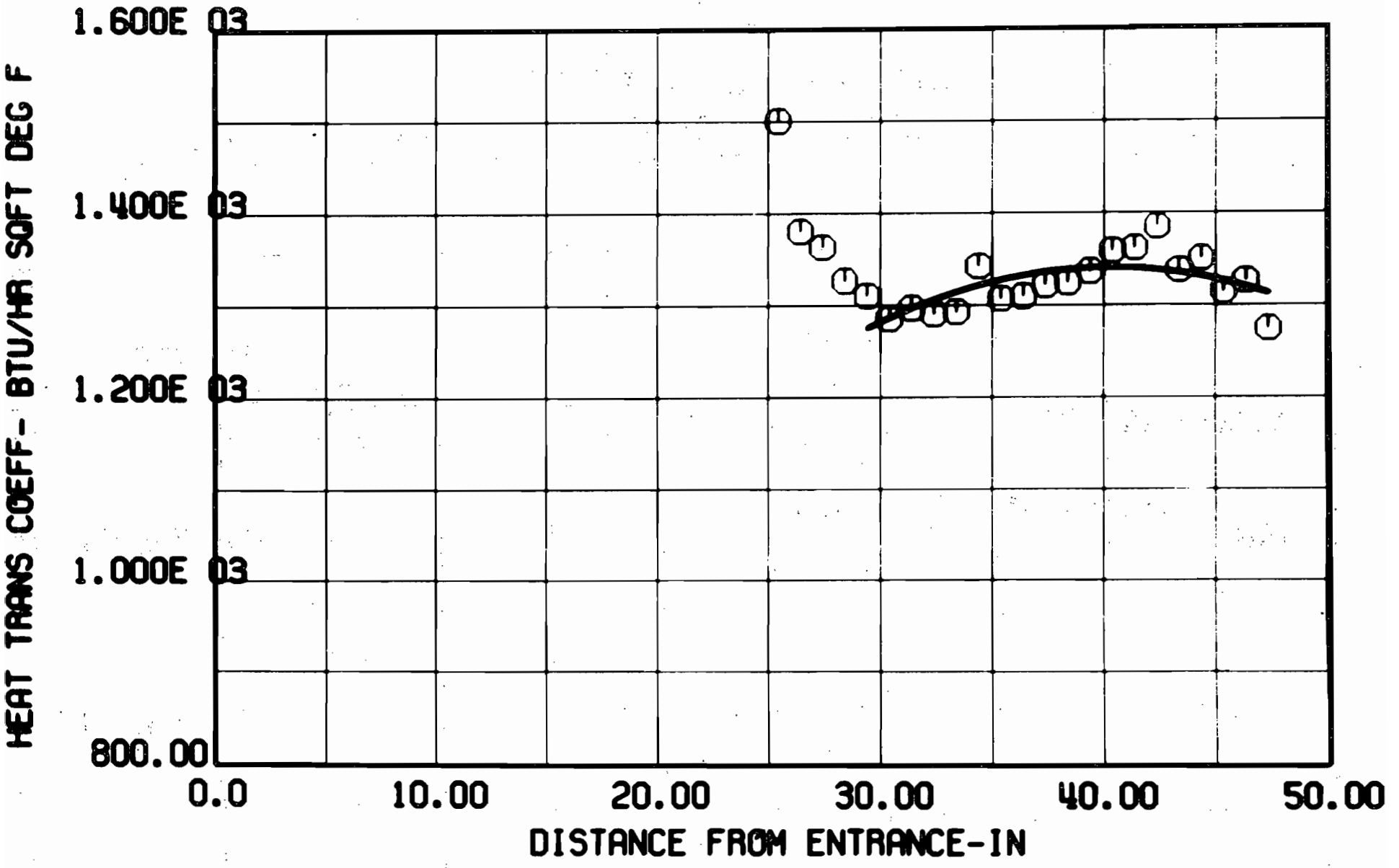

Fig. 10.4. Local Heat-Transfer Coefficient for Run 94.

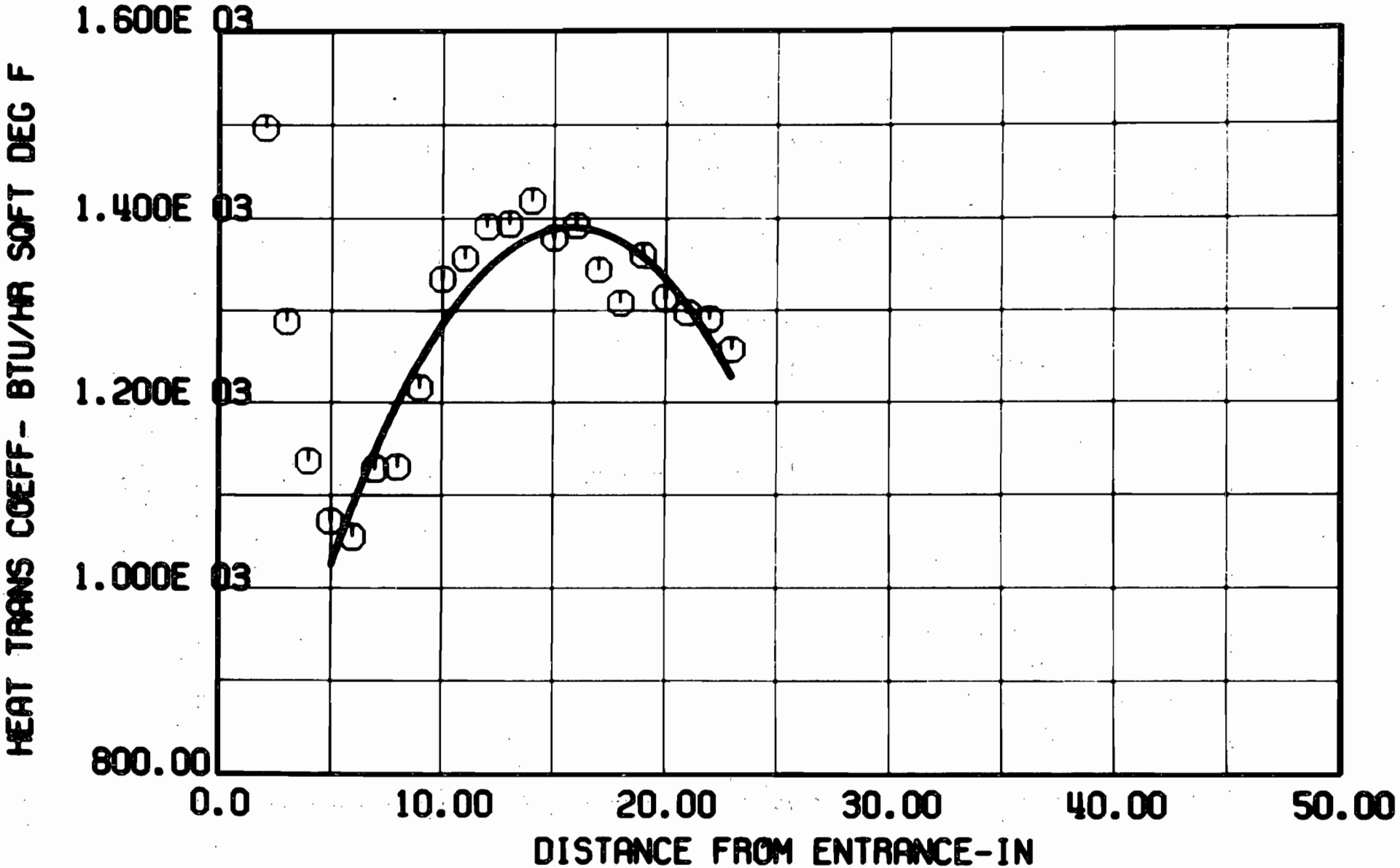

Fig. 10.5. Local Heat-Transfer Coefficient for Run 97.

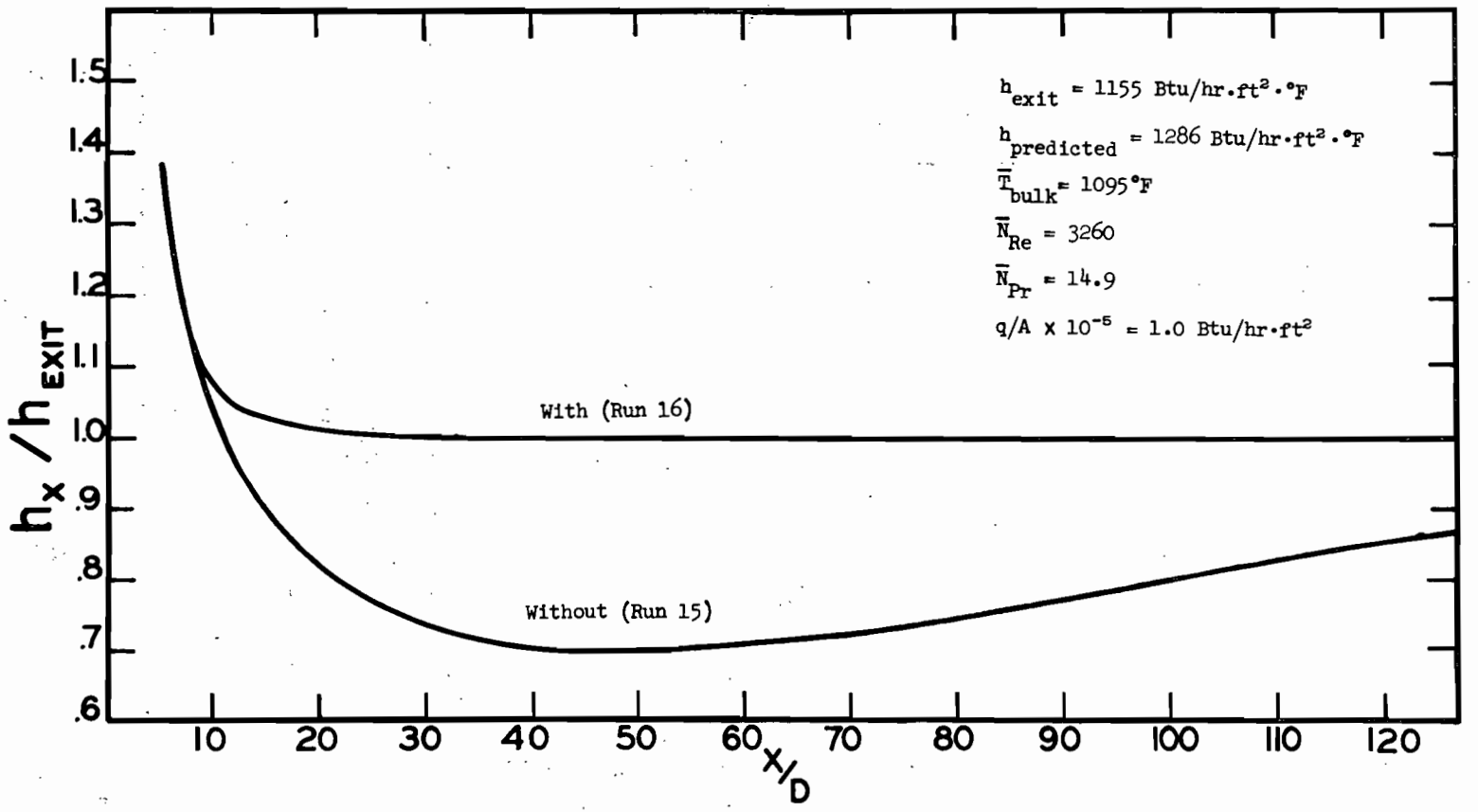

Fig. 10.6. Variation in Ratio of Local-to-Exit Heat-Transfer Coefficients With Distance from the Inlet to the Heater Section With and Without an Entrance Length.

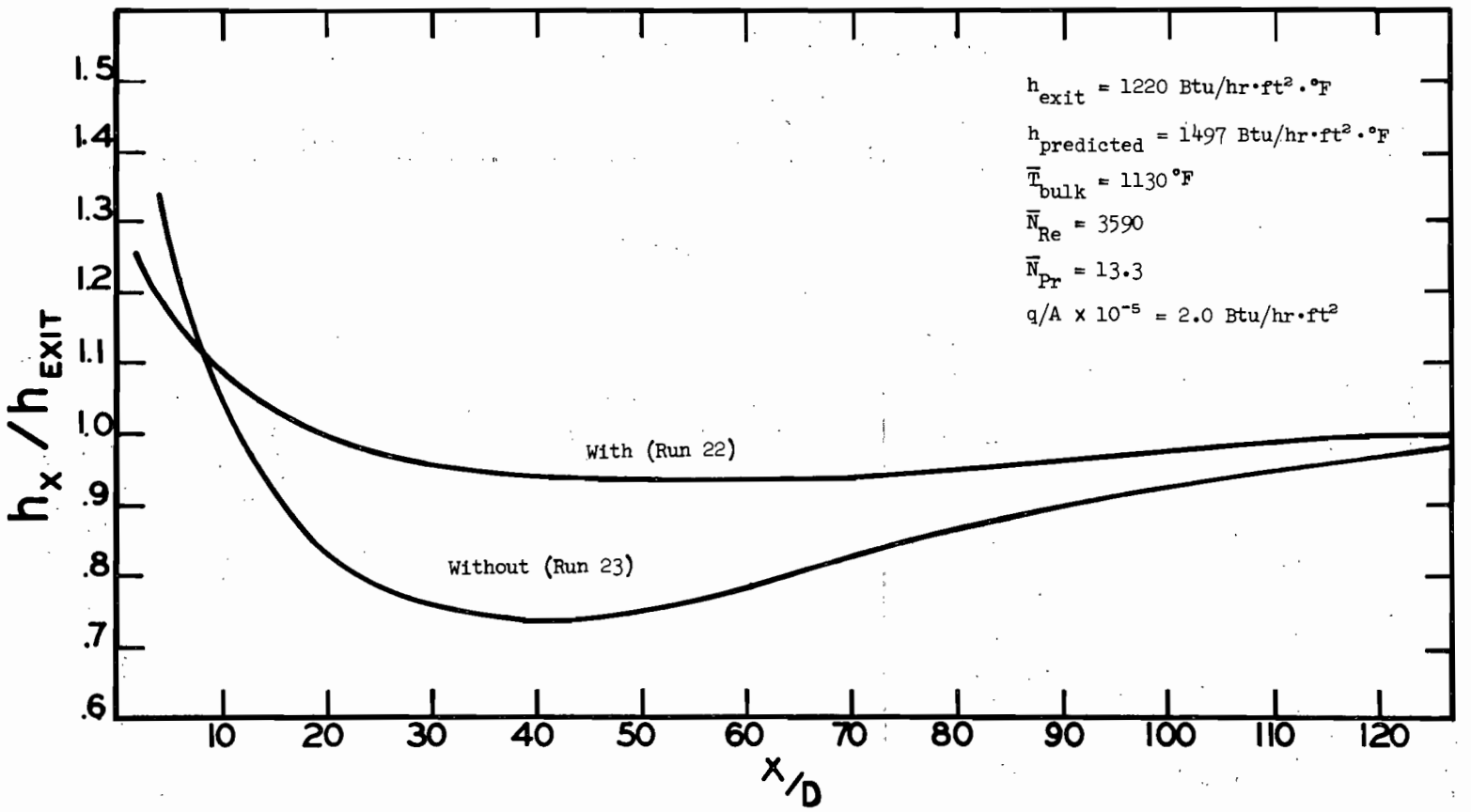

Fig. 10.7. Variation in Ratio of Local-to-Exit Heat-Transfer Coefficients With Distance from the Inlet to the Heater Section With and Without an Entrance Length.

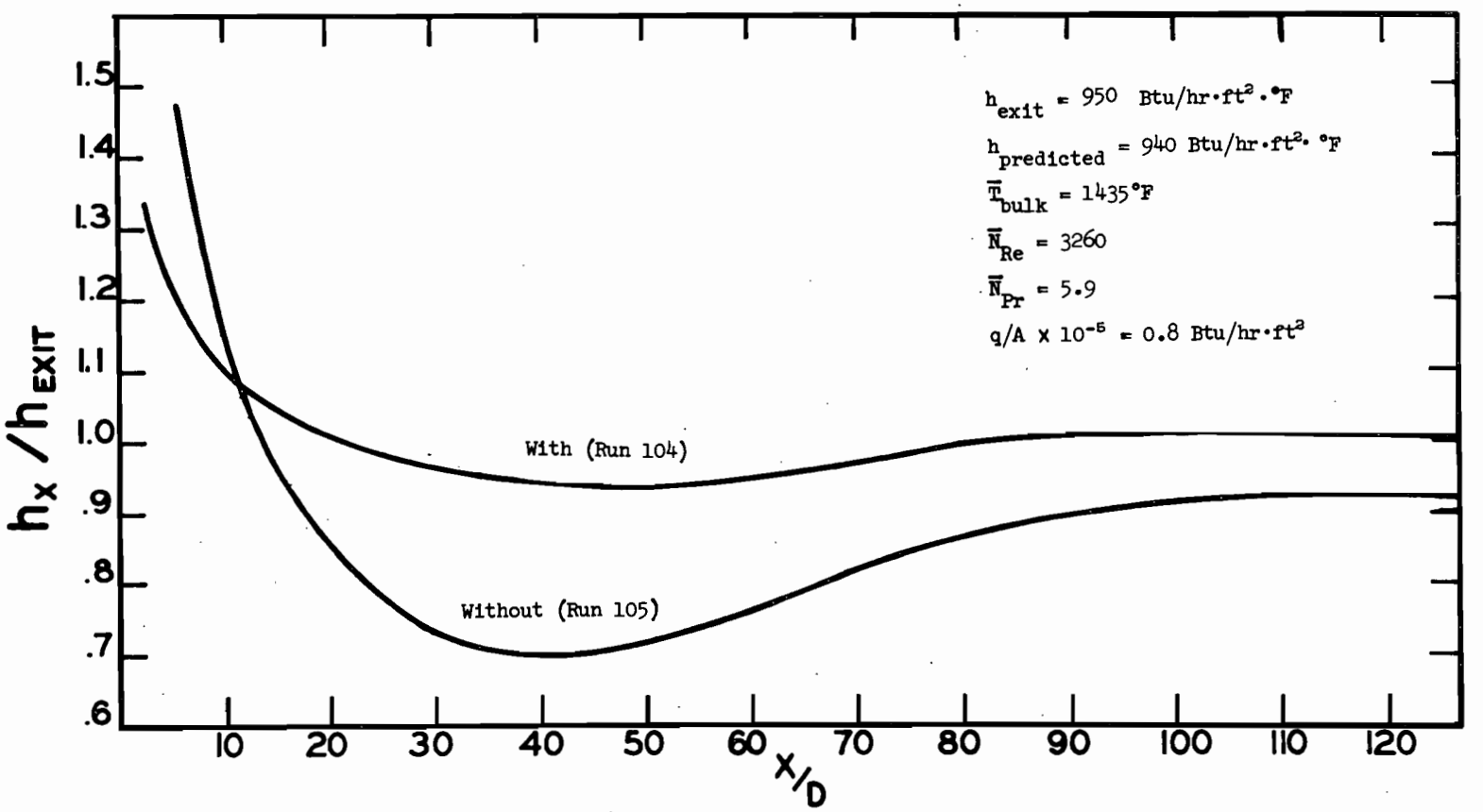

Fig. 10.8. Variation in Ratio of Local-to-Exit Heat-Transfer Coefficients With Distance from the Inlet to the Heater Section With and Without an Entrance Length.

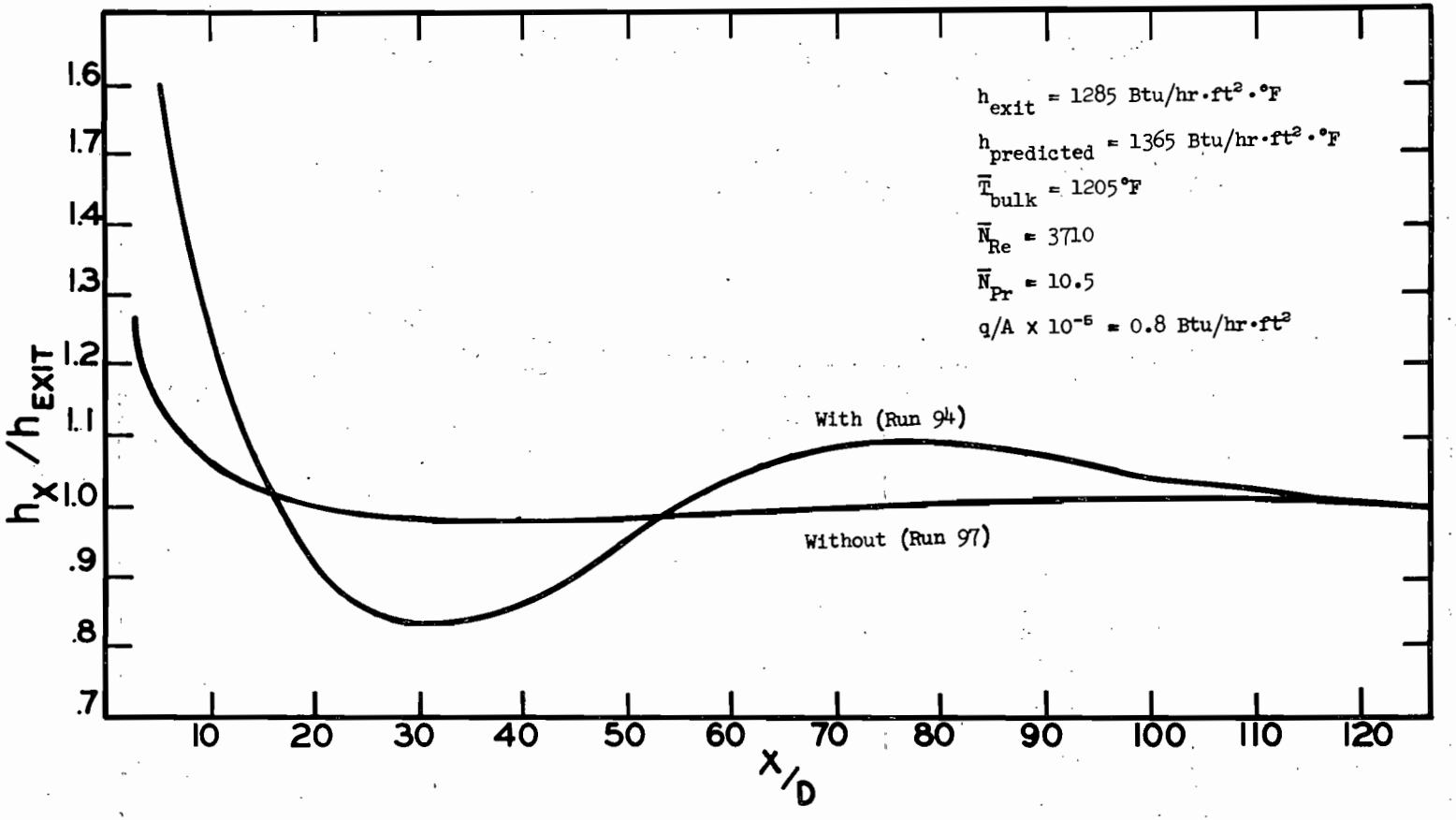

Fig. 10.9. Variation in Ratio of Local-to-Exit Heat-Transfer Coefficients With Distance from the Inlet to the Heater Section With and Without an Entrance Length.

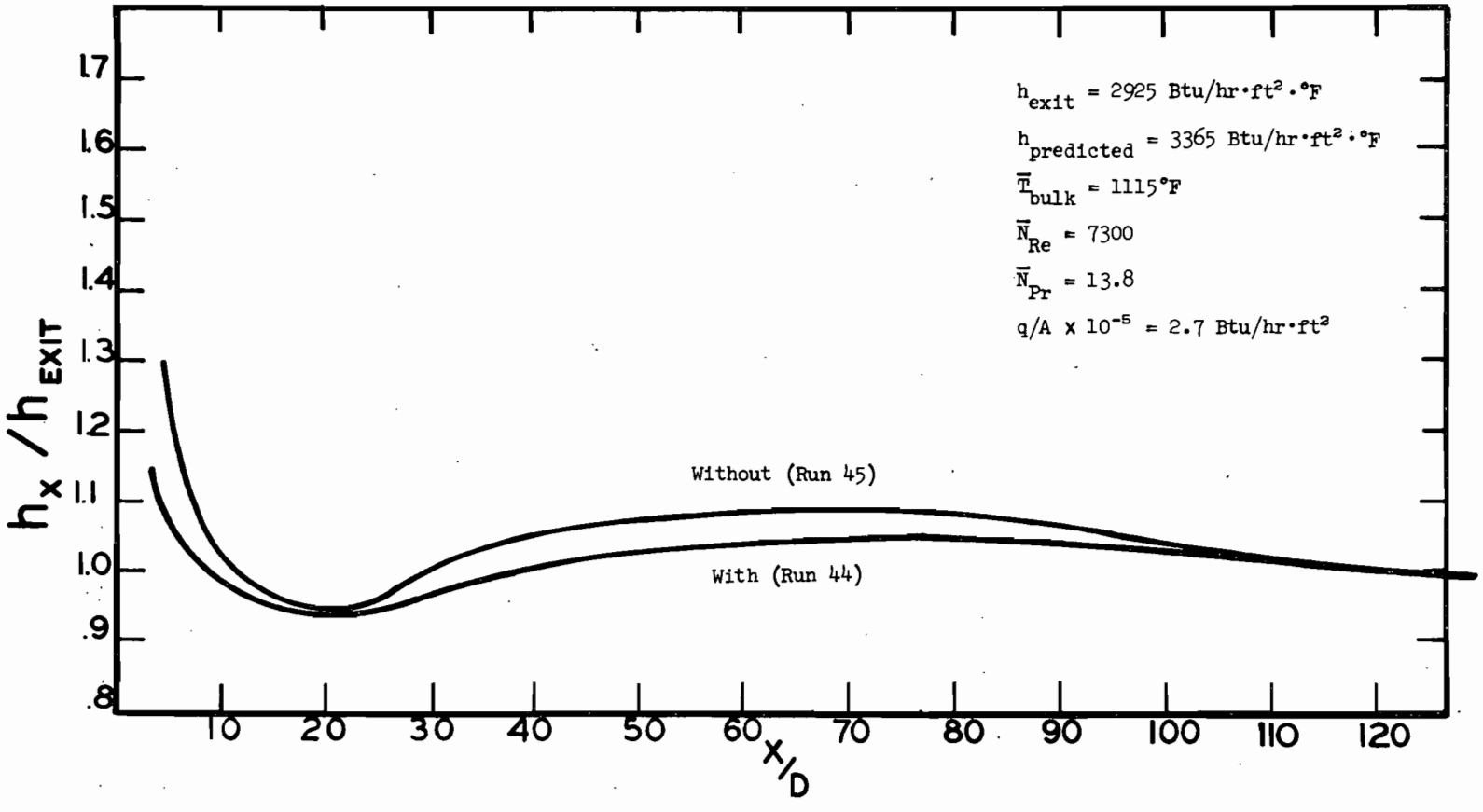

Fig. 10.10. Variation in Ratio of Local-to-Exit Heat-Transfer Coefficients With Distance from the Inlet to the Heater Section With and Without an Entrance Length.

Table 10.11. Accuracy Analysis: Source and Magnitude of Uncertainties Affecting the Accuracy of the Measurement of the Heat Transfer Coefficient and the Dimensionless Group $\overline{N}_{S-T} = \overline{N}_{Nu}/\overline{N}_{Pr}^{1/3}(\mu/\mu_S)^{0.14}$ [F_W = Weighting Factor]

Source	Maximum Magnitude (± per cent)			
	$q/A = 0.6 \times 10^5$ [a]		$q/A = 3 \times 10^5$ [a]	
	$\delta x/x$	$F_W \times (\delta x/x)$	$\delta x/x$	$F_W \times (\delta x/x)$
Heat Input, (EI)	±1.5	2.0	±2.0	2.5
Heat Loss, $(EI)_L$	1.5	0.1	2.0	0.1
Tube Diameter, Di	1.0	1.0	1.0	1.0
Tube Length, L	0.2	0.2	0.2	0.2
Mass Flow Rate, m	4.0	1.0	4.0	1.0
Salt Heat Capacity, C_p	4.0	1.0	4.0	1.0
Temperature Difference, ΔT ($T_{wall\ exit} - T_{bulk\ inlet}$)	4.0	5.0	1.0	1.2
Max error in heat transfer coefficient		±10.3		±7.0
Heat Input, (EI)	1.5	2.0	2.0	2.5
Heat Loss, $(EI)_L$	1.5	0.1	2.0	0.1
k_{salt}	12.0	8.0	12.0	8.0
Temperature Difference, ΔT	4.0	5.0	1.0	1.2
C_p, salt	4.0	2.3	4.0	2.3
μ salt	25.0	30.0	25.0	30.0
Mass Flow Rate	4.0	7.0	4.0	7.0
Tube Length	0.2	0.2	0.2	0.2
Tube Diameter	1.0	1.5	1.0	1.5
Maximum error in $\overline{N}_{S-T}$		±55.1		±52.8

[a] Btu/hr·ft²

11. Exploration of the Design of an MSR Demonstration Plant

E. S. Bettis

We have continued the design study of a medium powered [300 MW(e)] demonstration molten salt power plant. Work has involved a more detailed study of the containment, cell heating and cooling, primary salt expansion provision and heat exchanger design. As a result of further work there have been some changes made in these areas. The containment now consists of single stainless steel vessels for all cells. These are interconnected so that the cells can be heated by forced gas circulation from an external furnace thru all cells. The cell walls are cooling by water circulation thru pipes embedded in the concrete. The pump bowls are being made large enough to take care of all primary salt volume changes eliminating salt overflow to and pumpback from the drain tank. Thus jet pumps, except for the one used for filling the system, are eliminated from the drain tank resulting in simplification of primary salt piping. The sump tank of each pump is connected by a four-inch line to the outlet plenum of the reactor, providing a low impedance path thru which salt can flow into or out of the pump sump as temperature changes alter the volume of the primary salt. This line also permits pump fountain flow to return to the pump suction.

By far the most significant change in the design of the plant involves the addition of a third salt loop. A simplified flow diagram shown in Fig. 11-1 shows the incorporation of this loop into the molten salt plant. This flow diagram shows a lower performance steam system with 2400 psi steam at 900°F. These lower steam conditions were chosen as possibly being more conservative for a first of a kind plant. We are currently redesigning the plant for 3600 psi 1000°F steam. A plan view showing the equipment arrangement at the main level of the reactor building is shown in Fig. 11-2.

The third salt loop (a nitrate-nitrite eutectic) was put in for the purpose of trapping tritium and preventing its getting into the steam system. This represents a "brute force" solution to the tritium problem and more sophisticated ways of dealing with tritium may remove the necessity for the third loop. Because of the lower melting point of the nitrate-nitrite salt, the steam system can be considerably simplified over the system used when there is no low melting salt available for generating steam. Because of incompatibility with the primary salt, the nitrate-nitrite salt cannot be used as a secondary coolant. In addition to simplifying and giving greater choices in the steam system the third loop makes plant startup easier and also provides some desirable control possibilities, especially for off design conditions. We have not yet evaluated the cost of the third loop, since there are definite economics it effects in the steam system which at least partially off set the cost of the additional loop.

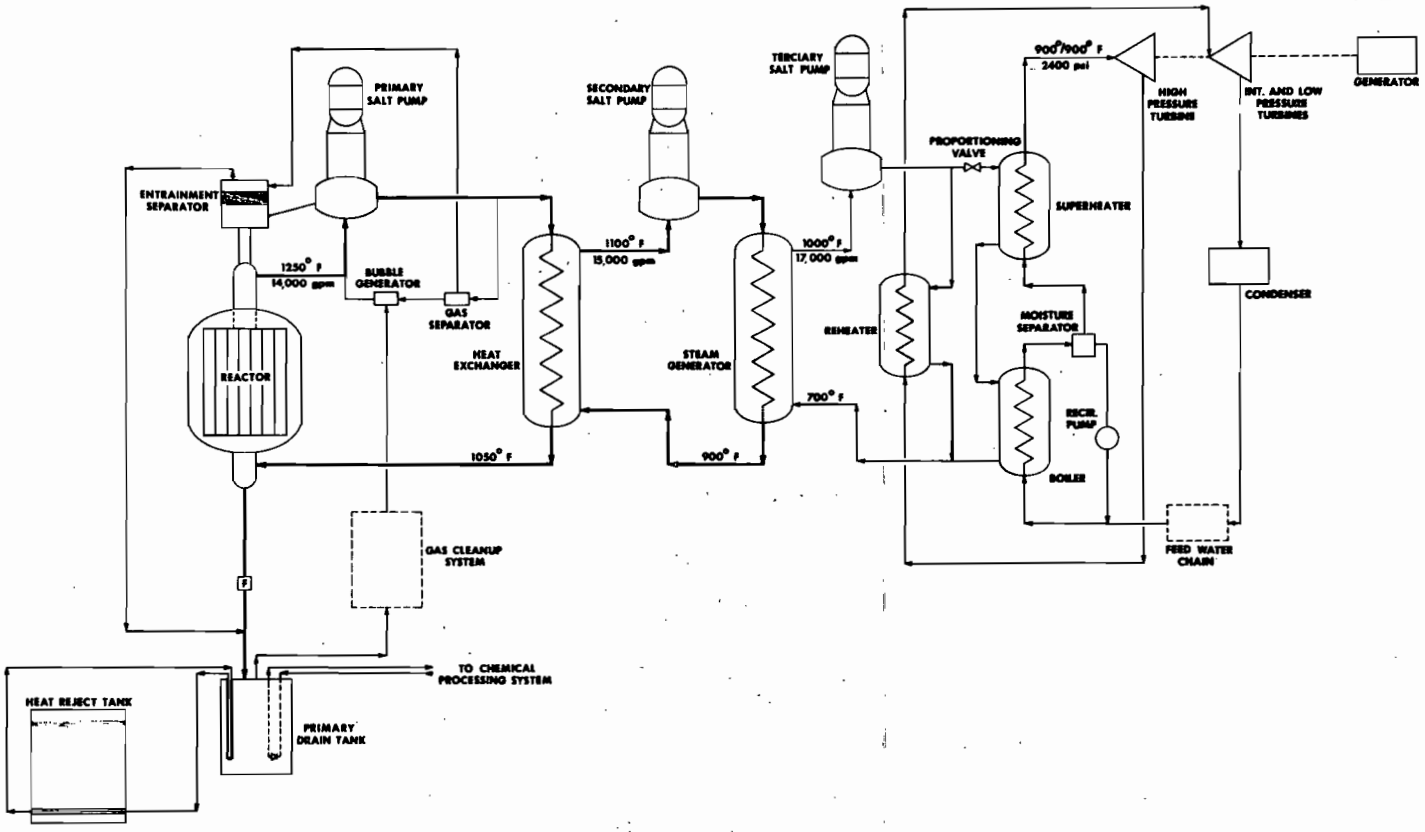

Fig. 11-1. SIMPLIFIED FLOWSHEET FOR 300-MW(e) MOLTEN-SALT DEMONSTRATION REACTOR

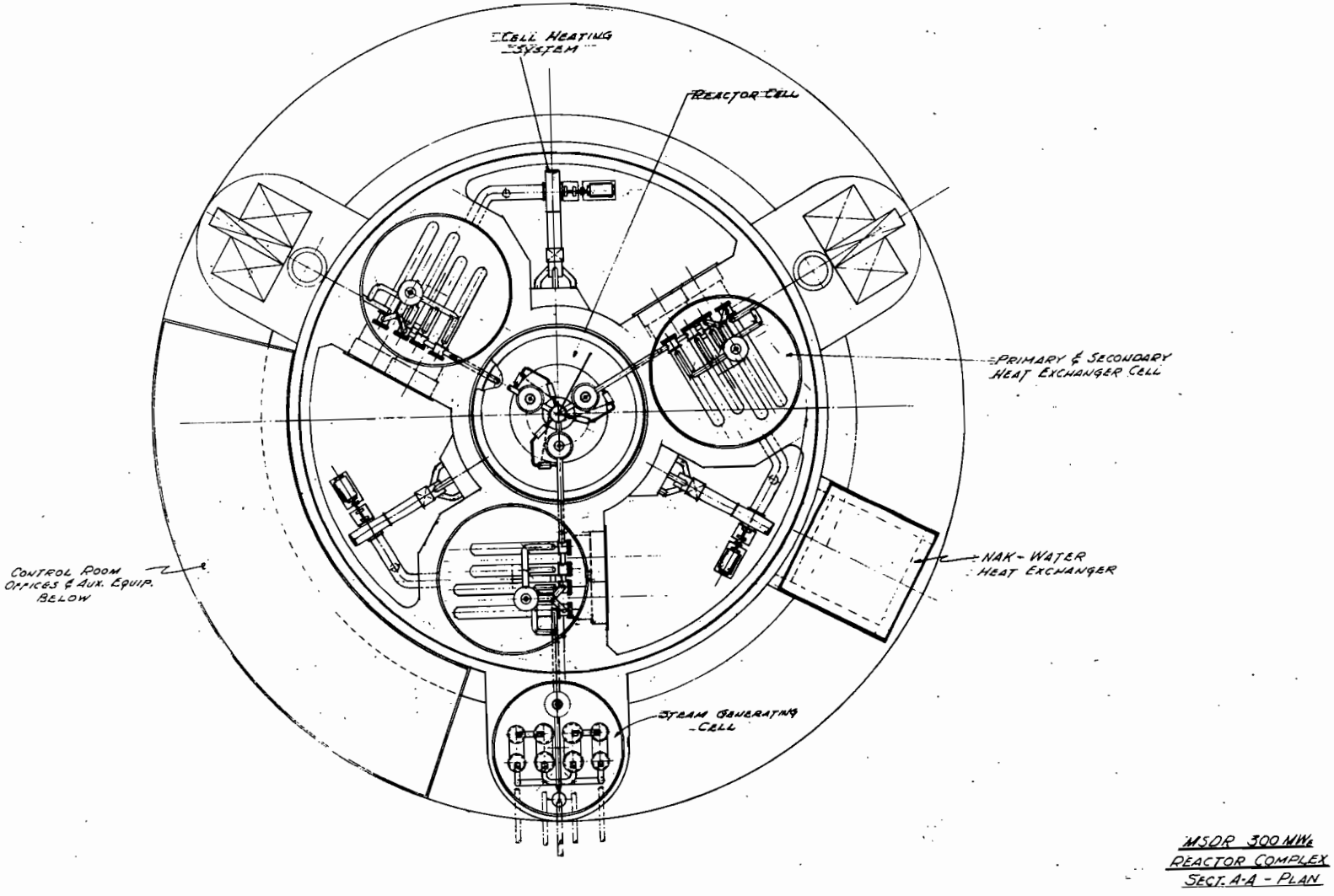

Fig. 11-2. MSDR EQUIPMENT LAYOUT PLAN

GENERAL REFERENCES ON MOLTEN SALT REACTORS

1. "The Status and Technology of Molten-Salt Reactors: A Review of Molten-Salt Reactor Work at the Oak Ridge National Laboratory", Nuclear Applications and Technology, 105-218, 8, Feb. 1970. (This is a set of eight papers covering the history of the molten-salt program, the MSRE, molten-salt chemistry, materials, fuel reprocessing, physics, fuel cycle analyses, and design features of breeder reactors.)

2. Molten-Salt Reactor Program Semiannual Progress Reports
   This series of 26 reports began in 1958. ORNL-3708 for the period ending July 31, 1964 gives a thorough review of the design, construction and supporting development work for the MSRE. The four most recent reports are:

   ORNL-4396 Period Ending February 28, 1969
   ORNL-4449 Period Ending August 31, 1969
   ORNL-4548 Period Ending February 28, 1970
   ORNL-4622 Period Ending August 31, 1970

3. Reactor Chemistry Division Annual Progress Reports
   This series of ten reports began in 1960 and includes basic work on the chemistry of molten-salts. The three most recent reports are:

   ORNL-4229 Period Ending December 31, 1967
   ORNL-4400 Period Ending December 31, 1968
   ORNL-4586 Period Ending May 31, 1970

4. Roy C. Robertson, R. B. Briggs, O. L. Smith, and E. S. Bettis, Two-Fluid Molten-Salt Breeder Reactor Design Study, ORNL-4528, August 1970.

5. Conceptual Design Study of a Single-Fluid Molten-Salt Breeder Reactor, ORNL-4541, (In press).

Central
Research Library
Document Collection

JUN 28 1971

R. J. DEBAKKER
BLDG. 7910